5-2014

The Development of APCI Mass Spectrometry Based Systems for Quantitative Real-Time Monitoring of Process-Scale Homogenous and Heterogeneous Reactions

Zhenqian Zhu
University of Tennessee - Knoxville, zzhu4@utk.edu

To the Graduate Council:

I am submitting herewith a dissertation written by Zhenqian Zhu entitled "The Development of APCI Mass Spectrometry Based Systems for Quantitative Real-Time Monitoring of Process-Scale Homogenous and Heterogeneous Reactions." I have examined the final electronic copy of this dissertation for form and content and recommend that it be accepted in partial fulfillment of the requirements for the degree of Doctor of Philosophy, with a major in Chemistry.

John E. Bartmess, Major Professor

We have read this dissertation and recommend its acceptance:

Jon P. Camden, Robert N. Compton, Stephen J. Paddison

Accepted for the Council:

Carolyn R. Hodges

Vice Provost and Dean of the Graduate School

(Original signatures are on file with official student records.)

The Development of APCI Mass Spectrometry Based Systems for Quantitative Real-Time Monitoring of Process-Scale Homogenous and Heterogeneous Reactions

A Dissertation Presented for the

Doctor of Philosophy

Degree

The University of Tennessee, Knoxville

Zhenqian Zhu

May 2014

Dedication

I dedicate this work to my dear grandma and grandpa, who passed away on the same day, Dec. 22, 2013, after SIXTY years of happy marriage.

Acknowledgements

First I would like to thank my advisor, Professor John E. Bartmess, for his guidance, encouragement, and support throughout my graduate study. I thank him for providing such a great platform for me to grow in the field of mass spectrometry. From him, I have learned how to work professionally when conducting scientific research and how to think critically as a chemist.

I would like to thank Professor Jon P. Camden, Professor Robert N. Compton, and Professor Stephen J. Paddison to serve on my committee. They have dedicated their time generously and I would like to thank them sincerely for their valuable comments and suggestions.

I would also like to thank Dr. Liguo Song for his generous support and great efforts dedicated to my research projects. I also want to thank him for training me to be a qualified operator in the Center of Mass Spectrometry.

My thanks go to our collaborators, Professor Kelsey D. Cook from University of Tennessee, Dr. Mary-Ellen McNally and Dr. Ron M. Hoffman from DuPont Crop Protection for their long-time support and precious industrial view on developing mass spectrometric methods to monitor batch slurry reactions in real time. I would also like to thank Dr. David S. Cho for his preliminary work in setup development and method validations. Without their contributions, this research might not have been possible.

I would like to thank Mr. Bill Gurley and Mr. Gary Wynn from Electronic Shop, and Mr. Tim Free from Mechanic Shop in Department of Chemistry at UTK, for their

great contributions to our setup development. I greatly thank the Department of Chemistry at University of Tennessee, the National Science Foundation for providing funding during my time in graduate school.

Lastly, I give very special thanks to my parents, my wife and her family for their full support, love, care and understanding. It is impossible to accomplish this work without them.

Zhengian Zhu

Abstract

The dissertation presents solutions to monitor industrial chemical processes quantitatively in real time by mass spectrometry. Chapter 1 presents the background of atmospheric pressure chemical ionization mass spectrometry (APCI-MS). Chapters 2-6 present methods developed based on flow injection analysis coupled to atmospheric pressure chemical ionization mass spectrometry (FIA/APCI-MS) for quantitative real-time monitoring of homogeneous and heterogeneous reactions conducted at molar concentrations.

Chapter 2 introduces auto-sampling FIA/APCI-MS with the ability to overcome potential sample overloading when molar concentration samples were analyzed without sample pretreatment procedures. A homogenous Michael-addition reaction between phenethylamine and acrylonitrile was conducted at room temperature and monitored quantitatively in real time at 1.63 M (molar) level. In chapter 3, auto-sampling FIA/APCI-MS was adapted for the quantitative real-time monitoring of a transesterification reaction, methanolysis of glycerol trioctanoate, which proceeded as a homogenous liquid system and a heterogeneous bi-phasic liquid-liquid system at an alcohol-to-oil molar ratio of 30:1 and 6:1, respectively. Simultaneous quantification of major compounds including two intermediates was achieved using calibrations based on the analysis of simulated reaction mixtures of standards and validated by parallel off-line reaction monitoring with HPLC/APCI-MS.

Chapter 4 introduces slurry FIA/APCI-MS with the ability to overcome potential instrumental clogging and sample overloading in quantitative real-time monitoring of a heterogeneous solid-liquid system, i.e. a batch slurry reaction. Slurry samples up to 30% (w/w) were successfully quantified. Chapter 5 describes an alternative slurry FIA/APCI-MS setup to accommodate a different mass spectrometer, aiming to prepare the slurry FIA/APCI-MS method to be used in quantitative real-time monitoring of a model batch slurry reaction at DuPont Crop Protection where a similar mass spectrometer was to be used. In Chapter 6, slurry FIA/APCI-MS was adapted for the quantitative real-time monitoring of a heterogeneous-catalyzed Pechmann condensation reaction using 50 g/L silica supported perchloric acid as catalyst.

Chapter 7 presents a study on the differentiation of underivatized monosaccharides from their stereoisomers using APCI quadrupole time-of-flight mass spectrometry (QTOF-MS). Identities of ions were assigned after accurate mass measurement by QTOF-MS. Distinctive fragmentation patterns were used to distinguish isomers of hexoses, methyl D-glucopyranosides, hexosamins and *N*-acetylhexosamines.

Chapter 8 presents the conclusion.

Table of Content

Chapter 1. Introduction 1
1.1 Background of APCI-MS 2
1.1.1 Chemical ionization mass spectrometry (CI-MS) 2
1.1.2 Atmospheric pressure chemical ionization mass spectrometry (APCI-MS) 5
1.1.3 Matrix effects in APCI-MS 9
1.2 Real-time reaction monitoring using APCI-MS 11
Reference 14
Chapter 2. Quantitative Real-time Monitoring of Chemical Reactions by Auto-sampling Flow Injection Analysis coupled with Atmospheric Pressure Chemical Ionization Mass Spectrometry 17
Abstract 18
2.1 Introduction 19
2.2 Experimental 22
2.2.1 Reagents 22
2.2.2 Instrumentation 23
2.2.3 Model reaction 27
2.2.4 Quantitative real-time reaction monitoring 29
2.3 Results and Discussion 29
2.3.1 Development of the auto-sampling FIA/APCI-MS system 29
2.3.2 Quantitative real-time monitoring of the model reaction 40
2.4 Conclusion 44
References 46
Chapter 3. Quantitative Real-time Monitoring of Transesterifications by Auto-sampling FIA/APCI-MS for the Improvement of Industrial Biodiesel Production 50
Abstract 51
3.1 Introduction 52

3.2 Experimental 54
3.2.1 Reagent 54
3.2.2 The model transesterification reaction 55
3.2.3 Real-time reaction monitoring 57
3.2.4 Quantitative calibration for real-time reaction monitoring 61
3.2.5 Off-line reaction monitoring 63
3.2.6 Quantitative calibration for off-line reaction monitoring 64
3.2.7 Kinetic modeling 64
3.3 Results and Discussions 66
3.3.1 Evaluation of the auto-sampling FIA/APCI-MS setup 66
3.3.2 Real-time reaction monitoring 67
3.3.3 Off-line reaction monitoring 69
3.3.4 Quantitative reaction monitoring 72
3.3.5 Kinetic results 75
3.4 Conclusion 82
Reference 83
Appendix A 86
Chapter 4. Slurry Flow Injection Analysis coupled with Atmospheric Pressure Chemical Ionization Mass Spectrometry for Quantitative Real-Time Monitoring of Batch Slurry Reactions 91
Abstract 92
4.1 Introduction 93
4.2 Experimental 96
4.2.1 Reagent 96
4.2.2 Model batch slurry reaction 97
4.2.3 Instrumentation 97
4.2.4 Quantitative calibration. 108
4.3 Results and Discussion 110

4.3.1 Development of the Slurry FIA/APCI-MS System 110
4.3.2 Quantitative Calibration 118
4.4 Conclusion 123
Reference 124
Chapter 5. Slurry Flow Injection Analysis coupled with APCI Mass Spectrometry for Quantitative Real-Time Monitoring of Batch Slurry Reactions: An Alternative Setup 129
Abstract 130
5.1 Introduction 131
5.2 Experimental 133
5.2.1 Reagent 133
5.2.2 Model batch slurry reaction 134
5.2.3 Instrumentation 134
5.2.4 Instrumental conditions 146
5.2.5 Quantitative calibration 147
5.3 Results and Discussions 148
5.3.1 Evaluation of the detached APCI-MS setup 148
5.3.2 Evaluation of the slurry FIA setup 150
5.3.3 Dynamic range of quantitation and LOD 156
5.3.4 Quantitative calibration 157
5.4 Conclusions 160
References 163
Appendix B 167
Chapter 6. Quantitative Real-time Monitoring of Heterogeneous-Catalyzed Reactions by Slurry FIA/APCI-MS 170
Abstract 171
6.1 Introduction 171
6.2 Experimental 172

6.2.1 Reagent 172
6.2.2 Model reaction 173
6.2.3 Instrumentation 173
6.2.4 Quantitative calibration 176
6.2.5 Quantitative real-time monitoring of the model reaction 177
6.3 Results and Discussions 177
6.4 Conclusion 182
Reference 183
Chapter 7. Differentiation of Underivatized Monosaccharides by Atmospheric Pressure Chemical Ionization Quadrupole Time-of-Flight Mass Spectrometry 184
Abstract 185
7.1 Introduction 186
7.2 Experimental 188
7.2.1 Chemicals 188
7.2.2 Mass spectrometry 189
7.3 Results and Discussion 190
7.3.1 Ionization products of hexoses by positive-ion APCI 190
7.3.2 Differentiation of Glc, Man and Gal 193
7.3.3 Differentiation between Me*α*Glc and Me*β*Glc 197
7.3.4 Differentiation of GlcN, ManN, and GalN 200
7.3.5 Differentiation of GlcNAc, ManNAc, and GalNAc 205
7.4 Conclusion 209
Reference 211
Appendix C 214
Chapter 8. Conclusion 216
Vita 220

List of Tables

Table 2.1 Matrix effects of PEA on the quantitation of PEAP. 42

Table 3.1 Reaction conditions of the model transesterification reaction. 58

Table 3.2 Changes of activation enthalpy and entropy of each step of the model transesterification reaction calculated from Eyring-Polanyi equation. 81

Table A1 Preparation of individual standard solution. 87

Table A2 Preparation of simulated reaction mixtures of standards based on a hypothetical reaction of TG+3MeOH→3FAME+Gly at an alcohol-to-oil molar ratio of 30:1.... 88

Table A3 Preparation of simulated reaction mixtures of standards based on a hypothetical reaction of TG+3MeOH→3FAME+Gly at an alcohol-to-oil molar ratio of 6:1..... 88

Table A4 Preparation of simulated reaction mixtures of standards based on a hypothetical reaction of TG+MeOH→DG+FAME at an alcohol-to-oil molar ratio of 30:1..... 89

Table A5 Preparation of simulated reaction mixtures of standards based on a hypothetical reaction of TG+MeOH→DG+FAME at an alcohol-to-oil molar ratio of 6:1..... 89

Table A6 Preparation of simulated reaction mixtures of standards based on a hypothetical reaction of TG+2MeOH→MG+2FAME at an alcohol-to-oil molar ratio of 30:1. .. 90

Table A7 Preparation of simulated reaction mixtures of standards based on a hypothetical reaction of TG+2MeOH→MG+2FAME at an alcohol-to-oil molar ratio of 6:1. 90

Table 4.1 Preparation of MSM slurry samples in xylenes with 25 mL volumetric flasks. 109

Table 4.2 Preparation of simulated slurry samples to represent the progress of the model batch slurry reaction at 30% (w/w) level upon completing using 25 mL volumetric flasks. 111

Table 4.3 Effects of the post-injection slurry mixer on relative standard deviation (RSD) and relative error (RE) of the quantitative calibration of MSM by the slurry FIA/APCI-MS system. 117

Table 4.4 Matrix effects of AMMT on the quantitation of MSM. 121

Table 5.1 Evaluation of the post-injection splitting using an aspirator. 153

Table 5.2 Evaluation of the post-injection splitting using a withdrawing syringe pump. 155

Table 5.3 Matrix effects of AMMT on the quantitation of MSM. 161

Table B1 Preparation of MSM solution and slurry samples in xylenes with 25 mL volumetric flasks. 168

Table B2 Preparation of simulated slurry samples to represent the progress of the model batch slurry reaction at 30% (w/w) level upon completing using 25 mL volumetric flasks. 169

Table 6.1 Preparation of standard mixtures simulating the progress of the model reaction. 178

List of Figures

Figure 1.1 Diagram of modern APCI source consisted of a heated nebulizer and a corona discharge needle. 8

Figure 1.2 Schematic diagram of the membrane interface for APCI-MS from reference [32]. 13

Figure 2.1 (A) Diagram of the auto-sampling FIA/APCI-MS system; (B) diagram of the automatic internal sample injector; (C) diagram of the detached APCI-MS setup; and (D) Diagram of the relative position of the ion-transport capillary, the corona discharge needle and the APCI probe. 24

Figure 2.2 Effect of the post-injection splitting on the upper-limit of quantitative calibration. (A) Splitting ratio, 0; upper-limit of linearity, 0.0255 M; (B) splitting ratio, 1:10; upper-limit of linearity, 0.103 M; and (C) splitting ratio, 1:100; upper limit of linearity, 0.413 M. Each point represents four replicated analyses. The R^2 of linear regression A, B and C are 0.9999, 0.9973 and 0.9958, respectively. A 1 μL automatic internal sample injector was incorporated into the FIA/APCI-MS system for these experiments. 31

Figure 2.3 Effect of the length of the 0.042-inch I.D. ion-transport capillary on the upper-limit of quantitative calibration. (A) Ion-transport capillary, 0 inch; upper-limit of linearity, 0.103 M; (B) ion-transport capillary, 6 inch; upper-limit of linearity, 0.413 M; and (C) ion-transport capillary, 4.5 inch; upper-limit of linearity, 0.825 M. Each point represents four replicated analyses. The R^2 of linear regression A, B and C are

0.9973, 0.9984 and 0.9987, respectively. A 1 μL automatic internal sample injector and a 1:10 post-injection splitter were incorporated into the FIA/APCI-MS system for these experiments. 35

Figure 2.4 Effect of the polarity of the analytes on the sampling interval of quantitative real-rime reaction monitoring. (A) XIP of 1.65 M PEAP at *m/z* 175; (B) XIP of 1.65 M isobutyrophenone at *m/z* 149. A 1 μL automatic internal sample injector, a 1:10 post-injection splitter and a 4.5-inch long 0.042-inch I.D. ion-transport capillary were incorporated into the FIA/APCI-MS system for these experiments. 37

Figure 2.5 Effect of the FIA solvent modifier on the upper-limit of quantitative calibration. (A) FIA solvent modifier, 0.05% (v/v) EA; upper-limit of linearity, 0.825 M; (B) FIA solvent modifier, 0.05% (v/v) IPA; upper-limit of linearity, 1.65 M; (C) FIA solvent modifier, 0.05% (v/v) TBA; upper-limit of linearity, 1.65 M. Each point represents four replicated analyses. The R^2 of linear regression A, B and C are 0.9972, 0.9927 and 0.9932, respectively. A 1 μL automatic internal sample injector, a 1:10 post-injection splitter and a 4.5-inch long 0.042-inch I.D. ion-transport capillary were incorporated into the FIA/APCI-MS system for these experiments. 39

Figure 2.6 Results of quantitative real-time monitoring of the model Michael-addition reaction of PEA and acrylonitrile. (A) Mass spectra of the reaction mixture at 10, 40 and 120 min reaction time; (B) Real-time molar concentration changes of PEA and PEAP. The reaction mixture was sampled and analyzed every 5 min..... 43

Figure 3.1 Detailed schematic diagrams of: A) the auto-sampling FIA/APCI-MS setup with a withdrawing syringe pump; B) the auto-sampling setup with an aspirator; C) the assembly of the aspirator..... 59

Figure 3.2 XIPs of the four targeted ions, i.e. $[TG+NH_4]^+$, $[DG+NH_4]^+$, $[MG+H]^+$ and $[FAME+H]^+$, as the model reaction progressed under conditions shown in entry 1 of Table 3.1 recorded by real-time reaction monitoring using auto-sampling FIA/APCI-MS..... 68

Figure 3.3 A mass spectrum at 14 minute of the model reaction under conditions shown in entry 1 of Table 3.1 recorded by real-time reaction monitoring using auto-sampling FIA/APCI-MS. The inserts are detailed mass spectra for ions related to TG, DG and MG. The ions that were selected to be monitored are marked in red. . 70

Figure 3.4 XICs of $[MG+H]^+$ at *m/z* 219, $[FAME+H]^+$ at *m/z* 159, $[DG+NH_4]^+$ at *m/z* 345 and $[TG+NH_4]^+$ at *m/z* 488 as a standard sample solution containing MG, FAME, DG and TG was analyzed by HPLC/APCI-MS..... 71

Figure 3.5 Concentration-time profiles of four targeted compounds for the model reaction under conditions shown in entry 1 of Table 3.1 with purple points representing off-line reaction monitoring by HPLC/APCI-MS and red points representing real-time reaction monitoring by auto-sampling FIA/APCI-MS using quantitative calibrations based on the analysis of simulated reaction mixtures of standards: (A) TG and FAME; (B) DG and MG. Quantitative data are presented every 5 min from 5-60 min of the reaction. 73

Figure 3.6 (A) Concentration-time profiles of experimental data (discrete points) and kinetic modeling results (contiguous curves) of the model reaction under conditions as shown in entry 1 of Table 3.1; (B) concentration-time profiles of kinetic modeling results of the model reaction under conditions as shown in in entry 1 to 5 of Table 3.1 for TG and FAME; (C) concentration-time profiles of experimental data (discrete points) and kinetic modeling results (contiguous curves) of the model reaction under conditions as shown in entry 6 of Table 3.1. 76

Figure 4.1 Diagram of the slurry FIA/APCI-MS system: (A) HPLC pump; (B) slurry auto-sampler; (C) post injection slurry mixer and (D) detached APCI-MS. 99

Figure 4.2 Operational principle of the slurry auto-sampler: (A) a 4-position flow-through selector valve in position #1; (B) a 4-position flow-through selector valve in position #2; (C) the slurry slurry auto-sampler in loading position with the 4-position flow-through selector valve, i.e. the auto-sampling valve, in position #3; (D) the slurry auto-sampler in injection position with the 4-position flow-through selector valve, i.e. the auto-sampling valve, in position #4..... 102

Figure 4.3 Diagram of the commercial APCI probe (A) and the slurry APCI probe (B). 107

Figure 4.4 Extracted ion profiles of the $[MSM + H]^+$ ion: (A) Analysis of a 0.039 M MSM solution sample in acetonitrile by the previously reported auto-sampling FIA/APCI-MS system; (B) analysis of a 1.71% (w/w) MSM slurry sample in xylenes (equivalent to 0.039 M) by the slurry FIA/APCI-MS system. 115

Figure 4.5 Mass spectra of simulated slurry samples representing the progress of the model batch slurry reaction at 30% (w/w) level upon completion: (A) 10%, (B) 40%; (C) 80% reaction completion..... 120

Figure 5.1 Schematic diagram of the new slurry FIA/APCI-MS setup. 137

Figure 5.2 Waters Quattro II triple quadrupole mass spectrometer with A) the commercial APCI-MS source, and B) the detached APCI-MS source. 138

Figure 5.3 Detailed schematic diagrams of: A) the detached APCI-MS setup, B) the base of the detached APCI source and C) the commercial APCI probe (left) and the slurry APCI probe (right). 139

Figure 5.4 Detailed schematic diagram of the post-injection splitter using an aspirator. 145

Figure 5.5 Effect of solvent preheating and post-injection splitting on the chromatographic peaks of the $[MSM + H]^+$ ion at *m/z* 382: A) without solvent preheating and post-injection splitting, B) with solvent preheating only, and C) with both solvent preheating and post-injection splitting. 151

Figure 5.6 Mass spectrum acquired by MS1 scan for simulated slurry mixture samples with reaction progress at 5%, 20% and 100% completion. 159

Figure 6.1 The slurry FIA/APCI-MS setup used for quantitative real-time monitoring of the model reaction. 175

Figure 6.2 Mass spectra of reaction mixtures at 5, 25 and 45 min of reaction time. 180

Figure 6.3 Yield-time profile of hymecromone obtained by quantitative real-time reaction monitoring using slurry FIA/APCI-MS. 181

Figure 7.1 Positive-ion APCI/QTOF mass spectrum of 1.0 mM Glc in H_2O. The mass spectrum was calibrated using the peaks representing ions of $[C_6H_{10}O_5 + H]^+$ and $[C_6H_6O_3 + H]^+$ with theoretical *m/z* values of 163.0607 and 127.0395, respectively. The *m/z* values of other peaks measured by APCI/QTOFMS are indicated in the figure. 191

Figure 7.2 (A) Positive-ion APCI/QTOF-MS^2 spectra of the $[M + NH_4]^+$ precursor ions at *m/z* 198.098 generated from 0.1 mM Glc, Man, and Gal in methanol containing 10 mM NH_4Ac. Collision energy was 9 V. Product ions are identified to be $[M + NH_4 - NH_3]^+$(*m/z* 181), $[M + NH_4 - H_2O]^+$ (*m/z* 180), $[M + NH_4 - H_2O - NH_3]^+$ (*m/z* 163) and $[M + NH_4 - 2H_2O - NH_3]^+$ (*m/z* 145). (B) Relative intensities of peaks at nominal *m/z* 180 to 163 in the APCI/QTOF-MS^2 spectra under different collision energy for Glc, Man and Gal. 194

Figure 7.3 (A) Negative- ion APCI/QTOF-MS^2 spectra of the $[M - H]^-$ ions at *m/z* 179.056 generated from 0.5 mM Man and Gal in methanol. Collision energy was at -10 V. Product ions are identified to be $[M - H_2O - H]^-$ (*m/z* 161), $[M - C_2H_4O_2 - H]^-$ (*m/z* 119) and $[M - C_3H_6O_3 - H]^-$ (*m/z* 89). (B) Relative intensities of peaks at nominal *m/z* 119 to 89 in the APCI/QTOF-MS^2 spectra under different collision energy for Man and Gal. 196

Figure 7.4 (A) Positive-ion APCI/QTOF-MS^2 spectra of the $[M + NH_4]^+$ precursor ions at *m/z* 212.113 generated from 0.1 mM Me*α*Glc and Me*β*Glc in methanol containing 10 mM NH_4Ac. Collision energy was 11 V. Product ions are identified to be $[M - 2H_2O + H]^+$ (*m/z* 144), $[M - 3H_2O + H]^+$ (*m/z* 126), $[M - CH_8O_4 + H]^+$ (*m/z* 96), $[M - C_2H_8O_4 + H]^+$ (*m/z* 84) and $[M - C_3H_8O_4 + H]^+$ (*m/z* 72). (B) Relative intensities of peaks at nominal *m/z* 180 to 195 in the APCI/QTOF-MS^2 spectra under different collision energy for Me*α*Glc and Me*β*Glc. 199

Figure 7.5 (A) Positive-ion APCI/QTOF-MS^2 spectra of the $[M - H_2O + H]^+$ precursor ions at *m/z* 162.076 generated from 0.1 mM GlcN, ManN and GalN in methanol containing 10 mM NH_4Ac. Collision energy was 18 V. Product ions are identified to be $[M - 2H_2O + H]^+$ (*m/z* 186) and $[M - C_2H_8O_4 + H]^+$ (*m/z* 126). (B) Relative intensities of peaks at nominal *m/z* 72 to 84 in the APCI/QTOF-MS^2 spectra under different collision energy for GlcN, ManN and GalN. 202

Figure 7.6 (A) Negative-ion APCI/QTOF-MS^2 spectra of the $[M + O_2]^-$ ions at *m/z* 211.070 generated from 0.5 mM GlcN, ManN and GalN. Collision energy was -8 V. Product ions are identified to be $[M - H]^-$ (*m/z* 178), $[M - 2H]^-$ (*m/z* 177), and $[M - H - H_2O]^-$ (*m/z* 160). (B) Relative intensities of peaks at nominal *m/z* 177 to 178 in the APCI/QTOF-MS^2 spectra under different collision energy for GlcN, ManN and GalN. (C) Relative intensities of peaks at nominal *m/z* 178 to 160 in the same spectra under same collision energies as in (B). 204

Figure 7.7 (A) Positive-ion APCI/QTOF-MS^2 spectra of the $[M - H_2O + H]^+$ precursor ions at *m/z* 204.087 generated from 0.1 mM GlcNAc, ManNAc and GalNAc in methanol containing 10 mM NH_4Ac. Collision energy was 9 V. Product ions are identified to be $[M - 2H_2O + H]^+$ (*m/z* 186) and $[M - C_2H_8O_4 + H]^+$ (*m/z* 126). (B) Relative intensities of peaks at nominal *m/z* 186 to 126 in the APCI/QTOF-MS^2 spectra under different collision energy for GlcNAc, ManNAc and GalNAc..... 207

Figure 7.8 (A) Positive-ion APCI/QTOF-MS^2 spectra of the $[M - 3H_2O + H]^+$ precursor ions at *m/z* 168.066 generated from 0.1 mM GlcNAc, ManNAc and GalNAc in methanol containing 10 mM NH_4Ac. Collision energy was 9 V. Product ions are identified to be $[M - 2H_2O + H]^+$ (*m/z* 186) and $[M - C_2H_8O_4 + H]^+$ (*m/z* 126). (B) Relative intensities of peaks at nominal *m/z* 126 to 138 in APCI/QTOF-MS^2 spectra under different collision energy for GlcNAc, ManNAc and GalNAc. 208

Figure C1 Structures of monosaccharides studied in this chapter. 215

List of Schemes

Scheme 2.1 The model reaction: Michael-addition reaction of phenethylamine and acrylonitrile. 28

Scheme 3.1 The model transesterification reaction of vegetable oils with three reversible steps..... 56

Scheme 4.1 The model slurry reaction: coupling reaction of AMMT and MIB for the production of MSM..... 98

Scheme 5.1 The model batch slurry reaction: coupling reaction of AMMT and MIB for the production of MSM..... 135

Scheme 6.1 The model reaction to synthesis hymecromone via Pechmann condensation 174

List of Abbreviations

AMMT: 2-Amino-4-methoxy-6-methyl-1,3,5-triazine

APCI: Atmospheric pressure chemical ionization

CI: Chemical ionization

DART: Direct analysis in real time

DESI: Desorption electrospray ionization

DG: Diglyceride

EASI: Easy Ambient Sonic-Spray Ionization

EESI: Extractive electrospray ionization

ELDI: Electrospray-assisted laser desorption/ionization

ESI: Electrospray ionization

eV: Electron volt

FA: Fatty acid

FAB: Fast atom bombardment

FAME: Fatty acid methyl ester

FIA: Flow injection analysis

FTIR: Fourier-Transform infrared

Gla: Galactose

GlaN: Galactosamine

GlaNAc: *N*-acetyl-galactosamine

GC: Gas chromatography

Glc: Gluctose

GlcN: Gluctosamine

GlcNAc: *N*-acetyl-glucosamine

GPC: Gel permission chromatography

^{1}H NMR: Proton Nuclear Magnetic Resonance

HPLC: High performance liquid chromatography

I.D.: Inner diameter

IE: Ionization energy

IPA: *iso*-Propylamine

IR: Infrared

LC: Liquid chromatography

Man: Mannose

ManN: Mannosamine

ManNAc: *N*-acetyl-mannosamine

MeαGlc: Mehtyl α-glucopyranoside

MeβGlc: Mehtyl β-glucopyranoside

MG: Mono-glyceride

MSM: Metsulfuron methyl

NI: Negative ion

O.D.: Outer diameter

PA: Proton affinity or Peak area

PEA: Phenethylamine

PEAP: Polyether ether ketone

PI: Positive ion

QTOF: Quadrupole time-of-flight

RSD: Relative standard deviation

TBA: *tert*-Butylamine

TG: Triglyceride

TOF: Time-of-flight

UV-vis: Ultraviolet–visible

XIP: Extracted ion profile

Chapter 1. Introduction

1.1 Background of APCI-MS

1.1.1 Chemical ionization mass spectrometry (CI-MS)

CI-MS was independently developed by Tal'roze *et al*[1] in 1950s and Munson *et al*[2-5] in 1960s. On the basis of studies made at source pressure up to 0.3 torr, researchers increased the pressure of pure methane (CH_4) up to 2 torr in the source, and observed that at higher than 0.5 torr, there was no perceptible change of CH_5^+ and $C_2H_5^+$ in the ionic concentration at increasing methane pressure, even though exothermic reactions can be written for them to further react with methane.[2] However, significant perceptible changes of CH_5^+ and $C_2H_5^+$ in the ionic concentration were observed at the presence of very small amount of other compounds, e.g. ethane, propane, water and ammonia.[3,4] In addition, the reactions of CH_5^+ and/or $C_2H_5^+$ with trace amount of other compounds produced abundant ions characteristic of added compounds. Subsequently, a systematic gas-phase ion reaction theory, i.e. CI, was introduced where mass spectra were produced from ion/molecule reactions of reactant ions with analyte compounds, and the CI spectra showed enhanced abundance of ions in the molecular weight region and much less fragmentations compared to EI (electron ionization) spectra.[5] Methane, isobutane and ammonia are commonly used reagent gases in CI-MS. In a typical CH_4 CI, formation of major primary ions and reactant ions can be described in Equation 1.1 to 1.4.

$$CH_4 + e^- \rightarrow CH_4^{+\bullet} + 2e^- \qquad \text{Equation 1.1}$$

$$CH_4 + e^- \rightarrow CH_3^+ + H^\bullet + 2e^- \qquad \text{Equation 1.2}$$

$$CH_4^{+\bullet} + CH_4 \rightarrow CH_5^+ + CH_3^\bullet \qquad \text{Equation 1.3}$$

$$CH_3^+ + CH_4 \rightarrow C_2H_5^+ + H_2 \qquad \text{Equation 1.4}$$

Ion/molecule reactions are essential in producing ions of analytes in CI. The ion/molecule reaction is a bimolecular process which relies on the sufficiently large number of collisions during the dwell time of reactants in the ion source. A "tight" ion source (pressure = 0.1-2 torr, compared with 10^{-5}-10^{-6} torr in EI source) is used in CI to maximize collisions, which results in increasing sensitivity.[6] Product ions of analyte M can be produced through proton transfer (Equation 1.5), adduct formation (Equation 1.6), hydride abstraction (Equation 1.7) and charge transfer (Equation 1.8) with reactant ion X^+ or $X^{+\bullet}$.[6-8] To take place, these ion/molecule reactions must be exothermic.

$$X^+ + M \rightarrow [X-H] + [M+H]^+ \qquad \text{Proton transfer} \qquad \text{Equation 1.5}$$

$$X^+ + M \rightarrow [M+X]^+ \qquad \text{Adduct formation} \qquad \text{Equation 1.6}$$

$$X^+ + M \rightarrow XH + [M-H]^+ \qquad \text{Hydride abstraction} \qquad \text{Equation 1.7}$$

$$X^{+\bullet} + M \rightarrow M^{+\bullet} + X \qquad \text{Charge transfer} \qquad \text{Equation 1.8}$$

Proton transfer is a dominant process when usual reagent gases are used in CI. To produce $[M+H]^+$, the proton affinity (PA) of the analyte molecule must be larger than that of the reagent gas. The greater the difference in proton affinities of the analyte and the reagent gas, the more energy will be transferred to the protonated molecule, and the greater will be the degree of subsequent fragmentation of the analyte. The protonation in

CI is generally exothermic by 1-4 eV and therefore the degree of fragmentation of $[M+H]^+$ is much lower than that observed under 70 eV condition in EI.[7] When the proton affinities of the analyte and the reagent gas are nearly equal, adduct ions may be observed instead of the protonated molecules. Selective ionization can be achieved to some extent in CI by choosing a reagent gas that has a proton affinity just slightly weaker than that of the analyte. Compounds with PAs weaker than that of the reagent gas will not be ionized and, therefore, will not interfere with the analysis. Similar to proton transfer, hydride abstraction occurs when hydride affinity of X^+ is larger than that of $[M-H]^+$. This process is seen most often in CI of hydrocarbons[9].

Charge exchange occurs when the ionic charge is transferred from ions to neutral molecules and can produce abundant molecular ion $M^{+\bullet}$ when a suitable reagent gas (e.g. chlorobenzene) is used. The ionization energy (IE) of M must be smaller than that of X for CE to take place (Equation 1.8). Predominant $M^{+\bullet}$ can be observed in spectra when $IE_{(X)} - IE_{(M)}$ is small, and extensive fragmentations are expected when $IE_{(X)} - IE_{(M)}$ is significant. Accordingly, the "softness" of CE can be adjusted by selecting a proper reagent gas.

In negative ion chemical ionization (NICI), electron capture (EC) is an important process to produce negative ions. The high number of collisions in CI helps generate a flux of low-energy electrons, including thermal electrons which further interact with reagent gas or analyte molecules to produce negative ions via three pathways of EC (Equation 1.9 to 1.11).

$$M + e^- \rightarrow M^{-\bullet}$$ Resonance electron capture Equation 1.9

$$M + e^- \rightarrow A + [M - A]^-$$ Dissociative electron capture Equation 1.10

$$M + e^- \rightarrow A^+ + [M - A]^- + e^-$$ Ion-pair formation Equation 1.11

Negative ions of analytes can also be formed by ion/molecule reactions, including proton abstraction (Equation 1.12), anion attachment (Equation 1.13) and charge exchange (Equation 1.14).

$$X^- + M \rightarrow XH + [M - H]^-$$ Proton abstraction Equation 1.12

$$X^- + M \rightarrow [M + X]^-$$ Anion attachment Equation 1.13

$$X^{\bullet -} + M \rightarrow M^{\bullet -} + X$$ Charge exchange Equation 1.14

OH^- is a frequently used reactant ion, and can be produced at the presence of N_2O and hydrogen-rich gas, e.g. H_2 and CH_4. The production of OH^- involves the formation of $O^{-\bullet}$ from N_2O by interacting with low energy electrons (Equation 1.15) and subsequent abstraction of $H^\bullet$ by $O^{-\bullet}$ (Equation 1.16).

$$N_2O + e^- \rightarrow O^{-\bullet} + N_2$$ Equation 1.15

$$O^{-\bullet} + X \rightarrow [X - H]^\bullet + OH^-$$ Equation 1.16

In general, CI-MS is an analytical application of ion/molecule reactions. Most analytes accessible to EI can be analyzed by CI and CI becomes especially useful when molecular ion peaks in EI is absent or weak.

1.1.2 Atmospheric pressure chemical ionization mass spectrometry (APCI-MS)

APCI-MS was first introduced by Horning and co-workers[10,11] in the early 1970s. A ^{63}Ni foil (a radioactive beta emitter) was used as a replacement for the heated filament

in CI which cannot be operated at atmospheric pressure. Shortly after, a corona discharge, typically in the range of 1-5 μA, was used to replace the ^{63}Ni foil in APCI[12]. The corona discharge is advantageous in providing about two orders of magnitude higher reactant ion densities in the region of the sampling aperture.[13]

The ionization of APCI is different from CI by operating at atmospheric pressure, where the mean free path between collisions is very short ($\times 10^{-9}$ m range). Therefore a large number of gas phase reactions occur and thermal equilibria are reached in a relative short period. The high density of reaction ions leads to high ionization efficiency, almost 100% ionization of analyte molecules if gas-phase chemistry is favored. On the other hand, typically non-equilibrium conditions exist in CI source, resulting in ionization of only a portion of the sample introduced and also product ions that are not collisionally stabilized.[14,15]

In APCI, ambient gas molecules are involved in the formations of primary ions and reactant ions. In positive ion (PI) mode, primary ions $N_2^{+\cdot}$, $O_2^{+\cdot}$, $NO^{+\cdot}$, and $H_2O^{+\cdot}$ may be produced; and in the presence of trace amount of water, cascade reactions leads to predominant protonated water clusters ions, i.e. $H_3O^+(H_2O)_n$, in the reaction ion mass spectrum (Equation 1.17 to 1.21).[10,16] Abundant $[M+H]^+$ ions are expected for basic compounds through proton transfer in spectrum, while little or no ions for non-polar compounds.

$$N_2 + e^- \rightarrow N_2^{+\bullet} + 2e^- \qquad \text{Equation 1.17}$$

$$N_2^{+\bullet} + 2N_2 \rightarrow N_4^{+\bullet} + N_2 \qquad \text{Equation 1.18}$$

$$N_4^{+\bullet} + H_2O \rightarrow H_2O^{+\bullet} + 2N_2$$ Equation 1.19

$$H_2O^{+\bullet} + H_2O \rightarrow H_3O^+ + OH^\bullet$$ Equation 1.20

$$H_3O^+ + nH_2O + N_2 \rightarrow H_3O^+(H_2O)n + N_2 \quad n=0\text{-}4$$ Equation 1.21

In negative ion (NI) mode, the dominant reactant ion is $O_2^{-\bullet}$. $O_2^{-\bullet}$ has strong proton affinity (PA=1477 kJ/mol) and will accept protons from analytes whose corresponding anions have lower PA, i.e. proton abstraction. In this manner, $[M-H]^-$ ion will dominant the NI APCI-MS spectra of many analyte compounds, e.g. carboxylic acids, benzoic acids, phenols, etc.. Halide reactant ions, i.e. X^-, can be generated when reagent compounds with a halide atom are presented and $[M+X]^-$ ions of analyte compounds will be observed through anion attachment.

A heated nebulizer, which was introduced by Henion and coworkers[17], is used extensively in modern APCI designs (Figure 1.1) to couple with reversed phase liquid chromatography (RPCL) with flow rates up to 2 mL/min. A heated nebulizer consists of a concentric pneumatic nebulizer and a quartz vaporizer extending beyond the tip of nebulizer capillary. Column eluent is nebulized with an inert gas (usually nitrogen) and the aerosol is swept through the heated tube (200-500 ℃), followed by corona discharge.

In LC/APCI-MS, the primary ions will react with solvent molecule to form solvent-derived reactant ions (Equation 1.22 and 1.23). Additive in the eluent may also change the composition of the reactant ions. For instance, if ammonium acetate is added to the eluent, the reactant ions are ammonium and acetate ions, clustered with water, ammonia, acetic acid, or other polar components in the eluent. The

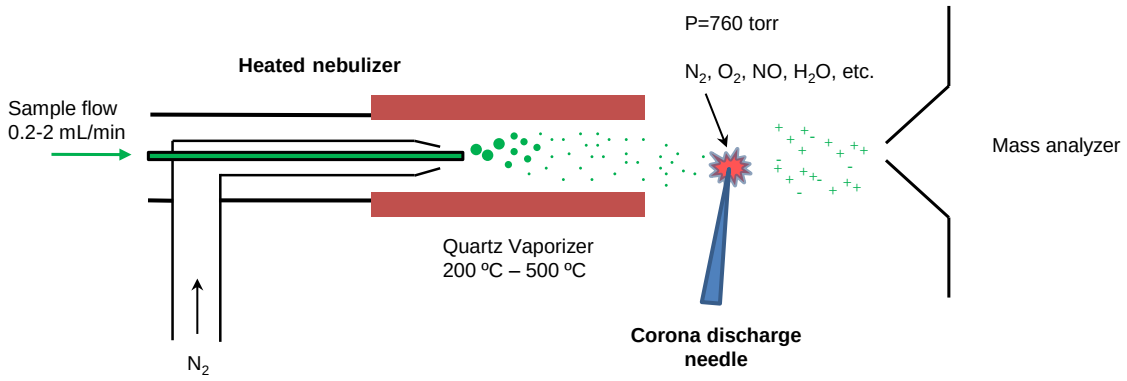

Figure 1.1 Diagram of modern APCI source consisted of a heated nebulizer and a corona discharge needle.

reactant ions will then react with the analyte M via ion/molecule reactions (Equation 1.24).

$$N_4^{+\bullet} + S \rightarrow S^{+\bullet} + 2N_2 \qquad \text{Equation 1.22}$$

$$S^{+\bullet} + S \rightarrow [S+H]^+ + [S-H]^\bullet \qquad \text{Equation 1.23}$$

$$[S+H]^+ + M \xrightarrow{\text{Proton transfer}} [M+H]^+ + S \qquad \text{Equation 1.24}$$

(When $PA_{(M)} > PA_{(S)}$)

Today, APCI and electrospray ionization (ESI) are the two most popular ionization methods for LC/MS applications. The APCI interface provides a stable ion beam, which is beneficial in establishing quantitative assays of chemical species that are known not to suffer thermal degradation effects. The heated nebulizer allows the accommodation of LC flow rates up to milliliters per minute, which enables large injection volume and in return offers low concentration detection limits. It has been reported that 20-30% of analyses dedicated to quantifying drugs in biological samples are conducted by APCI with the remainder by ESI. [14,18-21]

1.1.3 Matrix effects in APCI-MS

With the presence of a matrix or other interferences in the sample, the quantitative analysis with ESI or APCI can be substantially affected by the occurrence of ion suppression, or enhancement (very rare), which is referred to as "matrix effects".[22]

The mechanism of matrix effects has not been thoroughly understood. Using a dual ESI-APCI source and dual-sprayer ESI source, King and co-workers[23] demonstrated that suppression of ion signals in ESI majorly results from liquid phase processes. These

processes include competition for charges and available access to droplet surface between analyte and matrix compound[24,25], reduced rate of small droplet formation[23,26], and the induced precipitation or ion-paring phenomena by the presented matrix[23,27]. In the gas phase, on the other hand, the mechanisms responsible for ion suppression may involve neutralization reactions, charge transfer, and competition from gas-phase ion/molecule reactions due to interfering compounds.

Although not completely free from matrix effects, it has been suggested that APCI will not suffer from the same ion-suppression problem as those encountered with ESI[23,28-30], because APCI is known as a gas-phase ionization method and thus those liquid processes responsible for ion-suppression are absent. The suppression phenomena related to APCI are not fully understood. The concentration and gas-phase basicity or acidity of the matrix compounds may influence the extent of ion-suppression on analyte ion intensity in APCI-MS.

Several operational strategies have been suggested to minimize the interference of matrix compounds.[22] Improvement of sample pretreatment procedures (e.g. solid-phase extraction and liquid-liquid extraction) is commonly used to help remove specific matrix compounds. Modified chromatographic methods are also widely adopted by shifting the retention time of analyte far from the area severely affected by ion suppressions. Using appropriate calibration methods to compensate for the signal alterations can be another option.[31] Calibration strategies using external matrix-matched standards or stable isotope-labeled internal standards, as well as the standard-addition method, are extensively

employed in the laboratory. Furthermore, modifications of MS conditions can be performed to overcome the matrix effects, because the ion suppression may be different in the ionization mode, ion source designs and ionization techniques.

To develop MS based approaches for online real-time analysis, however, sample pretreatment and chromatographic methods are usually circumvented, where matrix effects are inevitably present. Therefore, in our study APCI is selected over ESI due to its inherent advantages of suffering less from matrix effects. Also, the ion suppressions due to matrix effects is further compensated by using external matrix–matched standards, which has been proven to be quite effective.

1.2 Real-time reaction monitoring using APCI-MS

Real-time online monitoring of reactions is of great importance because not only can it provide timely chemical information, but also can alleviate some of the difficulties encountered in the repetitive off-line sampling, which will further benefit process control in the chemical and pharmaceutical industries. Mass spectrometry based approaches have been reported for real-time monitoring of reactions (summarized in Chapter 2). However, prior to our work, the only method using APCI-MS for real-time monitoring of process-scale reactions was reported by Clinton and co-workers[32].

In their study, a system containing two solvent streams and a liquid-liquid membrane interface was used (Figure 1.2). As the reaction proceeded, a small portion of high-concentrated (1.65 molar level) reaction mixture was sampled and manually injected into a solvent donor stream (Figure 1.2 left). To avoid sample overloading for APCI-MS

analysis, a liquid–liquid membrane interface using a hydrophobic polyvinylidene fluoride microporous membrane with a pore size of 0.1 μm was incorporated into the system to achieve about 3×10^5 dilutions of the sample in the acceptor solvent stream (Figure 1.2 right).

The use of flow injection analysis (FIA) in solvent donor stream (Figure 1.2 left) avoids continuous introduction of high-concentrated samples into the system; and timely information of the process can still be provided with sufficient sampling frequency. However, the employment of the membrane interface, though it achieved on-line dilutions in one step, is not ideal for quantitative purposes or extended application of reaction monitoring. The ion responses were observed to be susceptible to the small changes in operational pressures, flow rates for the donor and acceptor streams and sample pulsing on both sides of the membrane from the reciprocating HPLC pumps.

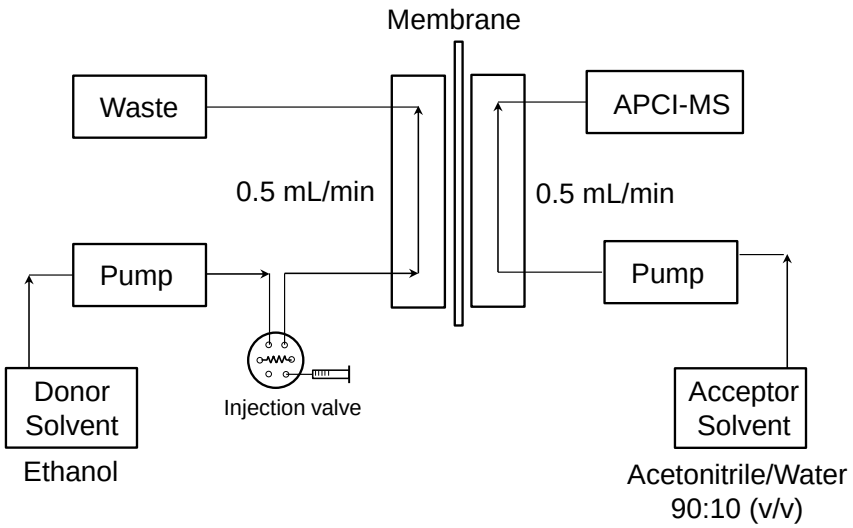

Figure 1.2 Schematic diagram of the membrane interface for APCI-MS from reference [32].

Reference

(1) Tal'roze, V. L.; Ljubimova, A. K. *J. Mass Spectrom.***1998**, *33*, 502-504.

(2) Field, F. H.; Munson, M. S. B. *J. Am. Chem. Soc.* **1965**, *87*, 3289.

(3) Munson, M. S. B.; Field, F. H. *J. Am. Chem. Soc.* **1965**, *87*, 3294.

(4) Munson, M. S. B.; Field, F. H. *J. Am. Chem. Soc.* **1965**, *87*, 4242.

(5) Munson, M. S. B.; Field, F. H. *J. Am. Chem. Soc.* **1966**, *88*, 2621.

(6) Watson, J. T.; Sparkman, O. D. In *Introduction to Mass Spectrometry*; John Wiley & Sons, Ltd, 2008, pp 449-484.

(7) Gross, J. H.; Roepstorff, P. *Mass Spectrometry: A Textbook*; Springer, 2011.

(8) Harrison, A. G. *Chemical Ionization Mass Spectrometry*; C R C Press LLC, 1983.

(9) Houriet, R.; Parisod, G.; Gaumann, T. *J. Am. Chem. Soc.* **1977**, *99*, 3599-3602.

(10) Horning, E. C.; Horning, M. G.; Carroll, D. I.; Dzidic, I.; Stillwel.Rn. *Anal. Chem.* **1973**, *45*, 936-943.

(11) Carroll, D. I.; Dzidic, I.; Stillwel.Rn; Horning, M. G.; Horning, E. C. *Anal. Chem.* **1974**, *46*, 706-710.

(12) Horning, E. C.; Carroll, D. I.; Dzidic, I.; Haegele, K. D.; Horning, M. G.; Stillwel.Rn. *J. Chromatogr.* **1974**, *99*, 13-21.

(13) Carroll, D. I.; Dzidic, I.; Stillwell, R. N.; Haegele, K. D.; Horning, E. C. *Anal. Chem.* **1975**, *47*, 2369-2373.

(14) Covey, T. R.; Thomson, B. A.; Schneider, B. B. *Mass Spectrom. Rev.* **2009**, *28*, 870-897.

(15) Mitchum, R. K.; Korfmacher, W. A. *Anal. Chem.* **1983**, *55*, 1485.

(16) Proctor, C. J.; Todd, J. F. J. *Org. Mass Spectrom.* **1983**, *18*, 509-516.

(17) Covey, T. R.; Lee, E. D.; Henion, J. D. *Anal. Chem.* **1986**, *58*, 2453-2460.

(18) Olah, T. V.; McLoughlin, D. A.; Gilbert, J. D. *Rapid Commun. Mass Spectrom.* **1997**, *11*, 17-23.

(19) Bogusz, M. J.; Maier, R. D.; Kruger, K. D.; Kohls, U. *J. Anal. Toxicol.* **1998**, *22*, 549-558.

(20) Singh, G.; Gutierrez, A.; Xu, K. Y.; Blair, I. A. *Anal. Chem.* **2000**, *72*, 3007-3013.

(21) Darius, J.; Banditt, P. *J. Chromatogr. B* **2000**, *738*, 437-441.

(22) Trufelli, H.; Palma, P.; Famiglini, G.; Cappiello, A. *Mass Spectrom. Rev.* **2011**, *30*, 491-509.

(23) King, R.; Bonfiglio, R.; Fernandez-Metzler, C.; Miller-Stein, C.; Olah, T. *J. Am. Soc. Mass Spectrom.* **2000**, *11*, 942-950.

(24) Cech, N. B.; Enke, C. G. *Anal. Chem.* **2000**, *72*, 2717-2723.

(25) Zhou, S. L.; Cook, K. D. *J. Am. Soc. Mass Spectrom.* **2001**, *12*, 206-214.

(26) Mallet, C. R.; Lu, Z. L.; Mazzeo, J. R. *Rapid Commun. Mass Spectrom.* **2004**, *18*, 49-58.

(27) Holcapek, M.; Volna, K.; Jandera, P.; Kolarova, L.; Lemr, K.; Exner, M.; Cirkva, A. *J. Mass Spectrom.* **2004**, *39*, 43-50.

(28) Barnes, K. A.; Fussell, R. J.; Startin, J. R.; Thorpe, S. A.; Reynolds, S. L. *Rapid Commun. Mass Spectrom.* **1995**, *9*, 1441-1445.

(29) Matuszewski, B. K.; Constanzer, M. L.; Chavez-Eng, C. M. *Anal. Chem.* **1998**, *70*, 882-889.

(30) Matuszewski, B. K.; Constanzer, M. L.; Chavez-Eng, C. M. *Anal. Chem.* **2003**, *75*, 3019-3030.

(31) Stuber, M.; Reemtsma, T. *Anal. Bioanal. Chem.* **2004**, *378*, 910-916.

(32) Clinton, R.; Creaser, C. S.; Bryant, D. *Anal. Chim. Acta* **2005**, *539*, 133-140.

Chapter 2. Quantitative Real-time Monitoring of Chemical Reactions by Auto-sampling Flow Injection Analysis coupled with Atmospheric Pressure Chemical Ionization Mass Spectrometry

A version of this chapter was originally published by Zhu, Z. Q.; Bartmess, J. E.; McNally, M. E.; Hoffman, R. M.; Cook, K. D.; Song, L. G.:

Zhu, Z. Q.; Bartmess, J. E.; McNally, M. E.; Hoffman, R. M.; Cook, K. D.; Song, L. G. *Anal. Chem.* **2012**, *84*. 7547-7554.

Abstract

Although qualitative and/or semi-quantitative real-time monitoring of chemical reactions have been reported with a few mass spectrometric approaches, to our knowledge, no quantitative mass spectrometric approach has been reported so far to have a calibration valid up to molar concentrations as required by process control. This is mostly due to the absence of a practical solution that could well address the sample overloading issue. In this study, a novel auto-sampling flow injection analysis coupled with atmospheric pressure chemical ionization mass spectrometry (FIA/APCI-MS) system, consisting of a 1 μL automatic internal sample injector, a post-injection splitter with 1:10 splitting ratio, and a detached APCI source connected to the mass spectrometer using a 4.5-inch long 0.042-inch inner diameter (I.D.) stainless-steel capillary, was thus introduced. Using this system together with an optional FIA solvent modifier, e.g. 0.05% (v/v) isopropylamine, a linear quantitative calibration up to molar concentration has been achieved with 3.4-7.2% relative standard deviations (RSDs) for 4 replicates. As a result, quantitative real-time monitoring of a model reaction was successfully performed at the 1.63 M level. It is expected that this novel auto-sampling FIA/APCI-MS system can be

used in quantitative real-time monitoring of a wide range of reactions under diverse reaction conditions.

2.1 Introduction

Monitoring of chemical/biochemical reactions has always been a significant subject in industries, not only because of the concerns of safety operations, but also due to the interests in improving production efficiency.[1] Real-time monitoring of chemical/biochemical reactions is particularly attractive because it can provide valuable timely chemical information and thus allows faster response to the monitored reaction, more accurate control of the end-point of the reaction, and better understanding of the reaction process. Mass spectrometry is an excellent analytical technique for real-time monitoring of chemical/biochemical reactions by offering fast response, high sensitivity and the capability of measuring multiple components simultaneously. [2,3]

Real-time monitoring of chemical/biochemical reactions by mass spectrometry has been the topic of many publications, once atmospheric pressure ionization (API), including electrospray ionization (ESI) and atmospheric pressure chemical ionization (APCI), gained popularity in the late 1980s.[4-16] However, the most frequently used approach in these publications, i.e. direct infusion/withdrawal of the reaction mixture coupled with API-MS, is not suited to monitor process-scale chemical/biochemical reactions due to sample overloading caused by molar concentrations of reaction mixtures. In 1999, Dell'Orco *et al*[15] reported real-time monitoring of process-scale reactions using a similar approach, except that the concentrations of the reaction mixtures were reduced

by approximately 3000-fold with the assistance of four HPLC pumps for 30 times dilution and a flow splitter for 1:100 splitting ratio. Although the ion current of the major observed species as a function of time was recorded, quantitation of these species remained problematic as calibrations were not performed and quantitation could only be possible on the assumption that the ionization efficiency for each species was identical.[10]

Real-time monitoring of chemical/biochemical reactions by mass spectrometry has also been reported using membrane inlet mass spectrometry (MIMS), where volatile or semi-volatile compounds are extracted selectively from a liquid stream, transported across the membrane, desorbed into a helium stream and detected by mass spectrometry.[17-19] However, this technique is limited to compounds with appreciable volatility and favorable permiselectivity. In 2005, Clinton *et al*[20] introduced a hybrid technique of MIMS and flow injection analysis atmospheric pressure chemical ionization mass spectrometry (FIA/APCI-MS) for real-time monitoring of a process-scale reaction, taking advantage of a liquid-liquid membrane interface with a high dilution factor of approximately five orders magnitude. However, the observed ion responses were very susceptible to the small changes in operational pressures and flow rates on both sides of the membrane. In addition, the sampling technique used by FIA was manual and the effectiveness of the membrane to dilute the reaction mixture was also highly compound dependent.

A few recently introduced ambient ionization techniques including desorption electrospray ionization (DESI)[21], low-temperature plasma (LTP)[22], extracted electrospray

ionization (EESI)[23,24], direct analysis in real time (DART)[25,26], probe ESI[27], electrospray-assisted laser desorption/ionization (ELDI)[28], easy ambient sonic-spray ionization (EASI)[29,30] and ultrasonic-assisted spray ionization (UASI)[31] have also been used in real-time monitoring of chemical/biochemical reactions; and LTP, EESI, and DART were demonstrated to be able to analyze reaction mixtures at molar concentrations.

Zhang and coworkers[22] reported the use of a LTP probe for real-time monitoring of an acetylation, a Schiff-base formation and an esterification reaction by directly pointing the LTP probe at the surface of the reaction, where sample desorption and ionization occur almost instantly at ambient conditions. Zenobi and coworkers[23] used EESI-MS in real-time monitoring of a Michael addition reaction and an acetylation reaction, where a continuous nitrogen flow was used to carry the gas phase above the reaction mixtures in a three-neck flask toward an electrospray plum jet for ionization. However, quantitative data was not reported by either LTP-MS or EESI-MS. In addition, the surface sampling techniques used by LTP-MS and EESI-MS might not be able to generate representative data for the actual composition of the bulk reaction mixtures.

DART-MS was recently evaluated by our group for quantitative monitoring of a model slurry reaction.[25] Well-stirred sample mixtures were manually deposited on the closed-end of melting-point capillaries followed by the automatic sample introduction with a home-made DART auto-sampler. The sampling process was demonstrated to be representative for semi-quantitative analysis. However, it was concluded that quantitative

analysis using DART-MS required better reproducibility and could not be achieved without a complicated, expensive and fully automated robotic auto-sampler.

In this study, a novel auto-sampling FIA/APCI-MS system was introduced for quantitative real-time monitoring of process-scale chemical/biochemical reactions. It was based on the conventional FIA/APCI-MS system because FIA produces chromatography-like peaks and has demonstrated good performance in quantitation.[32] In order to address the sample overloading issue, a few modifications with minimum involvement of compound-dependent elements were incorporated. Their quantitative ability was examined and the optimum system was further evaluated in quantitative real-time reaction monitoring of a model reaction in molar-concentration level.

2.2 Experimental

2.2.1 Reagents

Ethanol (190 proof) was purchased from Fisher Scientific (Pittsburgh, PA). Phenethylamine (PEA), acrylonitrile, ethylamine (EA) and tert-butylamine (TBA) were purchased from Sigma-Aldrich (St. Louis, MO). Isopropylamine (IPA) was purchased from Eastman Chemical Company (Kingsport, TN). Isobutyrophenone was purchased from Matheson Coleman & Bell (Norwood, OH). 3-(phenethylamino)propanenitrile (PEAP) was synthesized in our lab.[33]

2.2.2 Instrumentation

An auto-sampling FIA/APCI-MS system (Figure 2.1A), majorly containing an auto-sampling FIA and a detached APCI-MS setup, was developed for quantitative real-time monitoring of process-scale reactions.

The auto-sampling FIA setup. The auto-sampling FIA setup was based on a traditional FIA setup which consists of a syringe pump (Harvard Apparatus, Holliston, MA), an HPLC pump (Agilent, Santa Clara, CA) and a six-port manual injection valve (Rheodyne, Rohnert Park, CA) with a 10 μL sample loop. Automatic 1 μL sampling functionality was incorporated by using an automatic internal sample injector (Valco, Huston, TX) to replace the manual injection valve. The sampling volume was further reduced by incorporating a splitter (Upchurch Scientific, Oak Harbor, WA) for post-injection flow splitting.

As demonstrated in Figure 2.1B, the automatic internal sample injector had four ports, i.e. ion source (I), pump (P), sample (S), waste (W), and three internal passages (slot 1, 2 and 3). The positions of the four ports were fixed, while the three passages were engraved on the valve rotor. The movement of the valve rotor is controlled by a computer with in-house software.

Two separate streams flowed through the sample injector independently. FIA solvent flowed into port P and out of port I continuously, driven by the Agilent HPLC pump at 1 mL/min. Samples confined in a gas-tight syringe (Hamilton Company, Reno, NV) flowed into port S and out of port W continuously, driven by the Harvard Apparatus

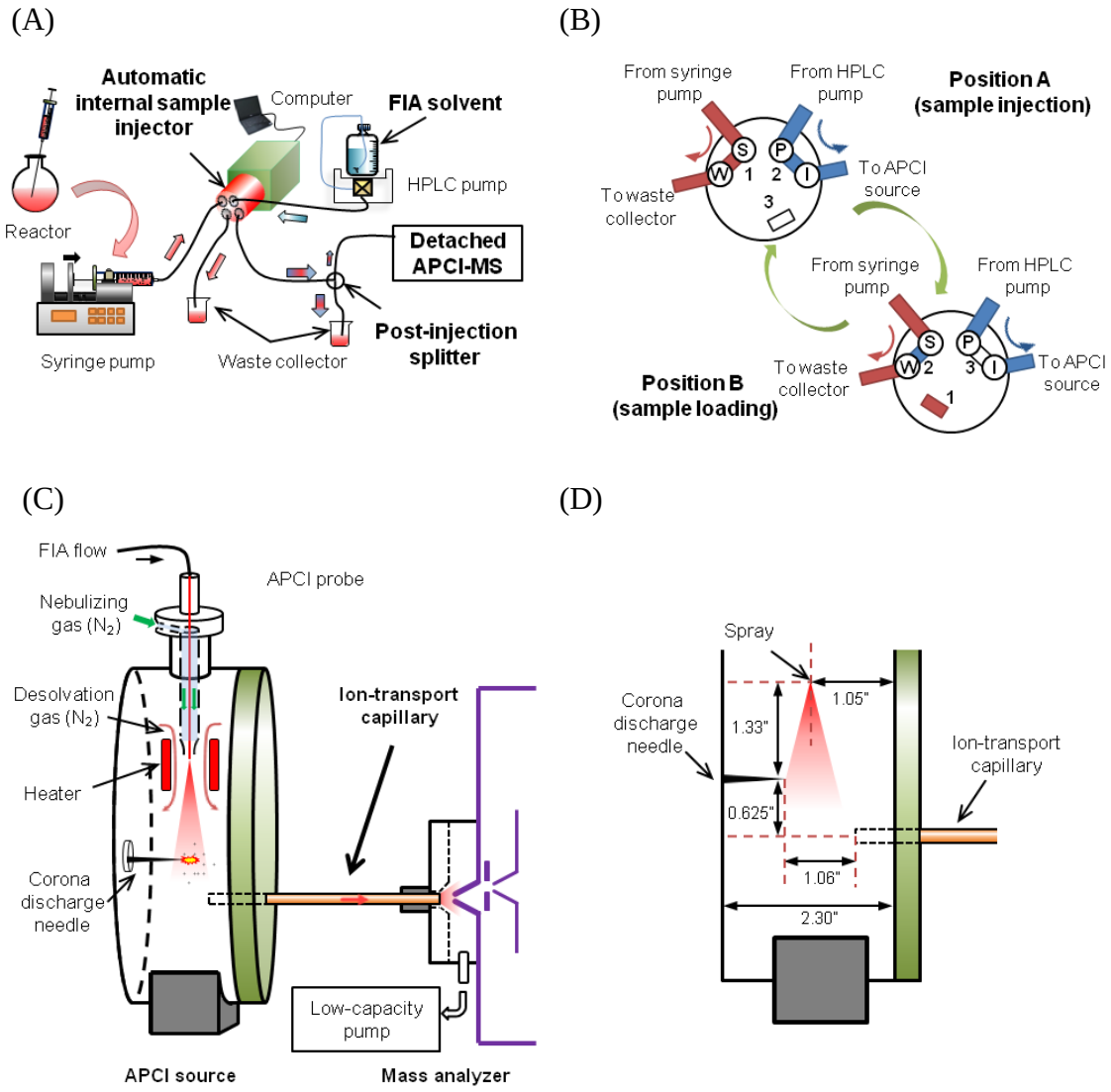

Figure 2.1 (A) Diagram of the auto-sampling FIA/APCI-MS system; (B) diagram of the automatic internal sample injector; (C) diagram of the detached APCI-MS setup; and (D) Diagram of the relative position of the ion-transport capillary, the corona discharge needle and the APCI probe.

syringe pump at 30 μL/min.

The auto-sampling was achieved by switching the automatic internal sample injector between position A and B. In position A, the FIA solvent stream flowed through slot 1 and sample stream flowed through slot 2, while slot 3 was not accessible. After the valve rotor was rotated counter-clock-wise to position B within 145 msec, sample trapped in slot 2 was injected into the FIA solvent stream. Meanwhile, slot 3 was connecting port S and W to maintain the continuous sample stream, while slot 1 was not accessible. Once the sample injection was completed, the injector returned to position A, preparing for the next injection cycle. The injection volume was determined by the volume of slot 2, which was 1 μL in this study though 0.5 μL could also be achieved with satisfactory quantitation using a different valve rotor.

The splitter consisted of one adjustable thumbscrew and three ports, i.e. one inlet and two outlet ports. The inlet port connected to the port I of the internal sample injector as mentioned above. The split stream flowed toward the APCI source in the downstream, while the waste stream flowed to a 600 mL waste-collection beaker. The split stream could be partially blocked by the thumbscrew while the waste stream port was designed to be completely open all the time. The splitting ratio was controlled by adjusting the position of thumbscrew. The more the split stream was blocked, the larger the split ratio would be.

The detached APCI-MS setup. The detached APCI-MS setup was based on a traditional APCI-MS setup used by an AccuTOF JMS-100LC time-of-flight (TOF) mass

spectrometer (JEOL, Peabody, MA) with an APCI source directly attached to the mass spectrometer. As illustrated in Figure 2.1C, the attached APCI source was replaced by a Vapur interface (Ionsense, Saugus, MA), while a stainless-steel capillary (Hamilton Company, Reno, NV), referred as ion-transport capillary in this study, was used to connect the center of the Vapur interface and the APCI source so that ions generated inside the detached APCI source were guided into the mass spectrometer. The position of the end of the ion-transport capillary inside the APCI source was optimized and illustrated in Figure 2.1D. The distance between the capillary exit and orifice of the analyzer is calculated to be 0.87-inch (22.1 mm). The optimization of the I.D. and the length of the ion-transport capillary were described in the Results and Discussion section. A VacTorr 20 vacuum pump (Gca/Precision Scientific, Chicago, IL) was used on the Vapur interface[34] to create pressure differential along the ion-transport capillary. The pressure in the intermediate region at the exit of the ion-transport capillary was measured to be 585 torr when the optimum 4.5-inch long ion-transport capillary was used.

The parameters of the APCI source were briefly optimized for 1 mL/min FIA flow rate with ethanol as solvent and set as follows: needle voltage, 4500 V; desolvation chamber temperature, 500 °C; desolvation gas flow, 4 L/min; nebulizing gas flow: 2 L/min. Nitrogen was used for both desolvation gas and nebulizing gas. The parameters of TOF mass spectrometer were briefly optimized for the detection of PEAP and set as follows: orifice 1 voltage, 20 V; orifice 2 voltage, 10 V; ring voltage, 3 V; peak voltage, 800 V. Chromatogram-like ion intensity profiles were recorded with mass range of *m/z*

100 to 500 and scan interval of 1.0 s. Integration of peaks from the extracted ion profiles (XIPs) were performed with TSSPRO 3.0 software (JEOL, Peabody, MA) .

In order to minimize exposure to vapors, the APCI ion source was put inside a wooden box which was connected to the lab exhaust pipe with good ventilation.

2.2.3 Model reaction

A Michael addition reaction of PEA and acrylonitrile (Scheme 2.1) was selected as the model reaction. At ambient temperature, PEA (20.5 mL, 0.163 mol) was mixed with ethanol (68.7 mL) in a 250 round-bottom flask. Acrylonitrile (10.8 mL, 0.163 mol) was then added into the mixture.

In order to test the upper limit of quantitative calibrations of different setups, standard solutions of PEAP with 0.0128, 0.0258, 0.0515, 0.103, 0.206, 0.413, 0.825, and 1.65 M concentrations were prepared in ethanol. In addition, standard solutions of PEA with 0.0825, 0.165, 0.33 0.825, 1.32, 1.65, 3.3, 6.6, 13.2, 20.6, 41.3 and 82.5 mM concentrations were also prepared in ethanol and used in some tests. In order to create a calibration curve for quantitative real-time monitoring of the model reaction using the optimum FIA/APCI-MS system, standard mixture solutions of PEA and PEAP with respective concentrations of 1.65, 0; 1.485, 0.165; 1.32, 0.33; 0.99, 0.66; 0.66, 0.99; 0.33, 1.32; and 0, 1.65 M were prepared to simulate the model reaction, representing 0, 10, 20, 40, 60, 80 and 100% reaction progress. All the standard solutions were analyzed in four replicates for quantitative calibration.

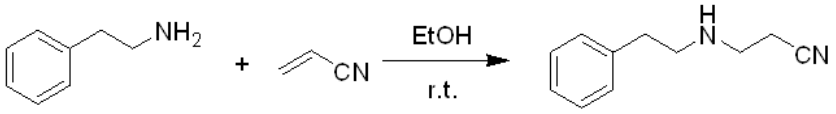

Phenetylamine (PEA) MW 121 | Acrylonitrile | 3-(phenethylamino)propanenitrile (PEAP) MW 174

Scheme 2.1 The model reaction: Michael-addition reaction of phenethylamine and acrylonitrile.

2.2.4 Quantitative real-time reaction monitoring

The two reactants were thoroughly mixed for one minute before 10 mL mixture was withdrawn into a 10 mL syringe (Hamilton Company, Reno, NV). Two minutes were then allowed to place the syringe in the syringe pump for infusion at 30 μL/min and prepare the automatic internal sample injector for the auto-sampling. Another two minutes were allowed for the infusion to form a continuous sample stream before the first injection was made. Sampling started at 5 min after the reaction was initiated and the sampling interval was 5 min. The reaction was monitored for 4 hours with total 47 samples being analyzed. The average response time between the injection of the reaction mixture by the automatic internal sample injector and the observation of a mass spectrometric response was approximately 45 s. However, since the reaction was quenched by IPA in the FIA solvent when the reaction mixture was injected, the mass spectrometric response reflected the molar concentration of the reaction mixture in real time.

2.3 Results and Discussion

2.3.1 Development of the auto-sampling FIA/APCI-MS system

The feasibility of the conventional FIA/APCI-MS system, consisting of the Harvard Apparatus syringe pump, the Agilent HPLC pump, the Rheodyne manual six-port injecting valve with a 10 μL sample loop, and the JEOL AccuTOF mass spectrometer with an attached APCI source was first tested for quantitation of the

reactant of the model reaction, i.e. PEA. In the obtained mass spectra, protonated molecular ion $[M + H]^+$ at *m/z* 122 was observed along with its in-source fragment ion $[M + H - NH_3]^+$ at *m/z* 105. Peak areas of the *m/z* 122 XIPs were plotted against PEA concentrations (detailed data not shown). The upper-limit of the quantitative linearity was 1.65 mM and the relative standard deviations (RSDs) varied from 9.7 to 19.2%. When the concentration of PEA was higher than the upper-limit of the quantitative linearity, non-linear behavior was observed, which should be a result of sample overloading. Since process-scale reactions typically are in molar concentrations, e.g. 1.63 M in the model reaction of this study, a series of modifications on this conventional FIA/APCI-MS system was performed to improve the upper limit of the quantitative linearity.

Incorporation of an automatic internal sample injector. The selection of the automatic internal sample injector was mainly due to the requirement of automatically rapid sampling by real-time monitoring of chemical reactions. In addition, the minimum sample volume of the internal sample injector can be decreased to 0.5 μL with extremely low dead volume, resulting in good sampling reproducibility. The performance of the FIA/APCI-MS using a 1 μL automatic internal sample injector was evaluated by analyzing PEAP from 0.0128 to 0.0515 M. In the obtained mass spectra, protonated molecular ion $[M + H]^+$ at *m/z* 175 was observed along with its in-source fragment ion $[M + H - C_3H_3N]^+$ at *m/z* 122 and $[M + H - C_3H_6N_2]^+$ at *m/z* 105. Peak areas of the *m/z* 175 XIPs were plotted against PEAP concentrations and shown in Figure 2.2 as Plot A.

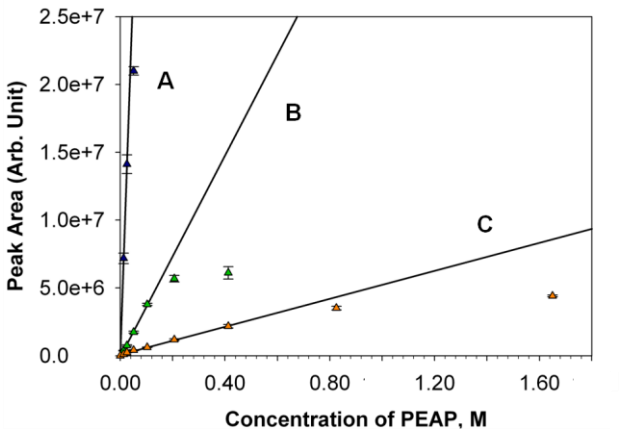

Figure 2.2 Effect of the post-injection splitting on the upper-limit of quantitative calibration. (A) Splitting ratio, 0; upper-limit of linearity, 0.0258 M; (B) splitting ratio, 1:10; upper-limit of linearity, 0.103 M; and (C) splitting ratio, 1:100; upper limit of linearity, 0.413 M. Each point represents four replicated analyses. The R^2 of linear regression A, B and C are 0.9999, 0.9973 and 0.9958, respectively. A 1 µL automatic internal sample injector was incorporated into the FIA/APCI-MS system for these experiments.

The upper-limit of linearity was observed to be 0.0258 M, with RSDs varying from 1.5 to 5.3%. Deviation from linearity was observed when 0.0515 M PEAP was injected. Therefore, the automatic internal sample injector was able to appreciably improve the upper-limit of quantitative linearity approximately 30 times over the traditional FIA/APCI-MS system. In addition, it also provided much better reproducibility.

Incorporation of a post-injection splitter. Post-injection flow splitting can be effective in reducing the sample loading amount into the APCI-MS system, but the reproducibility of the splitting ratio should be well controlled so that the RSDs of the quantitation is maintained. The performances of the FIA/APCI-MS system using a commercial flow splitter from Upchurch Scientific were evaluated with splitting ratios of 1:10 and 1:100 by analyzing PEAP from 0.0128 to 0.825 M; and the relationships between peak areas of the *m/z* 175 XIPs and PEAP concentrations were displayed in plot B and plot C of Figure 2.2, respectively. It can be seen that slopes of plot B and C were smaller than plot A by respective one and three orders of magnitude. The upper-limits of linearity were observed to be 0.103 M and 0.413 M for 1:10 and 1:100 splitting ratio, respectively.

Although the use of 1:10 splitting ratio obtained lower upper-limit of quantitative linearity, it resulted in better overall reproducibility than the use of 1:100 splitting ratio, i.e. 2.1-7.2 versus 3.2-16.1% RSDs. It may be that higher splitting ratio is more sensitive to the local-turbulence caused by the change of flow-path geometry. The use of 1:10 splitting ratio also resulted in a much shorter response time than the use of 1:100 splitting

ratio, i.e. 10 s versus 130 s, due to 10 times higher flow rate. Furthermore, less backpressure and less waste were generated. Therefore, the splitter with 1:10 splitting ratio was selected and incorporated in the setup for real-time quantitation of process-scale reactions; and the upper-limit of quantitative calibration was improved 4 times.

Incorporation of an ion-transport capillary. While reducing the sample loading amount into the APCI source was effective in addressing the sample overloading issue, the ion-transport efficiency, i.e. the fraction of ions that eventually entered the mass spectrometer over the total ions generated in the ion source, could also be manipulated to address the sample overloading issue. This can be achieved by distancing the APCI source from the mass spectrometer and narrowing the ion path between the APCI source and the mass spectrometer. In this study, we incorporated a Vapur interface from JEOL into APCI-MS for this purpose. The Vapur interface was originally designed for direct analysis in real time mass spectrometry (DART-MS) to enhance the ion-transport efficiency by creating an extra pumping chamber between the ions and the inlet of the mass spectrometer.[34] It used a 9-inch long 0.19-inch (4.75 mm) inner diameter (I.D.) ceramic capillary to achieve better ion-transport efficiency. In this study, narrower ion-transport capillaries were used to reduce the ion-transport efficiency. It is noted that the gas flow of the DART-MS was parallel to the ion path, but the gas flow of the APCI-MS was orthogonal to the ion path, This could be another reason why the ion-transport capillary were functioning differently between them, i.e. enhancing versus reducing ion-transport efficiency.

The FIA/APCI-MS system, incorporated with an ion-transport capillary, but without a splitter, was evaluated in the quantitation of PEAP. Stainless-steel capillary with 0.013-inch (0.31 mm) and 0.042-inch (1.07 mm) I.D.s were tested and the use of 0.013-inch I.D. was eventually abandoned due to weak ion intensities. Different length of 0.042-inch I.D. stainless-steel capillary, i.e. 2.5, 4.5, 6 and 8-inch, were further examined. Generally, the *m/z* 175 ion intensities were decreasing as the length of ion-transport capillary increased, except that the 6-inch generated slightly higher ion intensities than the 4.5-inch ion-transport capillary. It appeared to us that the flow conditions inside the ion-transport capillary were much more complicated than it was expected, but further research to interpret the experimental data were not performed. The highest upper-limit of quantitative linearity, i.e. 0.103 M, was achieved by using both 4.5 and 6-inch ion-transport capillaries with RSDs less than 4.1%.

The FIA/APCI-MS system, incorporated with either the 6-inch or the 4.5-inch ion-transport capillary together with the splitter with 1:10 splitting ratio, was further evaluated in the quantitation of PEAP. As shown in Figure 2.3, in comparison with the results obtained using the splitter with 1:10 splitting ratio only (Plot A), the use of additional either 6 (Plot B) or 4.5-inch ion-transport capillary (Plot C) showed respective 30 and 100-folds smaller slopes. Slightly higher ion intensities were still obtained by using the 6 than the 4.5-inch ion-transport capillary, which was consistent with the results described above. However, higher upper-limit of quantitative linearity was achieved by the 4.5 than the 6-inch ion-transport capillary, i.e. 0.825 versus 0.413 M. In addition,

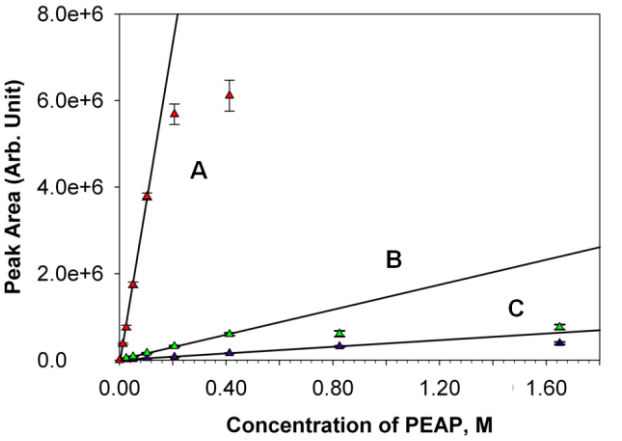

Figure 2.3 Effect of the length of the 0.042-inch I.D. ion-transport capillary on the upper-limit of quantitative calibration. (A) Ion-transport capillary, 0 inch; upper-limit of linearity, 0.103 M; (B) ion-transport capillary, 6 inch; upper-limit of linearity, 0.413 M; and (C) ion-transport capillary, 4.5 inch; upper-limit of linearity, 0.825 M. Each point represents four replicated analyses. The R^2 of linear regression A, B and C are 0.9973, 0.9984 and 0.9987, respectively. A 1 μL automatic internal sample injector and a 1:10 post-injection splitter were incorporated into the FIA/APCI-MS system for these experiments.

better reproducibility was also obtained by using the 4.5 than the 6-inch ion-transport capillary, i.e. 2.8-7.6 versus 3.8-10.6% RSDs. Therefore, the 4.5-inch capillary was eventually selected for the automatic FIA/APCI-MS system in quantitative real-time monitoring of process-scale reactions and the upper limit of quantitative linearity was improved 8 times.

Incorporation of an optional FIA solvent modifier. With the incorporation of a 1 μL automatic internal sample injector, a 1:10 post-injection flow splitter and a 4.5-inch long 0.042-inch I.D. ion-transport capillary, the upper-limit of quantitative calibration of the traditional FIA/APCI-MS system has been improved from 1.65 to 825 mM. However, as the PEAP concentration increased from 0.0258, 0.0515, 0.103, 0.206, 0.413, 0.825 to 1.65 M, its peaks tailed more and more. Consequently, the sampling interval was increased from 1.0, 1.2, 1.5, 2.4, 3.5, 5.5 to 8.0 min. It was believed that the peak tailing of PEAP was caused by its adsorption onto the inner surface of the FIA/APCI-MS system; and its polar functional group, i.e. –NH–, was responsible. This was confirmed by the analysis of a less polar compound, i.e. isobutyrophenone, at 1.65 M in ethanol under identical conditions. In the mass spectra of isobutyrophenone, protonated molecular ion $[M + H]^+$ at *m/z* 149 was observed along with its protonated dimer ion $[2M + H]^+$ at *m/z* 297. As shown in Figure 2.4, while the peak of the *m/z* 175 XIP from PEAP tailed and expanded about 8 min, the peaks of the *m/z* 149 XIP from isobuyrophenone had Gaussian-like profile and only covered approximately half minute. In order to reduce the peak tailing of PEAP, three small amines, i.e. EA, IPA and TBA, were selected as

(A)

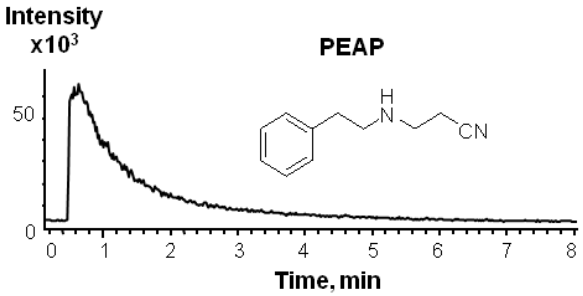

(B)

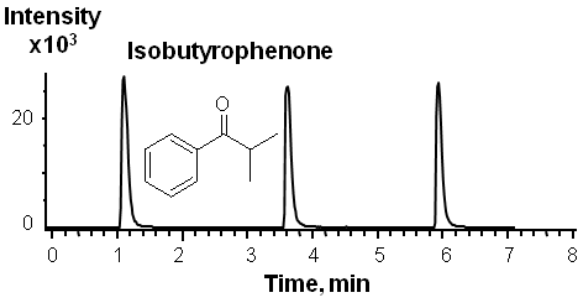

Figure 2.4 Effect of the polarity of the analytes on the sampling interval of quantitative real-rime reaction monitoring. (A) XIP of 1.65 M PEAP at *m/z* 175; (B) XIP of 1.65 M isobutyrophenone at *m/z* 149. A 1 µL automatic internal sample injector, a 1:10 post-injection splitter and a 4.5-inch long 0.042-inch I.D. ion-transport capillary were incorporated into the FIA/APCI-MS system for these experiments.

FIA solvent modifiers. It was believed that they could effectively compete with PEAP in the adsorption process on the inner surface of the FIA/APCI-MS system because their proton affinities (PA), i.e. 912.0, 923.8, and 934.1 kJ/mol, respectively, were close to PEAP (the PA of PEA was 936.2 kJ/mol).[35] In addition, they could also effectively compete with PEAP in the ionization/protonation process, therefore addressing the sample overloading issue through ion suppression.

The incorporation of 0.05% (v/v) EA, IPA and TBA into the FIA solvent, i.e. ethanol, resulted in trace amount of adduct ions of PEAP and the FIA solvent modifier, i.e. $[PEAP + H + EA]^+$ at *m/z* 220, $[PEAP + H + IPA]^+$ at *m/z* 234 or $[PEAP + H + TBA]^+$ at *m/z* 248, and decreased *m/z* 175 ion intensities, which was more obvious as the PA of the FIA solvent modifier increased. Peaks of *m/z* 175 XIPs covered 6.5, 5.0 and 5.0 min for 1.65 M PEAP when EA, IPA or TBA was used, respectively. Figure 2.5 shows the peak areas of *m/z* 175 XIPs against PEAP concentrations plots. The slopes of plot B from IPA and C from TBA were 8 and 12-fold smaller than that of plot A from EA, respectively. The upper-limits of linearity using 0.05% (v/v) EA, IPA and TBA as the FIA solvent modifier were 0.825, 1.65 and 1.65 M, respectively. IPA was eventually chosen over TBA due to better RSDs, i.e. 1.2-5.5 versus 2.8-8.1%. TBA might suppress the ionization of PEAP too much and therefore lead to worse reproducibility. The incorporation of 0.2% (v/v) IPA as FIA solvent modifier was also tested. It was not preferred due to worse RSDs, i.e. 2.4-8.6%. Again, it might suppress the ionization of PEAP too much.

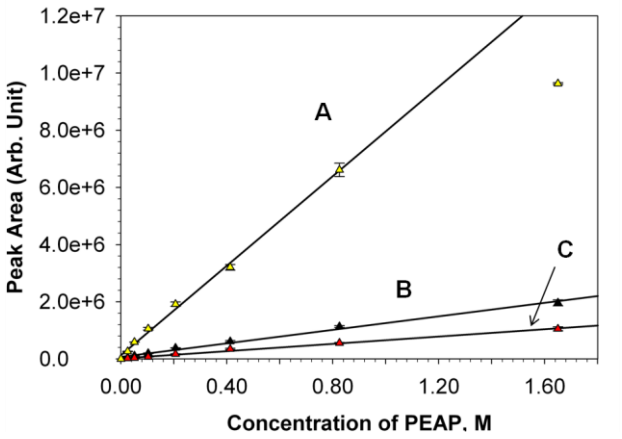

Figure 2.5 Effect of the FIA solvent modifier on the upper-limit of quantitative calibration. (A) FIA solvent modifier, 0.05% (v/v) EA; upper-limit of linearity, 0.825 M; (B) FIA solvent modifier, 0.05% (v/v) IPA; upper-limit of linearity, 1.65 M; (C) FIA solvent modifier, 0.05% (v/v) TBA; upper-limit of linearity, 1.65 M. Each point represents four replicated analyses. The R^2 of linear regression A, B and C are 0.9972, 0.9927 and 0.9932, respectively. A 1 µL automatic internal sample injector, a 1:10 post-injection splitter and a 4.5-inch long 0.042-inch I.D. ion-transport capillary were incorporated into the FIA/APCI-MS system for these experiments.

2.3.2 Quantitative real-time monitoring of the model reaction

Quantitative calibration. In order to quantitatively monitor a reaction, matrix effects on the mass spectrometric response of the component(s) to be quantitated should be considered. In this study, this was accomplished first by simulating the reaction progress using standard reagents of one reactant and the product, i.e. PEA and PEAP. The simulation omitted the other reactive reactant, i.e. acrylonitrile, due to its reactivity. At 1.65 M level, simulated reaction mixtures containing PEA and PEAP in ethanol were prepared to represent the progress of the model reaction at 0, 10, 20, 40, 60, 80 and 100%. Each simulated reaction mixture was analyzed by the optimized FIA/APCI-MS system, consisting of a 1 μL automatic internal sample injector, a 1:10 post-injection flow splitter, a 4.5-inch long 0.042-inch I.D. ion-transport capillary and 0.05% (v/v) IPA in the FIA solvent, under optimum mass spectrometric parameters with four replicates. Quantitative calibration of PEAP showed good linearity and reproducibility with 0.9948 R^2 and 3.4-7.2% RSDs. The linear regression equation was y = 1124835x + 113820, where y and x was the peak area and molar cocnetration, respectively. Quantitative calibration of PEA had 0.9901 R^2, 4.8 to 13.7% RSDs and y = 287986x + 214966 linear regression equation. It is noted that the mass spectrometric parameters were optimized for the *m/z* 175 ion from PEAP rather than the *m/z* 122 ion from PEA. In addition, the *m/z* 122 ion was from both the ionization of PEA and the fragmentation of the *m/z* 175 ion from PEAP. Therefore, the quantitative calibration of PEA was not as good as that of PEAP.

The matrix effect of PEA on the quantitation of PEAP was further investigated. Standard samples containing only PEAP and simulated reaction mixtures containing PEA and PEAP were prepared to represent the progress of the model reaction at 10, 40 and 80% of a 1.65 M level reaction. At each concentration, the simulated reaction mixtures were analyzed next to the standard PEAP samples for side-by-side comparison. As summarized in Table 2.1, the relative errors of peak areas of *m/z* 175 XIPs between the simulated reaction mixtures and the PEAP samples were comparable to the RSDs of the quantitative calibration as described above. Namely, the matrix effect of quantitative real-time reaction monitoring of the mode reaction was insignificant and the calibration curve could be simply obtained by analyzing standard PEAP samples.

Quantitative real-time monitoring. Figure 2.6A shows mass spectra of *m/z* 110 to 180 at 10, 40 and 120 min reaction time. The relative intensity ratio of the *m/z* 175 to 122 ion increased from 3.8 at 10 min, 16.0 at 40 min to 27.6 at 120 min, indicating the progression of the reaction. The intensity of the *m/z* 122 ion was low at the beginning of the reaction because the mass spectrometric parameters were optimized to detect *m/z* 175 ion. The possible by-product CPEAP as a double adduct, which could show up at *m/z* 228, was not observed (data not shown). This was in agreement with the results in a previous work when one equivalent of acrylonitrile was also used,[36] while the presence of double adduct was reported by a couple of other publications, when more than two equivalent of acrylonitrile was used [20,23]. Figure 2.6B shows the concentration change of PEA and PEAP during the reaction. The reaction proceeded rapidly in the first hour,

Table 2.1 Matrix effects of PEA on the quantitation of PEAP.

Simulated progress	**Standard containing only PEAP**			**Simulated sample containing PEA and PEAP**				**Deviation of averaged PEAP peak area**
	Conc. of PEAP	Averaged PEAP peak area	RSD	Conc. of PEAP	Conc. of PEA	Averaged PEAP peak area	RSD	
10%	0.165M	196775	4.9%	0.165M	1.49M	213778	3.3%	8.6%
40%	0.660M	769571	3.4%	0.660M	0.990M	763190	4.1%	0.82%
80%	1.32M	1443347	4.4%	1.32M	0.33M	1409969	3.2%	2.3%

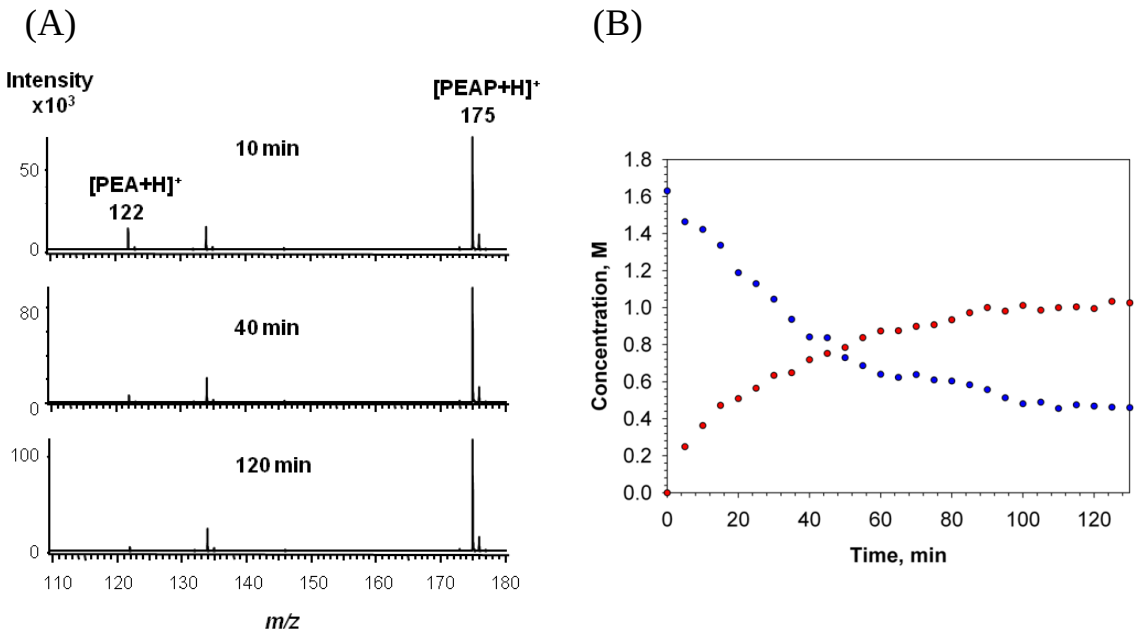

Figure 2.6 Results of quantitative real-time monitoring of the model Michael-addition reaction of PEA and acrylonitrile. (A) Mass spectra of the reaction mixture at 10, 40 and 120 min reaction time; (B) Real-time molar concentration changes of PEA and PEAP. The reaction mixture was sampled and analyzed every 5 min.

especially in the first 20 min. After 125 min, the reaction reached its end-point, which was in agreement with previous publications.[20,23] A conversion ratio of 66.1% was quantitated.

2.4 Conclusion

A novel auto-sampling FIA/APCI-MS system was developed based on a conventional FIA/APCI-MS system to address the sample overloading issue encountered in quantitative real-time monitoring of process-scale reactions. The system incorporated a 1 μL automatic internal sample injector, a post-injection splitter with 1:10 splitting ratio, and a detached APCI source connected to the mass spectrometer using a 4.5-inch long 0.042-inch I.D. ion-transport capillary, to extend the upper-limit of quantitative calibration approximately 30, 4 and 8 times without sacrificing the quantitative reproducibility. Consequently, quantitative linearity up to molar concentration has been achieved. Furthermore, the performance of the injector, the splitter and the ion-transport capillary were compound-independent, which should allow a wide range of reactions to be quantitatively monitoring in real time.

It is noted that quantitative real-time monitoring of reactions with high polarity products may require a FIA solvent modifier, e.g. 0.05% (v/v) IPA for the model Michael addition reaction of PEA and acrylonitrile, to alleviate the adsorption of high polarity compounds to the inner surface of the auto-sampling FIA/APCI-MS system. However, the sampling interval should be within 5 min, as demonstrated in this study for the model reaction. The sampling interval in quantitative real-time monitoring of reactions with low

polarity components, e.g. isobutyrophenone, should be as short as half minute without any FIA solvent modifier.

The automatic internal sample injector used in the system should also allow the use of more sophisticated sampling devices than an infusion syringe pump as used in this study. For instance, a withdraw syringe pump can be used to drive the sample stream directly from a traditional reactor vessel, where reactions can proceed under complicated conditions, e.g. air-tight, reflux, drop-wise adding, etc. Consequently, the auto-sampling FIA/APCI-MS system can be used for the quantitative real-time monitoring of a variety of reaction types.

The matrix effects of the reactant(s) on the mass spectrometric response of the product by the auto-sampling FIA/APCI-MS system during reaction monitoring may be negligible, possibly because APCI was not severely subject to ion suppression and/or the product of the reaction had higher PA than the reactants. Although it is appealing to generate a calibration curve using the product alone, i.e. without simulating the reaction using both the reactants and products, precaution should be taken dealing with specific reactions.

References

(1) Ponton, J. W. *Chem. Ind. (London)* **1993**, *9*. 315-318.

(2) Walsh, M. R.; LaPack, M. A. *ISA Trans.* **1995**, *34*. 67-85.

(3) Cook, K. D.; Bennett, K. H.; Haddix, M. L. *Ind. Eng. Chem. Res.* **1999**, *38*. 1192-1204.

(4) Lee, E. D.; Mueck, W.; Henion, J. D.; Covey, T. R. *J. Am. Chem. Soc.* **1989**, *111*. 4600-4604.

(5) Fabris, D. *Mass Spectrom. Rev.* **2005**, *24*. 30-54.

(6) Colgan, S. T.; Sharp, T. R.; Hammen, P. D.; Reed, R. H.; Horna, G. J.; Gwiazda, P. W. *Talanta* **1996**, *43*. 851-857.

(7) Hathout, Y.; Fabris, D.; Han, M. S.; Sowder, R. C., 2nd; Henderson, L. E.; Fenselau, C. *Drug Metab. Dispos.* **1996**, *24*. 1395-400.

(8) Arakawa, R.; Lu, J.; Mizuno, K.; Inoue, H.; Doe, H.; Matsuo, T. *Int. J. Mass Spectrom. Ion Processes* **1997**, *160*. 371-376.

(9) Zaia, J.; Fabris, D.; Wei, D.; Karpel, R. L.; Fenselau, C. *Protein Sci.* **1998**, *7*. 2398-404.

(10) Brum, J.; Dell'Orco, P. *Rapid Commun. Mass Spectrom.* **1998**, *12*. 741-745.

(11) Fligge, T.; Kast, J.; Bruns, K.; Przybylski, M. *J. Am. Soc. Mass Spectrom.* **1999**, *10*. 112-118.

(12) Kobayashi, N.; Fujimori, I.; Watanabe, M.; Ikeda, T. *Anal. Biochem.* **2000**, *287*. 272-278.

(13) Hogenboom, A. C.; de Boer, A. R.; Derks, R. J. E.; Irth, H. *Anal. Chem.* **2001**, *73*. 3816-3823.

(14) Dennhart, N.; Weigang, L. M. M.; Fujiwara, M.; Fukamizo, T.; Skriver, K.; Letzel, T. *J. Biotechnol.* **2009**, *143*. 274-283.

(15) Dell'Orco, P.; Brum, J.; Matsuoka, R.; Badlani, M.; Muske, K. *Anal. Chem.* **1999**, *71*. 5165-5170.

(16) Brum, J.; Dell'Orco, P.; Lapka, S.; Muske, K.; Sisko, J. *Rapid Commun. Mass Spectrom.* **2001**, *15*. 1548-1553.

(17) Kotiaho, T.; Lister, A. K.; Hayward, M. J.; Cooks, R. G. *Talanta* **1991**, *38*. 195-200.

(18) Hirabayashi, A.; Sakairi, M.; Koizumi, H. *Anal. Chem.* **1994**, *66*. 4557-4559.

(19) Johnson, R. C.; Cooks, R. G.; Allen, T. M.; Cisper, M. E.; Hemberger, P. H. *Mass Spectrom. Rev.* **2000**, *19*. 1-37.

(20) Clinton, R.; Creaser, C. S.; Bryant, D. *Anal. Chim. Acta* **2005**, *539*. 133-140.

(21) Li, J.; Dewald, H. D.; Chen, H. *Anal. Chem.* **2009**, *81*. 9716-9722.

(22) Ma, X.; Zhang, S.; Lin, Z.; Liu, Y.; Xing, Z.; Yang, C.; Zhang, X. *Analyst* **2009**, *134*. 1863-7.

(23) Zhu, L.; Gamez, G.; Chen, H. W.; Huang, H. X.; Chingin, K.; Zenobi, R. *Rapid Commun. Mass Spectrom.* **2008**, *22*. 2993-2998.

(24) McCullough, B. J.; Bristow, T.; O'Con nor, G.; Hopley, C. *Rapid Commun. Mass Spectrom.* **2011**, *25*. 1445-1451.

(25) Cho, D. S.; Gibson, S. C.; Bhandari, D.; McNally, M. E.; Hoffman, R. M.; Cook, K. D.; Song, L. *Rapid Commun. Mass Spectrom.* **2011**, *25*. 3575-3580.

(26) Petucci, C.; Diffendal, J.; Kaufman, D.; Mekonnen, B.; Terefenko, G.; Musselman, B. *Anal. Chem.* **2007**, *79*. 5064-5070.

(27) Yu, Z.; Chen, L. C.; Erra-Balsells, R.; Nonami, H.; Hiraoka, K. *Rapid Commun. Mass Spectrom.* **2010**, *24*. 1507-1513.

(28) Cheng, C.-Y.; Yuan, C.-H.; Cheng, S.-C.; Huang, M.-Z.; Chang, H.-C.; Cheng, T.-L.; Yeh, C.-S.; Shiea, J. *Anal. Chem.* **2008**, *80*. 7699-7705.

(29) Santos, V. G.; Regiani, T. s.; Dias, F. F. G.; Romão, W.; Jara, J. L. P.; Klitzke, C. c. F.; Coelho, F.; Eberlin, M. N. *Anal. Chem.* **2011**, *83*. 1375-1380.

(30) Nørgaard, A. W.; Vaz, B. G.; Lauritsen, F. R.; Eberlin, M. N. *Rapid Commun. Mass Spectrom.* **2010**, *24*. 3441-3446.

(31) Chen, T.-Y.; Chao, C.-S.; Mong, K.-K. T.; Chen, Y.-C. *Chem. Commun.* **2010**, *46*. 8347-8349.

(32) Calatayud, J. M., *Flow injection analysis of pharmaceuticals : automation in the laboratory*. Taylor & Francis: London ; Bristol, PA, 1996.

(33) Edwards, M. L.; Stemerick, D. M.; Bitonti, A. J.; Dumont, J. A.; McCann, P. P.; Bey, P.; Sjoerdsma, A. *J Med Chem* **1991**, *34*. 569-74.

(34) Yu, S.; Crawford, E.; Tice, J.; Musselman, B.; Wu, J.-T. *Anal. Chem.* **2009**, *81*. 193-202.

(35) Hunter, E. P.; Lias, S. G., "Pronton Affinity Evaluation", in **NIST Chemistry WebBook, NIST Standard Reference Database Number 69**, Eds. P. J. Linstrom and W. G. Mallard, National Institute of Standards and Technology: Gaithersburg MD, 20899, http://webbook.nist.gov.

(36) Ranu, B. C.; Dey, S. S.; Hajra, A. *Arkivoc* **2002**. 76-81.

Chapter 3. Quantitative Real-time Monitoring of Transesterifications by Auto-sampling FIA/APCI-MS for the Improvement of Industrial Biodiesel Production

Abstract

Auto-sampling FIA/APCI-MS, developed by us to enable quantitative real-time monitoring of chemical reactions, has been used to monitor a model transesterification reaction in real-time, which is of great interest in the biodiesel industry. Sample overloading caused by molar concentrations of targeted compounds was avoided by incorporating a 1 μL internal sample injector and a post-injection splitter with 1:15 splitting ratio. The detached APCI-MS setup, which was previously used to further address sample overloading, was found unnecessary in this study. The model transesterification reaction proceeded as a homogenous mono-phasic liquid system at an alcohol-to-oil molar ratio of 30:1 and a heterogeneous bi-phasic liquid system at an alcohol-to-oil molar ratio of 6:1; both of them were quantitatively monitored in real-time. Simultaneous quantification of the reactant, the product and the major intermediates were achieved using calibrations based on the analysis of simulated reaction mixtures of standards and validated by parallel off-line reaction monitoring with HPLC/APCI-MS. The model transesterification reaction was studied under six sets of reaction conditions. Kinetic modeling of the model transesterification reaction was then performed by following second-order kinetics. Subsequently, activation enthalpy changes of each step were estimated at the range of 7.4-10.38 kcal/mol, and negative entropy changes were obtained for both forward and reverse steps.

3.1 Introduction

Increasing price and depletion of fossil fuels along with the worldwide environmental concern about greenhouse effects are the major factors leading to the search for alternative fuels. Biodiesel is a renewable, biodegradable and nontoxic alternative to petroleum-based diesel with high flash point, excellent lubricity and low emission profiles (sulfur content, particulates, greenhouse gases, etc.).[1-2] Currently, biodiesel has not been widely commercialized due to its higher price than petroleum-based diesel, and thus is targeted towards regulated fleets and mining and marine markets in the United States, where higher priority is given to environmental and energy security concerns.

The most common method to produce biodiesel is the transesterification of vegetable oils or animal fats using a short-chain monohydric alcohol in the presence of a catalyst, e.g. NaOH, NaOMe or lipase.[3] Methanol is most frequently utilized as the short-chain monohydric alcohol because of its low cost and its physical and chemical advantages. The reaction rate and yield of a transesterification reaction are dependent on a variety of factors, including the alcohol-to-oil molar ratio, the catalyst and its concentration, the stirring type and speed, the reaction temperature and time, as well as the free fatty acids (FAs) and the water content of the vegetable oil or animal fat.[2,4] The complex dependence makes it of great interest to monitor transesterification reactions for research and development as well as commercial biodiesel production processes.

A variety of analytical techniques have been used to monitor transesterification reactions, including chromatographic methods such as gas chromatography (GC) with flame ionization or mass spectrometric detection[5-6]; liquid chromatography (LC) with UV, evaporative light scattering or mass spectrometric detection[7-8]; gel permission chromatography (GPC) with refractive index detection[9-10]; spectroscopic methods such as ^{1}H nuclear magnetic resonance (^{1}H NMR)[11-13], near infrared (NIR)[5,11,14-16], Fourier-Transform infrared (FTIR)[10,17-19], Raman[20] and laser[21] spectroscopy; and methods to measure physical properties such as refractive index[22] and viscometer[23]. An extensive review was published by Knothe[24]. Among these techniques, the spectroscopic and viscosity methods have been used to monitor transesterification reactions in real-time, while the chromatographic methods are generally used for off-line analysis as reference methods by providing detailed compositions of the reaction mixtures.

Mass spectrometry (MS) is one of the most powerful analytical tools and has been selected as an excellent detector for GC[6] and LC[7] methods during off-line monitoring of transesterification reactions. Atmospheric pressure chemical ionization (APCI) has been found as well-suited ionization approach for analyzing lipids and components involved in biodiesel production through transesterification.[7, 25] However, to our best knowledge, on-line monitoring of transesterification reactions has never been reported by MS, possibly because they are usually performed at molar concentrations which will easily cause sample overloading. Recently, APCI-MS has been coupled with auto-sampling flow injection analysis (FIA) in our lab[26] (Figure 2.1) to achieve

quantitative real-time monitoring of homogenous reactions; and a Michael-addition reaction between phenylethylamine and acrylonitrile was studied. The auto-sampling FIA/APCI-MS setup consisted of a 1 μL automatic internal sample injector, a post-injection splitter with 1:10 splitting ratio, and a detached APCI source connected to the mass spectrometer using a 4.5 in. long, 0.042 in. inner diameter (ID) stainless-steel capillary. Consequently, sample overloading caused by molar level reaction mixtures were successfully avoided without time-consuming sample pretreatment procedures.

In this study, the auto-sampling FIA/APCI-MS setup was employed with modifications in order to realize quantitative real-time monitoring of the transesterificaction of vegetable oils, which is a typical bi-phasic liquid system. A model reaction, transmethylation of glyceryl trioctanoate, was studied. Quantitative calibrations of the corresponding triglyceride (TG), diglyceride (DG), monoglyceride (MG) and fatty acid methyl ester (FAME) were created. Detailed concentration-time profiles of TG, DG, MG and FAME were obtained, which enabled kinetic study of the model transesterification reaction.

3.2 Experimental

3.2.1 Reagent

Water (H_2O, HPLC grade), methanol (MeOH, HPLC grade), certified A.C.S. grade methylene chloride, diethyl ether (anhydrous), pyridine, hexane, ethyl acetate, boric acid (powder) and solketal ((±)-2,2-dimethyl-1,3-dioxolane-4-methanol, 97%) were

purchased from Fisher Scientific (Suwanee, GA). Glycerol (Gly, >99.5%), sodium methoxide (MeONa, 33% (w/v) in MeOH), glyceryl trioctanoate (≥99%), methyl octanoate (99%), phosphoric acid (H_3PO_4, 85% (w/v) in H_2O), ammonium acetate (NH_4OAc), octanoyl chloride (99%) and trimethylborate (98%) were purchased from Sigma-Aldrich (St. Louis, MO). Glyceryl dioctanoate and glyceryl mono-octanoate were synthesized and purified in our lab. Briefly, solketal was mixed with 1.4 equivalents octanoyl chloride in methylene chloride at the presence of pyridine to give (2,2-dimethyl-1,3-dioxolan-4-yl)methyl octanoate, which was deprotected by 5 equivalents boric acid in trimethylborate. Glyceryl mono-octanoate was then obtained by recrystallization from diethyl ether.[27] Glycerol and 2.5 equivalents octanoyl chloride were mixed at the presence of pyridine in methylene chloride to produce the mixture of glyceryl dioctanoate and glyceryl mono-octanoate. Glyceryl dioctanoate was obtained after the product mixture separated by column chromatography using 1:1 hexane:ethyl acetate as the eluent.

3.2.2 The model transesterification reaction

Transmethylation of glyceryl trioctanoate was selected as the model reaction of transesterificaction of vegetable oils which were generally recognized as having three consecutive reversible esterification reactions (Scheme 3.1). Triglyceride (TG), i.e. glyceryl trioctanoate, was mixed with MeOH, which served as solvent and reactant, in a 250 mL three-neck flask, and into which a catalyst solution, i.e. MeONa dissolved in MeOH, was added. Diglyceride (DG), i.e. glyceryl dioctanoate, and monoglyceride

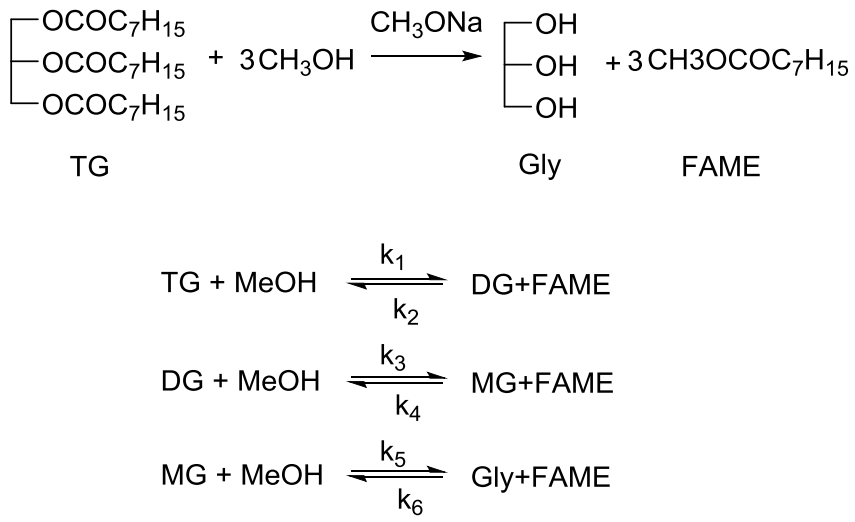

Scheme 3.1 The model transesterification reaction of vegetable oils with three reversible steps.

(MG), i.e. glyceryl mono-octanoate, were known as major intermediates. Three equivalents of fatty acid methyl ester (FAME), i.e. methyl octanoate, and one equivalent glycerol would be obtained if complete conversion was achieved.

Transesterificaction reactions of vegetable oils with alcohol-to-oil molar ratios from 5:1 to 60:1 have been previously studied[2]. In industrial biodiesel productions, transesterificaction reactions with an alcohol-to-oil molar ratio of 6:1 is commonly used.[2-3] In this study, two alcohol-to-oil (methanol-to-glyceryl trioctanoate) molar ratios, i.e. 30:1 and 6:1, were investigated. Because glyceryl trioctanoate has shorter hydrocarbon chains than conventional vegetable oils, a homogeneous system was observed at an alcohol-to-oil molar ratio of 30:1. However, a bi-phasic liquid system was observed at an alcohol-to-oil ratio of 6:1.

Other key conditions, including catalyst concentrations and reaction temperatures, were also investigated. Detailed reaction conditions were listed in Table 3.1.

3.2.3 Real-time reaction monitoring

Real-time reaction monitoring was performed using an auto-sampling FIA/APCI-MS setup, which consisted of an HPLC pump (Agilent, Santa Clara, CA), a 1 μL internal sample injector (Valco, Huston, TX), a post-injection splitter (Upchurch Scientific, Oak Harbor, WA) with 1:15 split ratio and a JEOL AccuTOF time-of-flight mass spectrometer (JEOL, Peabody, MA) with an APCI source (Figure 3.1A). The detached APCI-MS setup, which was used in our previous study to further address sample overloading[26], was found unnecessary in this study.

Table 3.1 Reaction conditions of the model transesterification reaction.

Entry	Key reaction conditions				Reaction monitoring mode
	Alcohol-to-oil molar ratio	Initial TG molar concentration	NaOMe/TG (wt./wt.)	Temperature (^{0}C)	
1	30:1	0.61	0.15	23	Real-time and off-line
2	30:1	0.61	0.50	23	
3	30:1	0.61	1.50	23	
4	30:1	0.61	0.15	0	Real-time
5	30:1	0.61	0.15	45	
6	6:1	1.36	0.05	45	

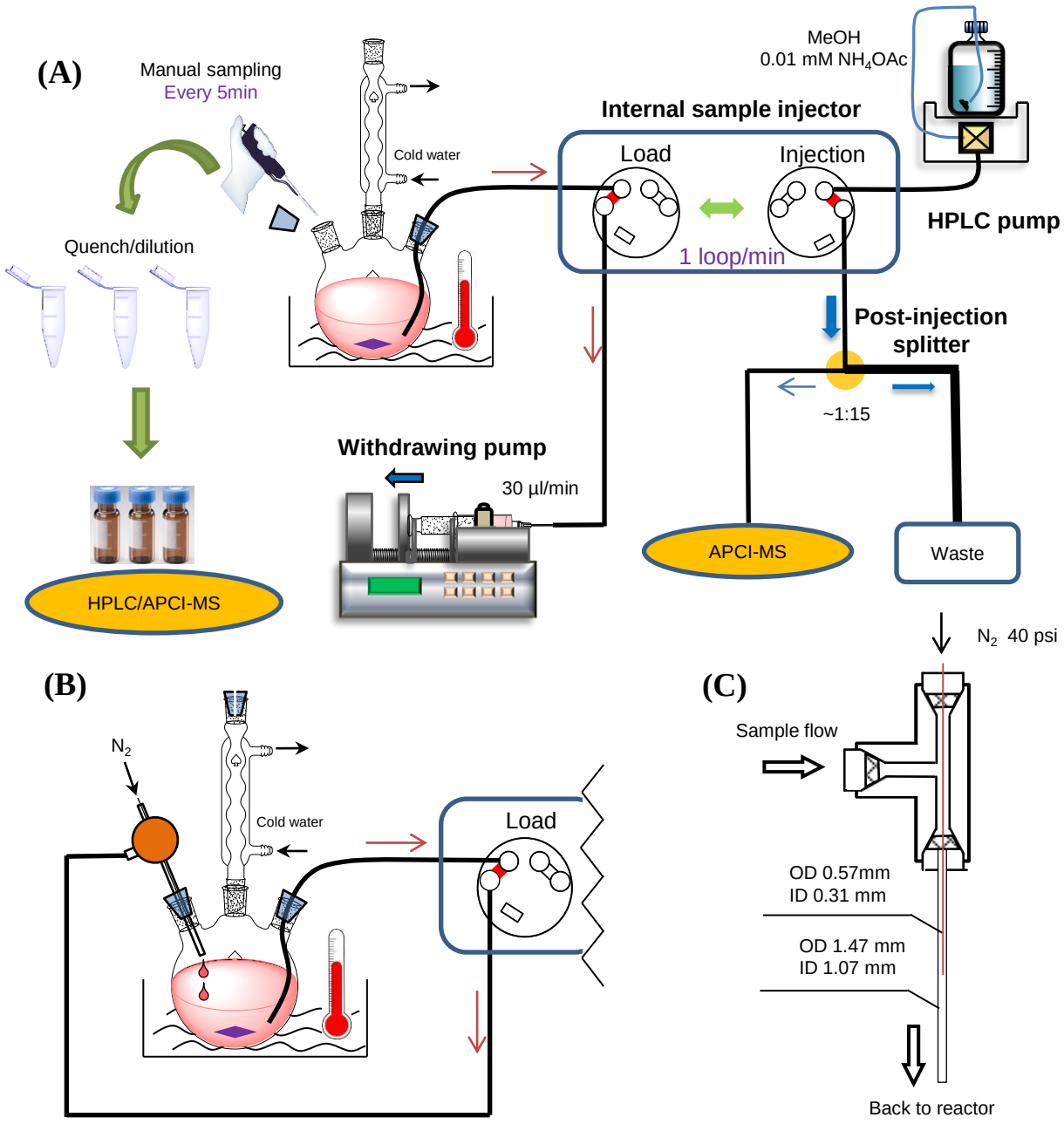

Figure 3.1 Detailed schematic diagrams of: A) the auto-sampling FIA/APCI-MS setup with a withdrawing syringe pump; B) the auto-sampling setup with an aspirator; C) the assembly of the aspirator.

For reactions performed at an alcohol-to-oil molar ratio of 30:1, homogenous systems were obtained. Online auto-sampling was achieved by using a withdrawing syringe pump (Harvard apparatus, Holliston, MA), which created a 30 μL/min sample flow to go through the 1 μL internal sample injector, where 1 μL sample was intercepted and transferred into the FIA flow as the internal sample injector switched from loading to injection position (Figure 3.1A). Because the reaction usually reached its completion within an hour or two, the total volume of the sample flow was only a few milliliters and not recycled back into the reactor flask.

For reactions performed at an alcohol-to-oil ratio 6:1, a bi-phasic liquid system was obtained. A sample flow with a much higher flow rate was required to avoid phase separation and consequently poor sampling reproducibility. Therefore, online auto-sampling was achieved by using an aspirator at a gas pressure of 40 psi, which created a sample flow with a flow rate of approximately one droplet per second. As illustrated in Figure 3.1B, the sample flow was recycled back into the reactor flask. The aspirator was assembled by centering a narrower stainless steel tube (0.57 mm O.D., 0.31 mm I.D. and 2.5 inch length) in a wider one (1.47 mm O.D., 1.07 mm I.D. and 4.5 inch length) through an appropriate tee (Valco, Huston, TX) (Figure 3.1C).

The FIA flow rate, which was delivered by the HPLC pump, was 2 mL/min. MeOH with 0.01 mM NH_4OAc was used as the FIA solvent. The maximum sampling rate was found to be 1 minute/injection without interferences between two adjacent samples.

The parameters of the APCI source were briefly optimized and set as follows: needle voltage, 4500 V; desolvation chamber temperature, 300 ℃; desolvation gas flow, 4 L/min; nebulizing gas flow, 2 L/min. Nitrogen was used for both desolvation and nebulizing gas. The parameters of the mass spectrometer were set as follows: orifice 1 voltage, 20 V; orifice 2 voltage, 10 V; ring voltage, 3 V; peak voltage, 800 V. Chromatogram-like total ion profiles (TIPs) were recorded with a mass range of *m/z* 100 to 500 and a scan interval of 1.0 s. Integration of peaks from the extracted ion profiles were performed with TSSPRO 3.0 software (JEOL, Peabody, MA). Good ventilation was adopted without safety concerns.

3.2.4 Quantitative calibration for real-time reaction monitoring

The initial concentrations of TG of the model transesterificaction reaction were calculated to be 0.61 and 1.36 M, respectively, at alcohol-to-oil molar ratios of 30:1 and 6:1. Therefore, a series of standard solutions of TG with concentration of 0.012, 0.024, 0.048, 0.096, 0.19, 0.38, 0.77 and 1.53 M was prepared for quantitative calibration based on individual standards (Table A1). Similarly, a series of standard solutions of DG with concentration of 0.0066, 0.013, 0.026, 0.053, 0.11, 0.21, 0.42 and 0.84 M was also prepared. The highest concentration of the DG standard solution was lower than 1.36 M because it was anticipated that DG would not reach 100% conversion as an intermediate product. Standard solutions of MG had respectively identical concentrations as those of DG (Table A1). The concentrations of standard FAME solutions were 0.036, 0.072, 0.14,

0.29, 0.57, 1.15, 2.29 and 4.58 M. The individual standard solutions were also used to test the upper-limit of quantitative calibration of the auto-sampling FIA/APCI-MS setup.

As matrix effects were anticipated for online real-time reaction monitoring using auto-sampling FIA/APCI-MS during analyte ionizations, simulated reaction mixtures of standards were further prepared to compensate the matrix effects in quantitative calibration. For the quantification of TG and FAME, simulated reaction mixtures of standards containing TG, FAME and Gly were prepared in MeOH, simulating the progress at 0, 10, 20, 40, 60, 80, and 100% completion of a hypothetically ideal reaction between TG and MeOH to produce FAME and Gly without intermediate steps, i.e. TG+3MeOH→3FAME+Gly (Table A2 and A3). For the quantification of DG, simulated reaction mixtures of standards containing TG, DG and FAME were prepared in MeOH, simulating the progress at 0, 5, 10, 30 and 50% completion of a hypothetically ideal reaction between TG and MeOH to produce DG and FAME without further steps, i.e TG+MeOH→DG+FAME (Table A4 and A5). It was anticipated that DG and MG would not reach beyond 50% conversion as intermediate products. Similarly, for the quantification of MG, simulated reaction mixtures of standards containing TG, MG and FAME were prepared in MeOH, simulating the progress at 0, 5, 10, 30 and 50% completion of a hypothetically ideal reaction between TG and MeOH to produce MG and FAME, i.e TG+2MeOH→MG+2FAME (Table A6 and A7). It was believed that these were the most appropriate simulation based on the reaction mechanism of the model reaction as described in Scheme 3.1.

All standard solutions were analyzed with three replicates by the auto-sampling FIA/APCI-MS under identical conditions optimized for online real-time reaction monitoring.

3.2.5 Off-line reaction monitoring

At the beginning in the development of the on-line reaction monitoring method, off-line HPLC/APCI-MS analysis was also performed for validation of the quantification. A Dionex Ultimate fully integrated micro-, capillary-, and nano-HPLC system (Sunnyvale, CA, USA) and an AB Sciex QSTAR Elite triple quadrupole time-of-flight (QTOF) mass spectrometer (Concord, Ontario, Canada) with an APCI heated nebulizer ion source were used for the off-line HPLC/APCI-MS analysis.

The HPLC separation used an XTerra MS C18 column (3.5 μm, 2.1mm ×150mm; Waters Corporation, Milford, MA) with an isocratic elution using water with 0.01mM NH_4OAc and MeOH with 0.01mM NH_4OAc at a 5:95 ratio. The LC column flow rate was 0.3 ml/min. The separation time for TG, DG, MG and FAME was 5 min and a 2 min column equilibration before the sample injection.

The general controlling parameters and settings for APCI-MS were nebulizer gas 40 (arbitrary unit), desolvation gas 40, source temperature 300 ℃, nebulizer current 1.0 μA, curtain gas 40, collision gas 3, declustering potential 30 V. Nitrogen gas (Airgas, Bowling Green, KY, USA) was used as the nebulizer, desolvation, curtain and collision gases. The acquisition mass range was *m/z* 100-500 and the acquisition time for each

spectrum was 1 second. Data were acquired and processed using Analyst 2.0 software (AB Sciex, Concord, Ontario, Canada).

During the reaction, 50 μL of the reaction mixture was sampled manually from the reactor flask (Figure 3.1A), quenched with 1.36 mM H_3PO_4 solution in MeOH, diluted by 20, 200 and 2000 times with the LC eluting solvent and then analyzed by HPLC/APCI-MS. Sampling was performed every 5 min for the first 60 minute of the reaction.

3.2.6 Quantitative calibration for off-line reaction monitoring

For offline reaction monitoring using HPLC/APCI-MS, chromatographic separations could result in minimum matrix effect during analyte ionizations. Therefore, quantitative calibrations for TG, DG, MG and FAME were established by analyzing a series of standard mixtures of TG, DG, MG and FAME with three replicates. The concentrations of each analyte in the standard mixtures were 0.025, 0.050, 0.125, 0.250, 0.500, 1.25, 2.50, 5.00, 12.5, 25.0 and 25.0 mM.

3.2.7 Kinetic modeling

After the concentration-time profiles of TG, DG, MG and FAME were obtained, a mechanistic study of the model transesterification reaction was performed. The mechanism of base-catalyzed transesterification of vegetable oils with alcohols has been reported in many studies, where the three reversible consecutive reactions (Scheme 3.1) were generally modeled by following second-order kinetics[28-33]. This kinetic model is described through a set of differential equations as flows.

$$\frac{d[TG]}{dt} = -k_1[TG][MeOH] + k_2[DG][FAME]$$

$$\frac{d[DG]}{dt} = k_1[TG][MeOH] - k_2[DG][FAME] - k_3[DG][MeOH] + k_4[MG][MeOH]$$

$$\frac{d[MG]}{dt} = k_3[DG][MeOH] - k_4[MG][MeOH] - k_5[MG][MeOH] + k_6[Gly][FAME]$$

$$\frac{d[FAME]}{dt} = k_1[TG][MeOH] - k_2[DG][FAME] + k_3[DG][MeOH]$$
$$- k_4[MG][MeOH] + k_5[MG][MeOH] + k_6[Gly][FAME]$$

$$\frac{d[Gly]}{dt} = k_5[MG][MeOH] + k_6[Gly][FAME]$$

$$\frac{d[MeOH]}{dt} = -\frac{d[FAME]}{dt}$$

In this study, the change in MeOH concentration was negligible at an alcohol-to-oil ratio of 30:1 due to its largely excessive amount. Therefore, term [MeOH] could be removed from the equations and the forward reactions were actually modeled following *pseudo*-first-order kinetics while the reversed reactions were modeled following second-order kinetics. However, at an alcohol-to-oil ration of 6:1 both the forward and reverse reactions were modeled following second-order kinetics.

Mathematical program. MATLAB (The Maths Works Inc., Natick, MA) was used for simultaneously fitting the differential equations into the experimental data. The methodology consisted of the following stages[34]:

(i) Estimation of initial rate constant values. After the concentration-time profiles of TG, DG, MG and FAME were obtained, the slopes of the plotted curves at any arbitrary time instant (t=5min was used here) were plugged into the differential equations to get the initial values of rate constant k_1 to k_6.

(ii) Optimization of rate constants. A simulation program (MATLAB ODE function) read the initial values of rate constants to give plots of simulated curves, which was compared with experimental data at each measured point. Deviations between experimental and calculated TG, DG, MG and FAME values were squared and summed up, from the initial time to final time, to form an objective function F:

$$F = \sum_{T_{inital}}^{T_{final}} [(TG_{\exp} - TG_{simu})^2 + (DG_{\exp} - DG_{simu})^2 + (MG_{\exp} - MG_{simu})^2 + (FAME_{\exp} - FAME_{simu})^2]$$

Optimal k_1 to k_6 were obtained when minimum F was reached.

(iii) Graphical representation of the experimental data and kinetic modelling results. These are described in detail in the **Results and Discussions** section**.**

3.3 Results and Discussions

3.3.1 Evaluation of the auto-sampling FIA/APCI-MS setup

The initial TG concentration of the model transesterificaction reaction was calculated to be 1.36 M at an alcohol-to-oil molar ratio of 6:1. Assuming a 100% conversion, the corresponding final concentration of FAME was calculated to be 4.08 M. Similarly, the corresponding highest concentration of DG and MG was estimated to be 0.78 M, assuming a 50% conversion of the intermediate reactions. Therefore, the requirement for the auto-sampling FIA/APCI-MS setup was to have linear calibrations up to 1.36, 0.78, 0.78 and 4.08 M for TG, DG, MG and FAME, respectively. In this study, sample overloading was addressed by using a 1 μL internal sample injector and a post-injection splitter with 1:15 splitting ratio. The detached APCI-MS setup, which was used

in our previous study to further address sample overloading[26], was found unnecessary. Individual standard solutions of TG, DG, MG and FAME with concentration range 0.012-1.53, 0.0066-0.84, 0.0066-0.84 and 0.036-4.58 M (Table A1), respectively, were analyzed in three replicates by using the auto-sampling FIA/APCI-MS setup. Linear responses were observed for peak areas of extracted ion profiles (XIPs) of $[TG+NH_4]^+$, $[DG+NH_4]^+$, $[MG+H]^+$ and $[FAME+H]^+$ versus the molar concentrations of TG, DG, MG and FAME, respectively. The correlation coefficients R^2 were 0.9990, 0.9980, 0.9993 and 0.9981 for TG, DG, MG and FAME, respectively; and the corresponding relative standard deviations (RSDs) were 1.4-5.8, 2.4-6.3, 0.74-5.4 and 0.85-3.2%.

3.3.2 Real-time reaction monitoring

The model transesterification reaction under conditions shown in entry 1 of Table 3.1 was first monitored in real-time using the auto-sampling FIA/APCI-MS setup. When methanol was used as the FIA solvent, abundant $[FAME+H]^+$ at *m/z* 159, $[MG+H]^+$ at *m/z* 219, $[DG+H]^+$ at *m/z* 345, $[DG+NH_4]^+$ at *m/z* 362 and $[TG+NH_4]^+$ at *m/z* 488 were observed. While $[FAME+H]^+$ and $[MG+H]^+$ were selected for the quantitation of FAME and MG, $[DG+NH_4]^+$ and $[TG+NH_4]^+$ were chosen for the quantitation of DG and TG. Consequently, 0.01, 0.1 and 1 mM NH_4Ac was added into the FIA solvent for better quantitative reproducibility and the optimum concentration was found to be 0.01 mM. Figure 3.2 demonstrates the XIPs of the four targeted ions as the model reaction progressed. Unlike the tailing peaks previously reported for amine compounds[26], Gaussian-like peaks for all targeted compounds were observed. Consequently, a much

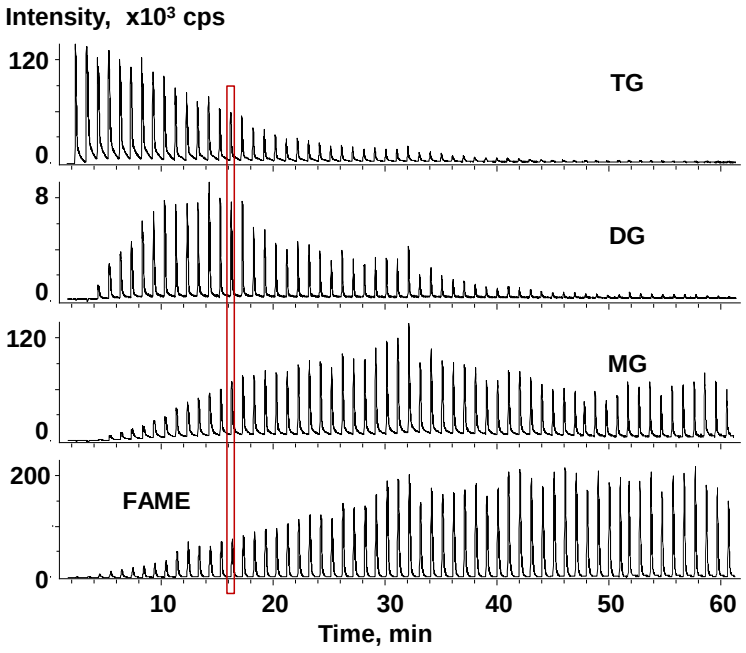

Figure 3.2 XIPs of the four targeted ions, i.e. $[TG+NH_4]^+$, $[DG+NH_4]^+$, $[MG+H]^+$ and $[FAME+H]^+$, as the model reaction progressed under conditions shown in entry 1 of Table 3.1 recorded by real-time reaction monitoring using auto-sampling FIA/APCI-MS.

faster sampling rate, i.e. 1 min versus 5 min/injection, was used for real-time monitoring without interferences between adjacent samples. Figure 3.3 demonstrates a mass spectrum at 14 minute of the model reaction under conditions shown in entry 1 of Table 3.1. Other than the ions mentioned above, weak $[TG+H]^+$ at *m/z* 471 and $[MG+NH_4]^+$ at *m/z* 236 were also observed. In addition, abundant ions at *m/z* 327, which could be $[TG+H-FA]^+$ and/or $[DG+H-H_2O]^+$ were also observed. Similarly, the abundant ion at *m/z* 201 could be $[DG+H-FA]^+$ and/or $[MG+H-H_2O]^+$. The extensive fragmentation of $[TG+H]^+$ agreed with previous study where saturated triglycerides were analyzed by APCI-MS[35].

3.3.3 Off-line reaction monitoring

In order to validate the quantification of real-time monitoring of the model reaction by using auto-sampling FIA/APCI-MS, off-line reaction monitoring by HPLC/APCI-MS was also performed as the model reaction progressed under conditions shown in entry 1 of Table 3.1. Figure 3.4 demonstrates extracted ion chromatograms (XICs) of $[MG+H]^+$ at *m/z* 219, $[FAME+H]^+$ at *m/z* 159, $[DG+NH_4]^+$ at *m/z* 345 and $[TG+NH_4]^+$ at *m/z* 488. The four targeted compounds were eluted in the order of MG, FAME, DG, and TG. During the reaction, 50 μL reaction mixture was sampled every 5 min for the first 60 minute of the reaction, immediately quenched, then diluted and analyzed by HPLC/APCI-MS.

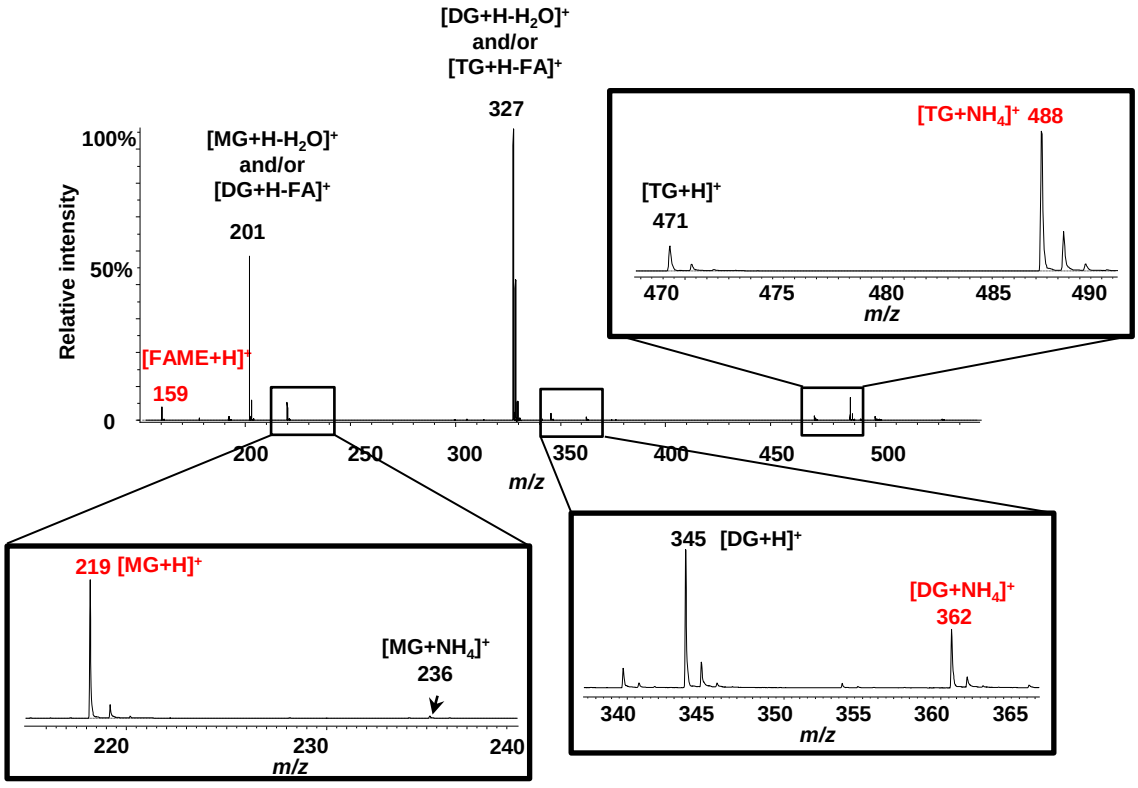

Figure 3.3 A mass spectrum at 14 minute of the model reaction under conditions shown in entry 1 of Table 3.1 recorded by real-time reaction monitoring using auto-sampling FIA/APCI-MS. The inserts are detailed mass spectra for ions related to TG, DG and MG. The ions that were selected to be monitored are marked in red.

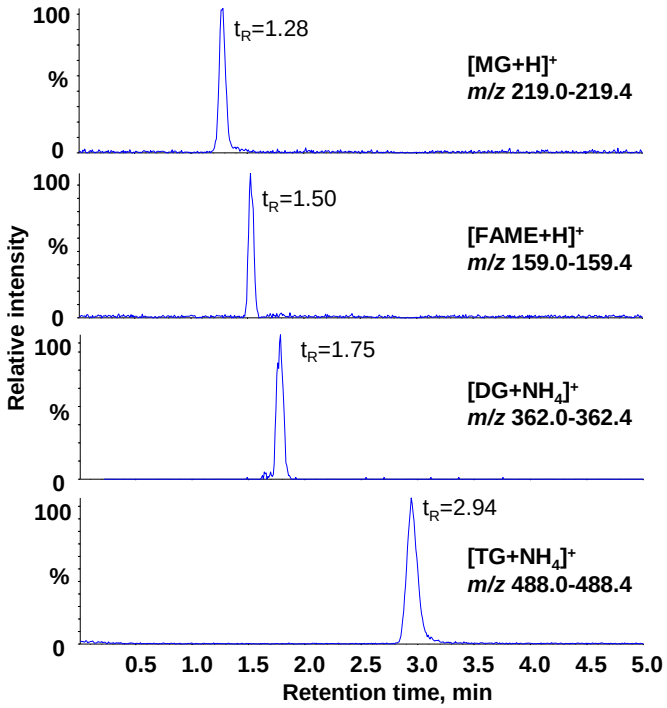

Figure 3.4 XICs of $[MG+H]^+$ at *m/z* 219, $[FAME+H]^+$ at *m/z* 159, $[DG+NH_4]^+$ at *m/z* 345 and $[TG+NH_4]^+$ at *m/z* 488 as a standard sample solution containing MG, FAME, DG and TG was analyzed by HPLC/APCI-MS.

3.3.4 Quantitative reaction monitoring

Quantitative reaction monitoring required quantitative calibrations so that the peak areas of the four targeted ions, i.e. $[FAME+H]^+$, $[MG+H]^+$, $[DG+NH_4]^+$ and $[TG+NH_4]^+$, obtained by either real-time or off-line reaction monitoring could be transformed into concentrations. Due to chromatographic separation, off-line reaction monitoring by HPLC/APCI-MS should suffer minimum ion suppression. Linear calibrations were established for four compounds with R^2 being 0.9975, 0.9953, 0.9966 and 0.9972 for TG, FAME, DG and MG, respectively; and the corresponding RSDs were 2.7-3.6, 0.61-5.3, 1.4-4.3 and 3.2-4.2%. The concentration-time profiles of TG, DG, MG and FAME for the model reaction under conditions shown in entry 1 of Table 3.1 were then calculated and illustrated in Figure 3.5 as purple points.

Quantitative calibrations for real-time monitoring by auto-sampling FIA/APCI-MS were first obtained by analyzing individual standard solutions; and the detailed results were already described in the "Evaluation of the auto-sampling FIA/APCI-MS setup" section. Subsequently, concentration-time profiles of TG, DG, MG and FAME for the model reaction under conditions shown in entry 1 of Table 3.1 were calculated (data not shown) and were found to significantly deviate from those obtained by HPLC/APCI-MS. Calibrations based on the analysis of individual standard solutions could only be accurate if the targeted compounds were not subject to significant ion suppression by other matrix compounds during APCI process. It is likely that ion suppression can be enhanced by a matrix compound with either stronger proton affinity (PA) or higher

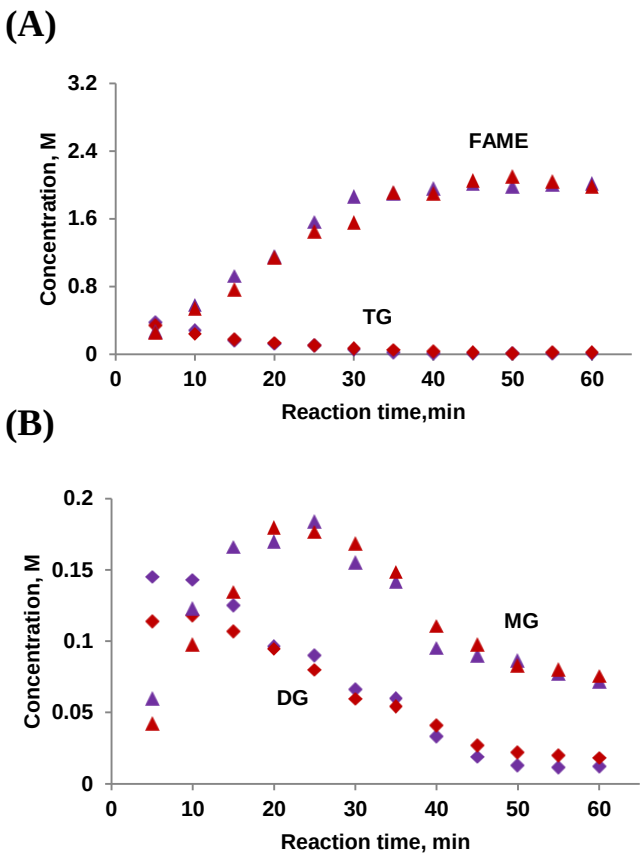

Figure 3.5 Concentration-time profiles of four targeted compounds for the model reaction under conditions shown in entry 1 of Table 3.1 with purple points representing off-line reaction monitoring by HPLC/APCI-MS and red points representing real-time reaction monitoring by auto-sampling FIA/APCI-MS using quantitative calibrations based on the analysis of simulated reaction mixtures of standards: (A) TG and FAME; (B) DG and MG. Quantitative data are presented every 5 min from 5-60 min of the reaction.

concentration. Unfortunately for the transesterification reaction, the reactant, i.e. TG, should have a stronger proton affinity than the intermediate products, i.e. DG and MG, and the final product, i.e. FAME. On the other hand, as reaction proceeded the concentration of FAME would quickly exceed other compounds.

Quantitative calibrations for real-time monitoring by auto-sampling FIA/APCI-MS were further obtained by analyzing simulated reaction mixtures of standards, which was used in our previous study on a Michael-addition reaction to compensate ion suppression by matrix compounds[26]. Unlike the one step Michael-addition reaction, however, accurate simulation of the progress of the model transesterificaction reaction with three reversible steps was impossible. Consequently, simulated reaction mixtures of standards were prepared based on three hypothetically ideal reactions as described in the "Experimental" section. Quantitative calibrations for real-time monitoring were then obtained by analyzing these simulated reaction mixtures of standards. Linear responses were observed for peak areas of extracted ion profiles (XIPs) of $[TG+NH_4]^+$, $[FAME+H]^+$, $[DG+NH_4]^+$ and $[MG+H]^+$ versus the molar concentrations of TG, FAME, DG and MG, respectively. For the model transesterification reaction at an alcohol-to-oil molar ratio of 30:1, R^2 were 0.9964, 0.9972, 0.9994 and 0.9990 for TG, FAME, DG and MG, respectively; and the corresponding RSDs were 3.4-7.9, 4.5-7.5, 1.7-9.1 and 3.4-7.2%. Subsequently, concentration-time profiles of TG, DG, MG and FAME for the model reaction under conditions shown in entry 1 of Table 3.1 were calculated and illustrated in Figure 3.5 as red points.

As shown in Figure 3.5, red points were very close to the purple points, indicating that the calibrations based on the analysis of simulated reaction mixtures of standards compensated ion suppression well. Among the four compounds, quantitative data of TG and FAME had great agreement between auto-sampling FIA/APCI-MS and HPLC/APCI-MS, indicating that the ion suppression by DG and MG on TG or FAME was negligible. This became reasonable in consideration that TG has the strongest PA and FAME would be dominant in concentration as the reaction proceeded.

3.3.5 Kinetic results

The concentration-time profiles of TG, DG, MG and FAME for the model reaction under conditions shown in entry 1 of Table 3.1, obtained by auto-sampling FIA/APCI-MS using calibrations based on the analysis of simulated reaction mixtures of standards, were input in the MATLAB program, with which rate constants of forward and reversed steps were calculated and optimized. Figure 3.6A shows graphic presentation of the experimental data (discrete points) and the kinetic modeling results (continuous curves) with a good fit. Equilibrium was reached at around 50 min for close to 100 % yield of FAME, while 3.1 mM TG, 13 mM DG and 43 mM MG were found remained in the mixture.

The effect of catalyst concentration was investigated by adjusting MeONa/TG concentration from 0.15 to 0.5 and 1.5% (Table 3.1, entry 1-3). Simulated TG and FAME curves based on optimized rate constants are demonstrated in Figure 3.6B, from which it is observed that reaction proceeded faster with increased concentration of catalyst. A

Figure 3.6 (A) Concentration-time profiles of experimental data (discrete points) and kinetic modeling results (contiguous curves) of the model reaction under conditions as shown in entry 1 of Table 3.1; (B) concentration-time profiles of kinetic modeling results of the model reaction under conditions as shown in in entry 1 to 5 of Table 3.1 for TG and FAME; (C) concentration-time profiles of experimental data (discrete points) and kinetic modeling results (contiguous curves) of the model reaction under conditions as shown in entry 6 of Table 3.1.

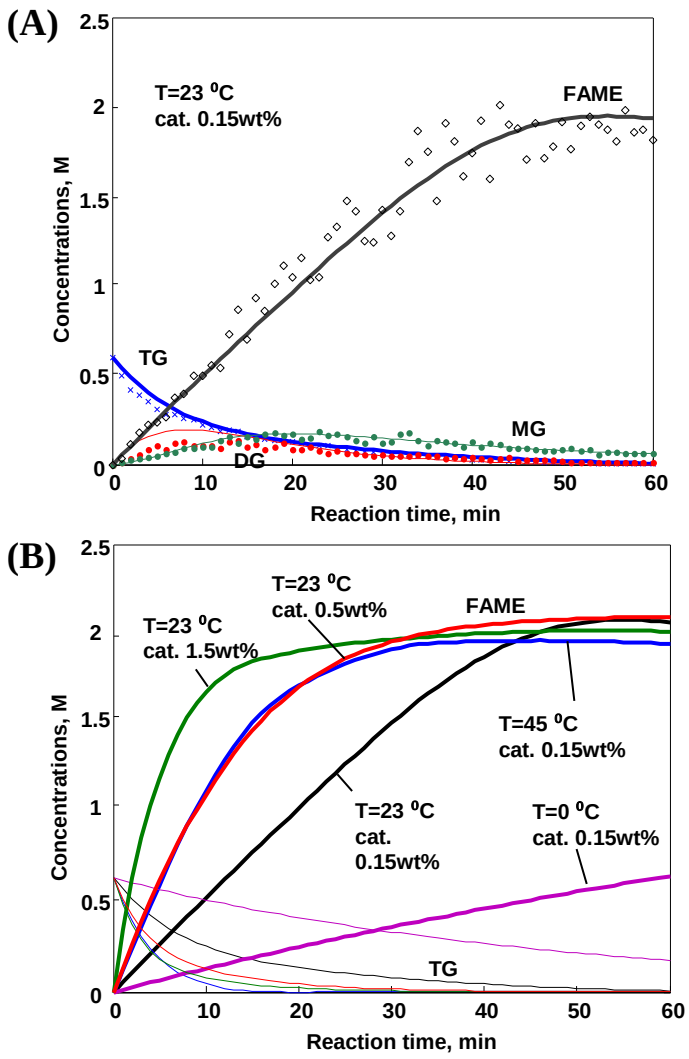

Figure 3.6 Continued.

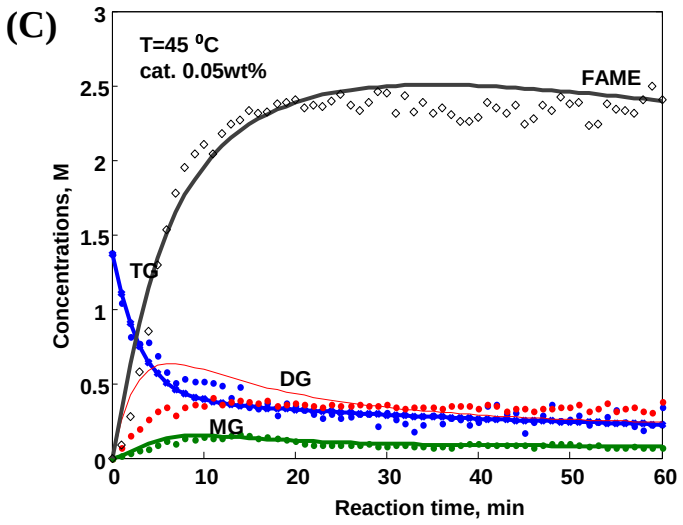

Figure 3.6 Continued.

limit of the improvement in reaction rate would be reached if concentration of catalyst was kept increasing, while the cost of using and disposition of catalyst is rising rapidly. Therefore, normally around 0.5-2% catalyst is used in commercial biodiesel production.[2]

The temperature dependence of the reaction rate (Table 3.1, entry 1, 4 and 5) in first 60 min is demonstrated in Figure 3.6B with simulated curves of TG and FAME. The reaction proceeded significantly faster from 0 ℃ to 45 ℃ as more thermal energy was provided. Besides, the improving solubility of oil in methanol at higher temperature might also contribute to the faster reaction rates from 0 ℃ to 23 ℃. Increases of calculated rate constants were observed for both forward and reverse reactions with rising reaction temperatures. Production yield of FAME was found to increase from 71% at 0 ℃ to almost 100% at 23 ℃ after 2.5 h, but no obvious improvement on the yield was observed when temperature was elevated further to 45 ℃. These suggest that improving solubility of oil in alcohol can greatly benefit the production of FAME.

The Erying-Polanyi equation[36] has been used to study the temperature dependency of the reaction rate constant. The following equation was derived from the Erying-Polanyi equation, based on which the logarithm of the ratio of rate constant (k) over absolute temperature (T) as a function of the reciprocal of absolute temperature (1/T) was set out. The k_B and h stand for Boltzmann constant and Plank's constant, respectively.

$$\ln\frac{k}{T} = -\frac{\Delta H^{\neq}}{R}\frac{1}{T} + \ln\frac{k_B}{h} + \frac{\Delta S^{\neq}}{R}$$

The activation enthalpy change ($\Delta H^{\neq}$) of each step can be determined by the slopes and the activation entropy change ($\Delta S^{\neq}$) by the y intercepts (Table 3.2). The calculated activation enthalpy changes for the three step reactions are roughly 7.4 to 10.38 kcal/mol, which are of the same order as those for the three step reactions obtained in previous studies[28-29, 31, 33]. The calculated activation entropy changes for both reversed and forward steps are negative, indicating a decrease in the degree of freedom, which is in agreement with the formation of the "tetrahedral transition state" for esterification reactions.

To achieve quantitative real-time monitoring of the model reaction conducted with an alcohol-to-oil ratio of 6 under conditions as shown in entry 6 of Table 3.1, calibrations based on the analysis of simulated reaction mixtures of standards were further established. The R^2 were 0.9888, 0.9976, 0.9900 and 0.9967 for TG, FAME, DG and MG, respectively; and the corresponding RSDs were 3.9-10.6, 3.3-9.4, 5.7-11.4 and 4.1-9.1%. Figure 3.6C shows the graphic presentation of the experimental data (discrete points) and kinetic modelling results (continuous curves). Similar to the industrial biodiesel production from transesterification of vegetable oils, a bi-phasic liquid system was involved throughout the reaction, and higher temperature and sufficient stirring were necessary to reduce the heterogeneity and accelerate the mass-transfer speed between two liquid phases. The production rate of FAME was slightly slower in the first 1 min and became faster after that, followed by the falling rate as reaction proceeded toward equilibrium. The initial slower rate may suggest a short mass-transfer controlled region,

Table 3.2 Changes of activation enthalpy and entropy of each step of the model transesterification reaction calculated from Eyring-Polanyi equation.

Step	$\Delta H^{\neq}$ (kcal·mol^{-1})	$\Delta S^{\neq}$ (cal·mol^{-1}·K^{-1})	Correlation coefficient R^2
TG→DG	7.4 ± 0.9	-38.5 ± 3.1	0.9852
DG→MG	9.1 ± 2.1	-32.9 ± 7	0.9498
MG→Gly	10.38 ± 2.7	-29.4 ± 9.1	0.9349
DG→TG	9.9 ± 2.6	-37.7 ± 9	0.9355
MG→DG	8.4 ± 0.7	-43.0 ± 2.4	0.9931
Gly→MG	7.4 ± 1.1	-46.9 ± 3.8	0.9780

which can be ignored in kinetic modeling.

3.4 Conclusion

Efforts have been made toward quantitative real-time monitoring of industrial bio-diesel production processes by mass spectrometry. The transmethylation of glyceryl trioctanoate, a simplified model of industrial bio-diesel production through the transesterification of vegetable oils, was able to be quantitatively monitored in real time by auto-sampling FIA/APCI-MS without sample overloading. For auto-sampling, a withdrawing syringe pump was used when the model reaction was a homogenous mono-phasic liquid system at an alcohol-to-oil molar ratio of 30:1, but a recycling loop driven by an aspirator was utilized when the model reaction was a heterogeneous bi-phasic liquid system at an alcohol-to-oil molar ratio of 6:1. Simultaneous quantification of the major compounds was achieved by using calibrations based on the analysis of simulated reaction mixtures of standards, which was labor-intensive but surprisingly successful. The resulting concentration-time profiles allowed kinetic study of the model reaction.

Improvement of the auto-sampling FIA/APCI-MS setup is anticipated before it can be used onsite for monitoring industrial bio-diesel production in real time because the feedstock of bio-diesel productions is far more complicated. However, quantification of all components may not be absolutely necessary as the production should be following one set of optimized reaction conditions.

Reference

(1) Knothe, G.; Dunn Robert, O.; Bagby Marvin, O., in **Biodiesel: The Use of Vegetable Oils and Their Derivatives as Alternative Diesel Fuels**, American Chemical Society, 1997.

(2) Abbaszaadeh, A.; Ghobadian, B.; Omidkhah, M. R.; Najafi, G. *Energy Convers. Manage.* **2012**, *63*. 138-148.

(3) Fukuda, H.; Kondo, A.; Noda, H. *J. Biosci. Bioeng.* **2001**, *92*. 405-416.

(4) Atadashi, I. M.; Aroua, M. K.; Aziz, A. A. *Renew. Energy* **2011**, *36*. 437-443.

(5) Richard, R.; Li, Y.; Dubreuil, B.; Thiebaud-Roux, S.; Prat, L. *Bioresour. Technol.* **2011**, *102*. 6702-6709.

(6) Panetta, R. J.; Jahren, A. H. *Rapid Commun. Mass Spectrom.* **2011**, *25*. 1373-1381.

(7) Holčapek, M.; Jandera, P.; Fischer, J.; Prokeš, B. *J. Chromatogr. A* **1999**, *858*. 13-31.

(8) Reddy, S. R.; Titu, D.; Chadha, A. *J. Am. Oil Chem. Soc.* **2010**, *87*. 747-754.

(9) Bhabhe, M. D.; Athawale, V. D. *J. Chromatogr. A* **1995**, *718*. 299-304.

(10) Dube, M. A.; Zheng, S.; McLean, D. D.; Kates, M. *J. Am. Oil Chem. Soc.* **2004**, *81*. 599-603.

(11) Knothe, G. *J. Am. Oil Chem. Soc.* **2000**, *77*. 489-493.

(12) Kouame, S. D. B.; Perez, J.; Eser, S.; Benesi, A. *Fuel Process. Technol.* **2012**, *97*. 60-64.

(13) Anderson, L. A.; Franz, A. K. *Energy & Fuels* **2012**, *26*. 6404-6410.

(14) Knothe, G. *J. Am. Oil Chem. Soc.* **1999**, *76*. 795-800.

(15) Richard, R.; Dubreuil, B.; Thiebaud-Roux, S.; Prat, L. *Fuel* **2013**, *104*. 318-325.

(16) de Lima, S. M.; Silva, B. F. A.; Pontes, D. V.; Pereira, C. F.; Stragevitch, L.; Pimentel, M. F. *Fuel* **2014**, *115*. 46-53.

(17) Trevisan, M. G.; Garcia, C. M.; Schuchardt, U.; Poppi, R. J. *Talanta* **2008**, *74*. 971-976.

(18) Mahamuni, N. N.; Adewuyi, Y. G. *Energy & Fuels* **2009**, *23*. 3773-3782.

(19) Zhang, F.; Adachi, D.; Tamalampudi, S.; Kondo, A.; Tominaga, K. *Energy & Fuels* **2013**, *27*. 5957-5961.

(20) Ghesti, G. F.; de Macedo, J. L.; Braga, V. S.; de Souza, A.; Parente, V. C. I.; Figueredo, E. S.; Resck, I. S.; Dias, J. A.; Dias, S. C. L. *J. Am. Oil Chem. Soc.* **2006**, *83*. 597-601.

(21) De Boni, L. A. B.; da Silva, I. N. L. *Fuel Process. Technol.* **2011**, *92*. 1001-1006.

(22) Xie, W. L.; Li, H. T. *J. Am. Oil Chem. Soc.* **2006**, *83*. 869-872.

(23) Ellis, N.; Guan, F.; Chen, T.; Poon, C. *Chem. Eng. J.* **2008**, *138*. 200-206.

(24) Knothe, G. *T. Asae* **2001**, *44*. 193-200.

(25) Byrdwell, W. C. *Lipids* **2001**, *36*. 327-346.

(26) Zhu, Z. Q.; Bartmess, J. E.; McNally, M. E.; Hoffman, R. M.; Cook, K. D.; Song, L. G. *Anal. Chem.* **2012**, *84*. 7547-7554.

(27) Counsell, R. E., Strawn, Laurie Radioiodinated diacylglycerol analogues and methods of use. US Patent 4,925,649, **1990**.

(28) Freedman, B.; Butterfield, R. O.; Pryde, E. H. *J. Am. Oil Chem. Soc.* **1986**, *63*. 1375-1380.

(29) Noureddini, H.; Zhu, D. *J. Am. Oil Chem. Soc.* **1997**, *74*. 1457-1463.

(30) Karmee, S. K.; Chandna, D.; Ravi, R.; Chadha, A. *J. Am. Oil Chem. Soc.* **2006**, *83*. 873-877.

(31) Vicente, G.; Martinez, M.; Aracil, J. *Energy & Fuels* **2006**, *20*. 1722-1726.

(32) Doell, R.; Konar, S. K.; Boocock, D. G. B. *J. Am. Oil Chem. Soc.* **2008**, *85*. 271-276.

(33) Stamenkovic, O. S.; Todorovic, Z. B.; Lazic, M. L.; Veljkovic, V. B.; Skala, D. U. *Bioresour. Technol.* **2008**, *99*. 1131-1140.

(34) Seoud, A. A. a. L. A. M. A. *Am. J. Appl. Sci.* **2010**, *7*. 509-517.

(35) Laakso, P. *Eur. J. Lipid Sci. Technol.* **2002**, *104*. 43-49.

(36) Laidler, K. J.; King, M. C. *J. Phys. Chem.* **1983**, *87*. 2657-2664.

Appendix A

For

Chapter 3. Quantitative Real-time Monitoring of Transesterifications by Auto-sampling FIA/APCI-MS for the Improvement of Industrial Biodiesel Production

Table A1 Preparation of individual standard solution.

Analyte	Molar concentration of standard solutions							
TG	0.012	0.024	0.048	0.096	0.19	0.38	0.77	1.53
DG	0.0066	0.013	0.026	0.053	0.11	0.21	0.42	0.84
MG	0.0066	0.013	0.026	0.053	0.11	0.21	0.42	0.84
FAME	0.036	0.072	0.14	0.29	0.57	1.15	2.29	4.58

Table A2 Preparation of simulated reaction mixtures of standards based on a hypothetical reaction of TG+3MeOH→3FAME+Gly at an alcohol-to-oil molar ratio of 30:1.

Content	Amount of each compound in the simulated standards (g)[a]						
	Simulated progress of the hypothetical reaction						
	0%	10%	20%	40%	60%	80%	100%
TG	1.44	1.30	1.15	0.86	0.58	0.29	0
MeOH	2.94	2.91	2.88	2.82	2.76	2.71	2.65
FAME	0	0.15	0.29	0.58	0.87	1.16	1.45
Gly	0	0.03	0.06	0.11	0.17	0.23	0.28

a. The total volume is 5 mL.

Table A3 Preparation of simulated reaction mixtures of standards based on a hypothetical reaction of TG+3MeOH→3FAME+Gly at an alcohol-to-oil molar ratio of 6:1.

Content	Amount of each compound in the simulated standards (g)[a]						
	Simulated progress of the hypothetical reaction						
	0%	10%	20%	40%	60%	80%	100%
TG	3.20	2.88	2.56	1.92	1.28	0.64	0
MeOH	1.31	1.24	1.18	1.05	0.92	0.78	0.65
FAME	0	0.32	0.65	1.29	1.94	2.58	2.23
Gly	0	0.06	0.13	0.25	0.38	0.50	0.63

a. The total volume is 5 mL.

Table A4 Preparation of simulated reaction mixtures of standards based on a hypothetical reaction of TG+MeOH→DG+FAME at an alcohol-to-oil molar ratio of 30:1.

Content	Amount of each compound in the simulated standards (g)[a]				
	Simulated progress of the hypothetical reaction				
	0%	5%	10%	30%	50%
TG	1.44	1.37	1.30	1.01	0.72
MeOH	2.94	2.94	2.93	2.91	2.89
DG	0	0.05	0.11	0.32	0.53
FAME	0	0.02	0.05	0.15	0.24

a. The total volume is 5 mL.

Table A5 Preparation of simulated reaction mixtures of standards based on a hypothetical reaction of TG+MeOH→DG+FAME at an alcohol-to-oil molar ratio of 6:1.

Content	Amount of each compound in the simulated standards (g)[a]				
	Simulated progress of the hypothetical reaction				
	0%	5%	10%	30%	50%
TG	1.98	1.88	1.78	1.38	0.99
MeOH	0.81	0.80	0.79	0.77	0.74
DG	0	0.07	0.14	0.43	0.72
FAME	0	0.03	0.07	0.20	0.33

a. The total volume is 5 mL.

Table A6 Preparation of simulated reaction mixtures of standards based on a hypothetical reaction of TG+2MeOH→MG+2FAME at an alcohol-to-oil molar ratio of 30:1.

Content	Amount of each compound in the simulated standards (g)[a]				
	Simulated progress of the hypothetical reaction				
	0%	5%	10%	30%	50%
TG	1.44	1.37	1.30	1.01	0.72
MeOH	2.94	2.93	2.92	2.88	2.84
MG	0	0.03	0.07	0.20	0.33
FAME	0	0.05	0.10	0.29	0.48

a. The total volume is 5 mL.

Table A7 Preparation of simulated reaction mixtures of standards based on a hypothetical reaction of TG+2MeOH→MG+2FAME at an alcohol-to-oil molar ratio of 6:1.

Content	Amount of each compound in the simulated standards (g)[a]				
	Simulated progress of the hypothetical reaction				
	0%	5%	10%	30%	50%
TG	1.98	1.88	1.78	1.38	0.99
MeOH	0.81	0.79	0.78	0.73	0.67
MG	0	0.05	0.09	0.28	0.46
FAME	0	0.07	0.13	0.40	0.66

a. The total volume is 5 mL.

Chapter 4. Slurry Flow Injection Analysis coupled with Atmospheric Pressure Chemical Ionization Mass Spectrometry for Quantitative Real-Time Monitoring of Batch Slurry Reactions

Abstract

Although batch slurry reactions are widely used in the fine chemical and pharmaceutical industries, to our knowledge, no methods have been reported for their quantitative real-time monitoring. In order to develop a corresponding mass spectrometric method, two issues have to be addressed: sample overloading caused by real life molar concentrations in the reaction mixtures and system clogging caused by solid particles from process-scale batch slurry reactions. In this study, an innovative slurry flow injection analysis coupled with atmospheric pressure chemical ionization mass spectrometry (slurry FIA/APCI-MS) system is introduced. It is based on our recently reported auto-sampling FIA/APCI-MS system for quantitative real-time monitoring of homogeneous reactions, where three strategies had been introduced to address the sample overloading. To avoid the system clogging, in addition to the use of wider tubing and fittings and higher sample flow rate, further modifications on hardware were made. First, a slurry auto-sampler, which consisted of a 10 μL auto-sampling valve, an aspirator and a flow-switch valve, was constructed to replace the 1 μL automatic internal sample injector and the syringe pump. The second modification was the construction of a slurry APCI probe to replace the commercial version. Finally, a post-injection slurry mixer was incorporated into the slurry FIA/APCI-MS system. The optimized system was tested with a model batch slurry reaction at 30% (w/w) slurry concentration upon completion; and a linear quantitative calibration has been achieved for the product with 0.7-6.0% relative standard deviation (RSD) for five replicates.

4.1 Introduction

The mission of process analytical chemistry is to provide physical properties and chemical compositions during an industrial manufacturing process so that production control and preventive assurance of product quality can be enabled[1]. Industries such as chemical, pharmaceutical, petro-chemical, bio-fuels, and food are examples that benefit from reliable process analytical technology for optimal process guidance. Off-site process analysis carried out at a central analytical laboratory can result in lost opportunities for real-time process adjustments. Conversely, on-site process analysis usually involves real-time measurements, which enable automated manufacturing control and further improvement of safety, product quality and manufacturing cost efficiency.

For on-site real-time reaction monitoring, optical spectroscopic techniques including ultraviolet-visible (UV-Vis), infrared (IR) and especially near infrared (NIR) spectroscopy, using optical immersion probes to directly analyze reaction components without sampling, are recognized as useful tools by science-based regulatory guidance publications[2-5]. Despite their robustness and ease in handling and operation, these in-line techniques usually do not have sufficient chemical selectivity, therefore they require sophisticated chemometric data processing[6]. Recently, direct on-line coupling of more selective analytical techniques such as nuclear magnetic resonance (NMR) spectroscopy[7] and mass spectrometry (MS)[8] to the reaction vessel with sampling systems, transfer lines or bypass loops has attracted more and more attention.

Both high-resolution (HR，≥300 MHz)[9-12] and medium-resolution (MR, 10-85 MHz) quantitative on-line NMR instruments[13-17] have been successfully utilized in real-time reaction monitoring. For the control of an industrial manufacture process, modern HR-NMR instruments have the disadvantage of high cost and the spatial and environmental needs of cryogenic magnets. In contrast, traditional MR-NMR instruments are usually equipped with small low-field permanent magnets and therefore are low cost, robust and offer easy operation. However, reaction monitoring requires a spectral resolution of at least 0.1 ppm full width at half maximum (FWHM) for a flowing liquid stream, which is not routinely achievable by many low-field NMR instruments, and consequently sophisticated chemometric method had to be applied in data processing[14].

Unlike NMR spectroscopy, MS has been developed to perfectly couple with flow liquid streams on-line. In fact, real-time reaction monitoring by on-line MS has been the topic of many publications so far[18-31], but these procedures are not suited to measure reaction mixtures with molar concentrations in an industrial manufacturing process due to sample overloading. Recently, we have addressed this[8] with a novel auto-sampling flow injection analysis system coupled with atmospheric pressure chemical ionization mass spectrometry (FIA/APCI-MS) system using a 1 μL automatic internal sample injector, a post-injection splitter with 1:10 splitting ratio, and a detached APCI source connected to the mass spectrometer using a 4.5 in. long, 0.042 in. inner diameter (ID) ion-transport capillary (Figure 2.1). Sample overloading can also be circumvented with some of the

newly developed ambient ionization techniques, but real-time monitoring of chemical reactions have yet to be reported quantitatively[32-37].

On-line real-time monitoring of heterogeneous reactions is challenging. When optical spectroscopic instruments are used, multiplicative light scattering effects would "scale" the entire spectral measurement and hence mask the spectral variations relating to the content differences of chemical compounds in the samples[38]. Although a number of chemometric preprocessing methods[38-47] have been proposed to counteract this, they have been applied only to relatively simple heterogeneous mixture samples rather than the ones from batch slurry reactions. When NMR is used, the homogeneity of the magnetic field can be severely perturbed by the different magnetic susceptibilities of solids and liquids. So far, on-line NMR spectroscopy was utilized only to monitor heterogeneously catalyzed reactions[9,11-12] and filters were utilized at the sampling point of the reactor vessels to avoid having solid particles in the detection region of the NMR probe. Recently, direct analysis in real time mass spectrometry (DART-MS) has been evaluated by Cho *et. al.*[35] for the on-site monitoring of a batch slurry reaction. Well-stirred slurry mixture samples were manually deposited on the closed end of melting-point capillaries and then automatically introduced for DART ionization with a homemade DART auto-sampler. Although semi-quantitative results were obtained, it was concluded that a complicated, expensive, and fully automated robotic auto-sampler was necessary before a quantitative analysis could be conducted.

Batch slurry reactions are widely used in the fine chemical and pharmaceutical industries because the products can be easily separated from the solvents and the solvents recycled. Currently, these reactions are typically monitored at the central analytical laboratory with conventional analytical methods such as liquid chromatography (LC) with UV detection. In this case, a representative reaction mixture is sampled-out, quenched if necessary, and dissolved in a suitable solvent. Based on our previous experience with quantitative real-time monitoring of process-scale homogeneous reactions by mass spectrometry, FIA/APCI-MS is the most feasible approach for real-time monitoring of batch slurry reactions due to the acceptable quantitation we obtained. This report highlights our efforts to overcome system clogging which interferes with making our design a routine automated operation for quantitative real-time monitoring of batch slurry reactions.

4.2 Experimental

4.2.1 Reagent

2-Amino-4-methoxy-6-methyl-1,3,5-triazine (AMMT) and metsulfuron methyl (MSM) were industrial grade and provided by DuPont Crop Protection (Newark, Delaware). Certified A.C.S. grade xylenes, generally a mixture of the *ortho*-, *meta*- and *para*-isomers and perhaps containing some ethylbenzene, was purchase from Fisher Scientific (Pittsburgh, PA). It was used as the liquid component of simulated slurry samples because the corresponding industrial grade reagent is currently used in the

commercial manufacture of MSM by DuPont Crop Protection. AMMT and MSM have very limited solubility in xylenes, approximately 1.73 mM (0.245 mg/mL) and 2.76 mM (1.05 mg/mL), respectively, by experiments after ultrasonication. HPLC grade acetonitrile was also purchased from Fisher Scientific (Pittsburgh, PA). It was used as FIA solvent. The solubility of AMMT and MSM in acetonitrile was approximately 10.0 mM (1.40 mg/mL) and 65.6 mM (21.2 mg/mL), respectively, after ultrasonication.

4.2.2 Model batch slurry reaction

Metsulfuron methyl is a sulfonylurea herbicide for broadleaf weeds and some annual grasses. As shown in Scheme 4.1, Metsulfuron methyl is synthesized by a coupling reaction between 2-Amino-4-methoxy-6-methyl-1,3,5-triazine and methyl 2-(isocyanatosulfonyl) benzoate (MIB) in xylenes. This is a typical batch slurry reaction due to the extremely low solubility of AMMT and MSM in xylenes. Of the three compounds involved in this reaction, MIB has much higher solubility in xylenes than AMMT and MSM and can remain dissolved up to 1 M. However, MIB is moisture sensitive and can be easily hydrolyzed in air. In the commercial manufacture, this slurry reaction is usually performed at 30% (w/w). Upon completion of the reaction an average particle size of less than 10 μm has been determined for MSM.

4.2.3 Instrumentation

A slurry FIA/APCI-MS system (Figure 4.1), consisting of a slurry FIA setup and a detached APCI-MS setup, was developed for quantitative real-time monitoring of batch slurry reactions.

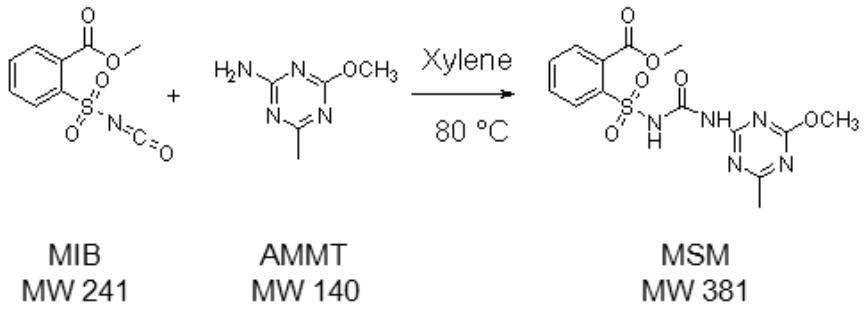

Scheme 4.1 The model slurry reaction: coupling reaction of AMMT and MIB for the production of MSM.

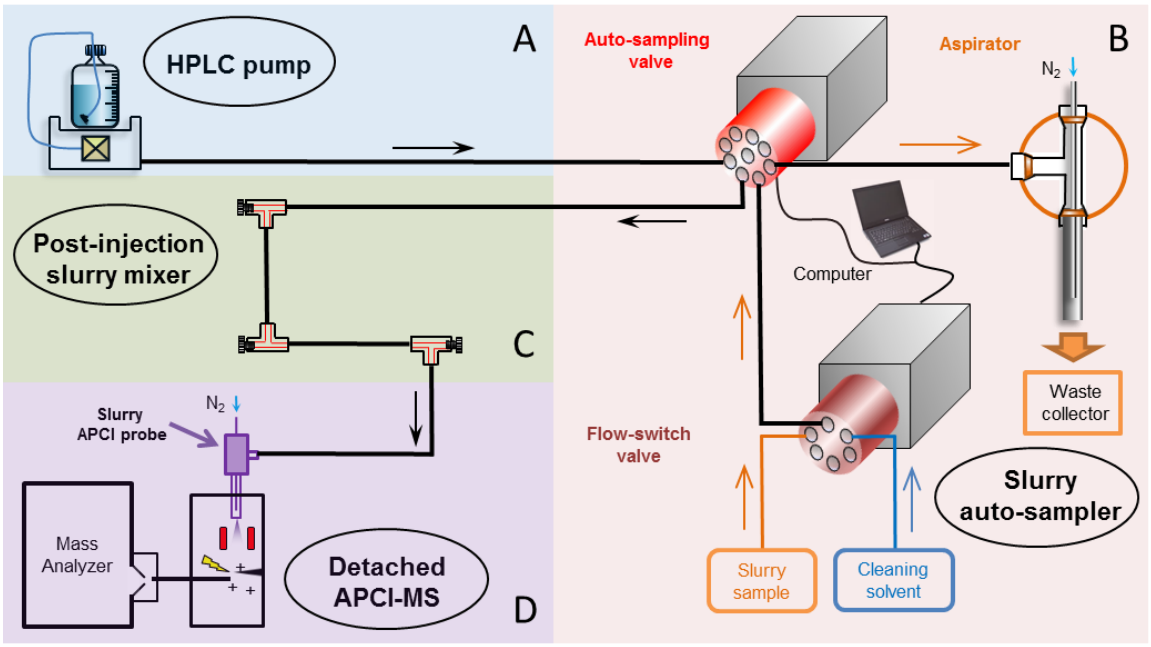

Figure 4.1 Diagram of the slurry FIA/APCI-MS system: (A) HPLC pump; (B) slurry auto-sampler; (C) post injection slurry mixer and (D) detached APCI-MS.

Slurry FIA Setup. The slurry FIA system consisted of an HPLC pump (Agilent, Santa Clara, CA), a slurry auto-sampler and a post-injection slurry mixer. It was based on a previously developed auto-sampling FIA setup for homogenous sample analysis[75], which consisted of an HPLC pump (Agilent, Santa Clara, CA), an automatic internal sample injector (Valco, Huston, TX), a syringe pump (Harvard Apparatus, Holliston, MA) and a splitter (Upchurch Scientific, Oak Harbor, WA). Modifications were made so that slurry samples could be handled without a clogging problem. The first modification was to use wider tubing and fittings (Valco, Huston, TX) to avoid clogging of the pipeline: the slurry FIA setup used PEEK tubing with 0.06 in. (1.52 mm) inner diameter (I.D.) and 1/8 in. outer diameter (O.D.), while the previous auto-sampling FIA setup used PEEK tubing with 0.03 in. (0.076 mm) I.D. and 1/16 in. O.D. The second modification was to construct a slurry auto-sampler, which consisted of an auto-sampling valve, an aspirator and a flow-switch valve, so that slurry samples could be injected without clogging. The auto-sampling valve had the same function as the automatic internal sample injector, while the aspirator functioned to create a slurry sample flow, similar to the syringe pump. An additional flow-switch valve was incorporated to save slurry samples because the slurry flow rate was maintained at approximately 1.5 mL/s to avoid clogging problems.

There were two prominent requirements for an auto-sampling valve: 1) appropriate ports to host 0.06 in. I.D. and 1/8 in. O.D. PEEK tubing to avoid clogging; and 2) minimal length grooves on the valve rotor so that the injected sample volume from

one of the grooves was as small as possible to avoid sample overloading. A 4-position flow-through selector valve with 0.06 in. ports (Valco, Huston, TX) was eventually selected as the best fit. As demonstrated in Figure 4.2, the 4-position flow-through selector is designed to have 4 independent flow streams, with the selected stream flowing through the central outlet port for further analysis. Other streams flow through their own independent outlet ports. However, these so-called independent streams with their own independent outlet ports actually share the grooves, which are engraved on the valve rotor, so that the independent streams could maintain their continuity when not selected. When the 4-position flow-through selector valve is in position #1 as shown in Figure 4.2A, the selected stream S1 uses inlet port P2, the selected stream outlet port and the selected stream groove G1. Under this condition, the independent streams S2, S3 and S4 use inlet ports P4, P6 and P8, outlet ports P3, P5 and P7, and the grooves G2, G3 and G4, respectively. When the 4-position flow-through selector valve is rotated clockwise to be in position #2 as shown in Figure 4.2B, the selected stream S2 used the selected stream groove G1, while the independent streams S3, S4 and S1 used the grooves G2, G3 and G4, respectively. When the 4-position flow-through selector valve is further rotated clockwise to be in position #3 as shown in Figure 4.2C, the selected stream is supposed to be S3 (purposely closed in Figure 4.2C as described in the next paragraph) which would use groove G1, while the independent streams should be S4 (purposely closed in Figure 2C as described in the next paragraph), S1 and S2, which would use grooves G2, G3 and G4, respectively. When the 4-position flow-through selector valve is rotated clockwise

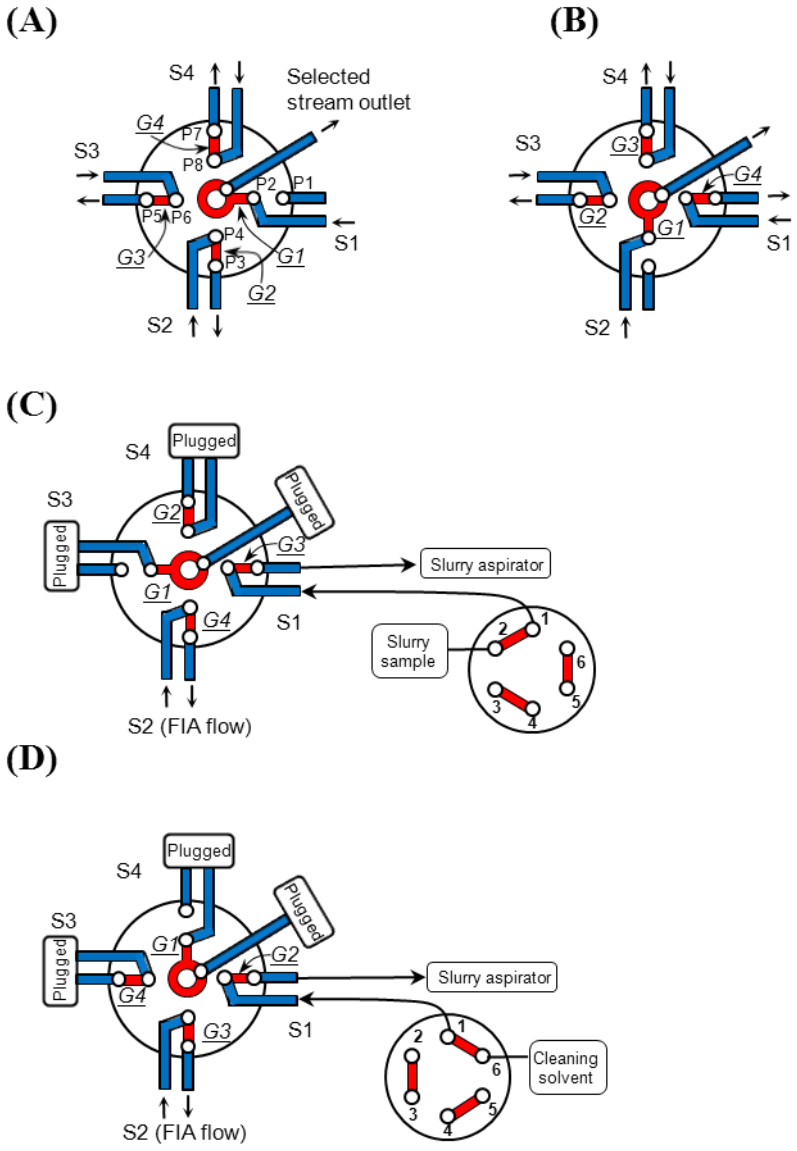

Figure 4.2 Operational principle of the slurry auto-sampler: (A) a 4-position flow-through selector valve in position #1; (B) a 4-position flow-through selector valve in position #2; (C) the slurry slurry auto-sampler in loading position with the 4-position flow-through selector valve, i.e. the auto-sampling valve, in position #3; (D) the slurry auto-sampler in injection position with the 4-position flow-through selector valve, i.e. the auto-sampling valve, in position #4.

one more step to be in position #4 as shown in Figure 4.2D, the selected stream is supposed to be S4 (purposely closed in Figure 4.2D as described in the next paragraph) which would use groove G1, while the independent streams should be S1, S1 and S3 (purposely closed in Figure 4.2D as described in the next paragraph), which would use grooves G2, G3 and G4, respectively.

Figure 4.2C and 4.2D demonstrated how this 4-position flow-through selector valve functioned as an auto-sampling valve in this study. Inlet port P2, groove G3 and outlet port P1 were utilized to allow a slurry sample flow stream at a flow rate of approximately 1.5 mL/s driven by a home-made aspirator. Inlet port P4, groove G4 and outlet port P3 were utilized to allow a FIA solvent flow stream at a flow rate of 2 mL/min driven by an HPLC pump. At the same time, ports 5-8 and the common outlet port were plugged to avoid possible interference from air bubbles. The movement of the valve rotor was controlled by a computer with in-house software. When the valve rotor is in position #3 as shown in Figure 4.2C, groove G3 was loaded with slurry sample (approximately 10 μL). Then the valve rotor is rotated to be in position #4 as shown in Figure 4.2D and slurry sample trapped in groove G3 was injected into the FIA flow stream.

The aspirator (Figure 4.1B) was assembled by centering a narrower stainless steel capillary (O.D. 1.47 mm, I.D. 1.07 mm) in a wider one (O.D. 3.05 mm, I.D. 2.39 mm) through an appropriate tee (Valco, Huston, TX). It was able to aspirate the slurry sample through the auto-sampling valve at a flow rate of approximately 1.5 mL/s when 80 psi of nitrogen gas passed through the narrower capillary. This aspiration is the result of the

Venturi effect, which generates negative pressure at the outlet of the nitrogen gas flow. Notably, the sufficient inter-space between the inner and outer stainless steel capillaries was able to prevent the aspirator from being clogged by slurry samples.

The additional flow-switch valve was a 6-port and 2-position switching valve (Valco, Huston, TX). In one position as shown in Figure 4.2C, it allowed a slurry sample flow stream for sample loading purposes. In the second position as shown in Figure 4.2D, it allowed not only the slurry sample flow to turn off for sample conservation after loading but also generated a cleaning solvent flow for better reproducibility and less clogging. As shown in Figures 4.2C and 4.2D, ports 2 and 6 were the inlets for slurry samples and cleaning solvent, respectively, while port 1 was the common outlet for both solvent and slurry sample. The flow-switch valve was controlled by the same in-house software as the auto-sampling valve to allow synchronized rotations of both valve rotors.

For the injection of slurry samples, 1 second was allowed for the valves at positions in Figure 4.2C so that a slurry flow was initiated and groove G3 of the auto-sampling valve was filled with slurry sample. Once the valve rotors were rotated clockwise to be at positions as shown in Figure 4.2D, the slurry sample trapped in groove G3 of the auto-sampling valve was carried downstream by the FIA solvent for APCI-MS analysis. For each cycle, 5 mL cleaning solvent (acetonitrile) was consumed to clean the pipeline after each injection. Subsequent injection occurred when the valve rotors were rotated counter-clockwise to be at positions as shown in Figure 4.2C.

This slurry FIA setup omitted the incorporation of a splitter used in the previously reported auto-sampling FIA setup because sample overloading was not observed for the model slurry reaction. However, it incorporated an additional post-injection slurry mixer as shown in Figure 4.1C. Acetonitrile, which exhibits good solubility towards the slurry samples, was selected as FIA solvent because the slurry samples had limited solubility in the reaction solvent, xylenes. The incorporation of a post-injection slurry mixer, constructed by introducing up to four tees (Valco, Huston, TX) into the FIA flow path to force the FIA flow to make 90 degree turns, promoted mixing, dissolution and diffusion of the slurry samples into the FIA solvent.

Detached APCI-MS. The detached APCI-MS setup (Figure 4.1D) used in this work, was previously reported to address sample overloading in quantitative real-time monitoring of homogenous process-scale reactions[75]. Briefly, a directly attached APCI source to an AccuTOF JMS-100LC time-of-flight (TOF) mass spectrometer (JEOL, Peabody, MA) was detached. Instead, a Vapur interface (Ionsense, Saugus, MA) was directly attached to the AccuTOF mass spectrometer and a 4.5 in. long and 1.07 mm I.D. stainless-steel capillary (Hamilton Company, Reno, NV), referred as the ion-transport capillary, was used to connect the center of the Vapur interface and the APCI source. A VacTorr 20 vacuum pump (Gca/Precision Scientific, Chicago, IL) was used on the Vapur interface to create pressure differential along the ion-transport capillary. The pressure in the intermediate region at the exit of the ion-transport capillary was measured to be approximately 585 Torr.

The APCI probe was modified to eliminate clogging in the analysis of slurry samples. As shown in Figure 4.3A, the commercial APCI probe used a metal capillary with 0.1 mm I.D. and 0.2 mm O.D. to conduct homogenous liquid flow, which was centered inside a wider metal capillary with a 0.3 mm I.D. tip for the nebulizing gas. The construction of a slurry APCI probe was similar. As shown in Figure 4.3B, an appropriate tee (Valco, Huston, TX) was used to center a narrow stainless steel capillary into a wider one. However, unlike the commercial APCI probe, the slurry APCI probe allows the FIA solvent flow through the inter-space between the inner and outer capillaries and the nebulizing gas through the inner capillary. This design of the slurry APCI probe provided significantly higher tolerance to heterogeneous samples.

The parameters of the APCI source were briefly optimized for 2 mL/min FIA flow rate with acetonitrile as solvent and set as follows: needle voltage, 4500 V; desolvation chamber temperature, 300 ℃; desolvation gas flow, 4 L/min. Nitrogen was used for both desolvation gas and nebulizing gas. The pressure of the nebulizing gas was optimized according to the dimension of the APCI probe and described in the RESULTS AND DISSCUSSION section. The parameters of TOF mass spectrometer were briefly optimized for the detection of MSM and set as follows: orifice 1 voltage, 20 V; orifice 2 voltage, 10 V; ring voltage, 3 V; peak voltage, 1200 V. Chromatogram-like ion intensity profiles were recorded with a mass range of *m/z* 50 to 500 and scan interval of 1.0 s.

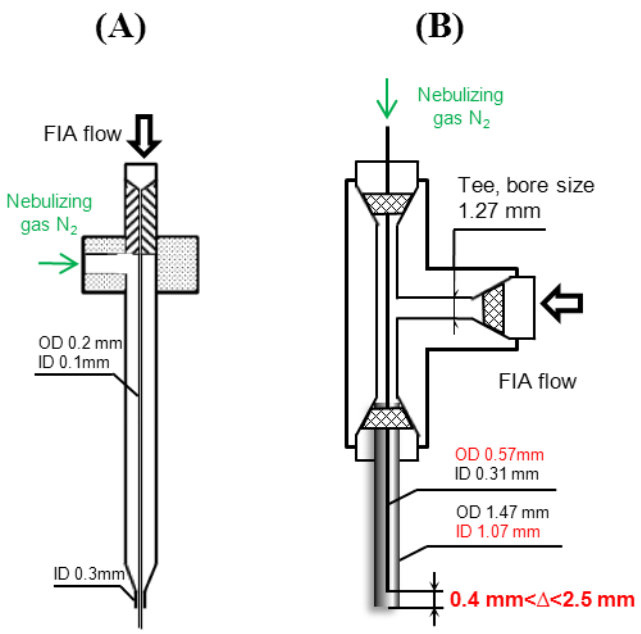

Figure 4.3 Diagram of the commercial APCI probe (A) and the slurry APCI probe (B).

Integration of peaks from the extracted ion profiles were performed with TSSPRO 3.0 software (JEOL, Peabody, MA). In order to minimize exposure to vapors, the APCI ion source was put inside a wooden box which was connected to the well ventilated lab exhaust pipe.

4.2.4 Quantitative calibration

The slurry auto-sampler was designed to load a constant volume of slurry sample, the same as a homogenous sample. Thus, the quantitative calibration for the analysis of slurry samples by the slurry FIA/APCI-MS system is a linear relationship between the peak areas of the extracted ion profiles and the equivalent molar concentration of the slurry sample. This molar concentration is calculated assuming the slurry samples are prepared as homogeneous samples. Therefore, the weight/weight concentration, which is generally used for slurry samples, for example, a 30% (w/w) MSM slurry sample in xylenes, was converted into the equivalent molar concentration before a linear regression of the quantitative calibration was performed. The relationship between the weight/weight concentration and the equivalent molar concentration of even the simplest slurry, one solid and one liquid component, is usually non-linear. Table 4.1 shows the relationship between the weight/weight concentration and the equivalent molar concentration of six MSM slurry samples in xylenes. These samples were prepared for the test of the upper limit of quantitative calibration during the development of the slurry FIA/APCI-MS system. The preparation used 25 mL volumetric flasks, an accurate MSM amount and the appropriate volume of xylenes. These preparations provided MSM slurry

Table 4.1 Preparation of MSM slurry samples in xylenes with 25 mL volumetric flasks.

Entry	W_{MSM}(g)	V_{xylene}(mL)	Concentration	
			% (w/w)	M
1	0.369	24.52	1.71	0.039
2	0.741	24.29	3.41	0.078
3	1.48	23.82	6.70	0.16
4	2.95	22.62	13.1	0.31
5	4.96	21.40	21.2	0.52
6	7.30	19.70	30.0	0.77

samples with accurate equivalent molar concentrations. Their corresponding weight/weight concentrations were calculated by using the MSM weight, the volume of xylenes and the density of xylenes, 0.864 g/mL.

To complete the calibration for quantitative real-time monitoring of the model batch slurry reaction, simulated slurry samples containing AMMT, MSM and xylenes were further prepared to represent 0%, 10%, 20%, 40%, 60%, 80% and 100% reaction progress. Table 4.2 shows the required AMMT amount, MSM amount and xylenes volume when they were mixed into 25 mL volumetric flasks. To further assess the existence of AMMT on the calibration, corresponding slurry samples containing only the MSM and xylenes were also prepared to represent 10%, 20%, 40%, 60% and 80% reaction progress (Table 4.2). All slurry samples were sonicated for 20 min and thoroughly stirred before being sampled by the slurry auto-sampler.

4.3 Results and Discussion

4.3.1 Development of the Slurry FIA/APCI-MS System

The slurry FIA/APCI-MS system was based on a previously reported auto-sampling FIA/APCI-MS which was successfully used in quantitative real-time monitoring of homogeneous process-scale reactions up to molar concentrations. In order to address the sample overloading problem caused by molar concentration samples, the auto-sampling FIA/APCI-MS system used a 1 μL automatic internal sample injector, a post-injection splitter with 1:10 splitting ratio and a detached APCI source connected to

Table 4.2 Preparation of simulated slurry samples to represent the progress of the model batch slurry reaction at 30% (w/w) level upon completing using 25 mL volumetric flasks.

Reaction progress	Simulated samples			Product only	
	W_{AMMT} (g)	W_{MSM} (g)	V_{xylene} (mL)	W_{MSM} (g)	V_{xylene} (mL)
0%	2.68	0	23.20	--	--
10%	2.41	0.730	22.65	0.730	24.30
20%	2.15	1.46	22.38	1.46	23.78
40%	1.61	2.92	21.66	2.92	22.75
60%	1.07	4.38	21.23	4.38	21.83
80%	0.537	5.84	20.56	5.84	20.82
100%	0	7.30	19.70	--	--

the mass spectrometer using a 4.5 in. long, 0.042 in. I.D. ion-transport capillary. It also used a syringe pump to deliver homogenous samples. To transform this system for the quantitative real-time monitoring of heterogeneous process-scale reactions, a few replacements were made to avoid clogging.

Replacement of the Commercial APCI Probe with a Slurry APCI Probe. To use an APCI probe for slurries requires more passage room for the FIA solvent and the slurry sample than a commercial APCI probe so that clogging of the tubing is avoided. The probe should still provide sufficient nebulization of the FIA solvent and slurry sample so that quantitative mass spectrometric analysis can be achieved. Figure 4.3 illustrates the design of such a slurry APCI probe compared to the commercial APCI probe. The dimension of the outer stainless steel capillary was first chosen as the same dimension as the commercial APCI source to be 1.07 mm I.D., 1.47 mm O.D and 4.5 in. length. The I.D. and O.D. of the inner stainless steel capillary were 0.31 and 0.57 mm, respectively. The length of the inner capillary and the pressure of the nebulizing gas were then optimized at an FIA solvent flow rate of 2 mL/min without the APCI source chamber. Visual observation of the spray indicated that the best spray was formed when the outlet of the inner capillary was approximately 0.4 to 2.5 mm inside the outlet of the outer capillary. With this APCI probe setup, better spray was usually generated with higher nebulizing gas pressure, e.g. 80 psi.

The slurry APCI probe setup was then evaluated off-line to assess its tolerance to slurry samples. When working offline, the slurry APCI probe functioned similar to the

aspirator. Slurry samples were aspirated into the slurry APCI probe directly from the sample container through a short piece of 0.06 in. I.D. PEEK tubing. Then the sample was nebulized out of the APCI probe by the nebulizing gas. When the nebulizing gas pressure was higher than 80 psi, a 30% (w/w) MSM slurry sample in xylenes was successfully sprayed without clogging.

Finally, the performance of the slurry APCI probe was compared with the commercial APCI probe for the FIA/APCI-MS analysis of a 0.039M MSM solution in acetonitrile. No significant differences were observed for either the average peak width or peak area in the extracted ion profiles of *m/z* 382 (the protonated molecular ion of MSM). However, the analyses by the slurry APCI probe did have a slightly larger RSD of five replicates than the analyses by the commercial APCI probe, i.e. 4.0% vs. 2.3%, which could be the result of larger dead volume or a less stable spray. Nevertheless, the slurry APCI probe was proven to yield acceptable quantitative results as well as the ability to handle slurry samples up to 30% (w/w).

Replacement of the 1 μL Automatic Internal Sample Injector with a 10 μL Auto-Sampling Valve. Although the auto-sampling valve functioned similarly to the automatic internal sample injector, its passage was wider so that slurry samples would not cause a clogging problem. Subsequently, its injection volume was larger. In addition, since it was originally manufactured as a 4-position flow-through selector valve, its reproducibility as an auto-sampling valve was unknown. Therefore, after the replacement, the auto-sampling valve was assessed for the FIA/APCI-MS analysis of a 0.039 M MSM solution

in acetonitrile. While obvious increase of both the peak height and the peak width in the XIPs of *m/z* 382 was observed, the RSD of five replicate analyses only increased slightly for the auto-sampling valve in comparison with the automatic internal sample injector, i.e. 5.0% vs. 4.0%.

Replacement of the Syringe Pump with an Aspirator. The third step to transform the previously reported auto-sampling FIA/APCI-MS system for homogenous samples to a slurry FIA/APCI-MS system is the introduction of an aspirator instead of a syringe pump. In addition, PEEK tubing with 0.06 in. I.D. and 1/8 in. O.D. replaced the 0.03 in. I.D. and 1/16 in. O.D. PEEK tubing, along with changes to the corresponding fittings. This aided in eliminating clogging problems. As described previously, a flow-switch valve was also incorporated in the system to save slurry samples and allow a cleaning solvent flow through the tubing for better reproducibility and less risk of clogging. The transformed slurry FIA/APCI-MS system was finally tested for the analysis of a 1.71% (w/w) MSM slurry sample in xylenes (equivalent to 0.039 M as shown in Table 4.1) and compared with the analysis of a 0.039 M MSM solution sample in acetonitrile by the previously reported auto-sampling FIA/APCI-MS system. As shown in Figure 4.4, both the peak height and the peak width in the extracted ion profiles of *m/z* 382 were increased, i.e. 2582 vs. 5136 cps and 0.27 vs. 1.50 min., which is the result of the larger sample volume and longer diffusion time before APCI-MS analysis. The injection volume was increased from 1 to 10 μL and the diffusion time was increased from 4 to 21 seconds (the length of the tubing between the auto-sampling valve and the slurry APCI

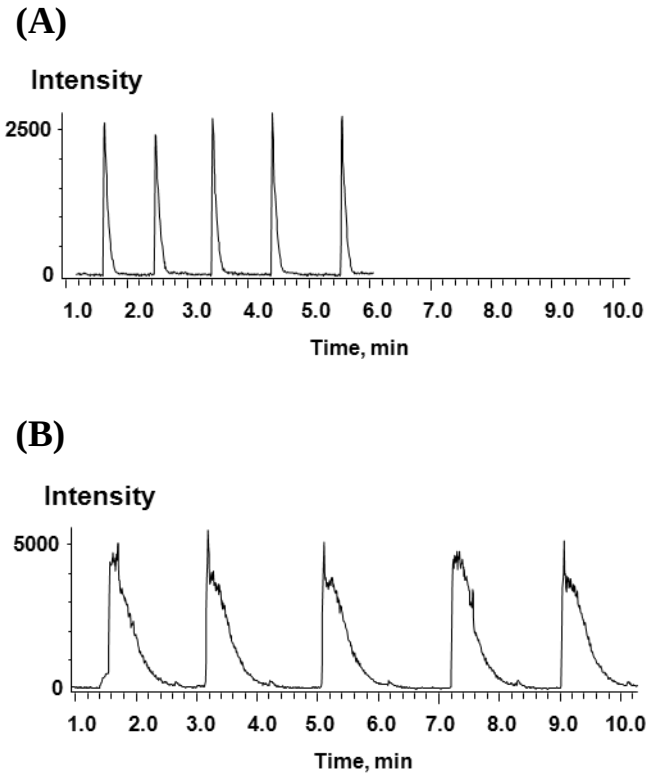

Figure 4.4 Extracted ion profiles of the $[MSM + H]^+$ ion: (A) Analysis of a 0.039 M MSM solution sample in acetonitrile by the previously reported auto-sampling FIA/APCI-MS system; (B) analysis of a 1.71% (w/w) MSM slurry sample in xylenes (equivalent to 0.039 M) by the slurry FIA/APCI-MS system.

probe was 12 inches). The relative standard deviation for five replicates of the two measurements was 2.3% for the analyses by the auto-sampling FIA/APCI-MS system and 5.4% by the slurry FIA/APCI-MS system. Both RSDs were satisfactory for quantitative real-time monitoring of batch slurry reactions. Most importantly, no clogging was observed by the slurry FIA/APCI-MS system for the analysis of the 1.71% (w/w) MSM slurry sample in xylenes.

Incorporation of a Post-injection Slurry Mixer. The last step to complete the slurry FIA/APCI-MS system was the incorporation of a post-injection slurry mixer. This mixer was found to be necessary when higher concentration, i.e. 3.41, 6.70, 13.1, 21.2, and 30% (w/w), MSM slurry samples in xylenes were analyzed. Without a post-injection slurry mixer, the original linear calibration (r^2=0.9907) by plotting peak areas of extracted ion profiles of *m/z* 382 against equivalent molar concentrations of slurry samples deviated after 6.7% (w/w); and larger relative errors (REs), i.e. -22.5, -38.6 and -43.0%, were observed as the slurry concentration increased to be 13.1, 21.2 and 30 % (w/w), respectively (Table 4.3). It is hypothesized that these high errors are the result of the dissolution process of MSM originally dispersed in xylenes as slurry samples comes into contact with the acetonitrile used as the FIA solvent. The post-injection slurry mixer was constructed by using up to four tees in the FIA flow path to force the FIA flow making 90 degree turns while maintaining the total length of the tubing between the auto-sampling valve and the slurry APCI probe constant at 48 inches (Figure 4.1C). The post-injection slurry mixer promoted turbulence so that mixing, dissolution and diffusion of

Table 4.3 Effects of the post-injection slurry mixer on relative standard deviation (RSD) and relative error (RE) of the quantitative calibration of MSM by the slurry FIA/APCI-MS system.

Number of 90 ° turns	W/W Conc. (Molar Conc.)	1.71% (0.039)	3.41% (0.078)	6.70% (0.16)	13.1% (0.31)	21.2% (0.52)	30.0% (0.77)	Correlation coefficient R^2
0	Mean (M)	0.042	0.084	0.149	*0.240*[a]	*0.320*	*0.437*	0.9907
	RSD (%)	4.5	5.2	6.1	*9.8*	*11.2*	*15.2*	
	RE (%)[b]	7.3	7.1	-3.7	*-22.5*	*-38.6*	*-43.0*	
1	Mean (M)	0.041	0.083	0.148	0.311	*0.421*	*0.591*	0.9965
	RSD (%)	4.8	11.4	2.3	2.2	*8.4*	*6.3*	
	RE (%)	5.0	6.1	-4.3	0.3	*-19.1*	*-22.8*	
2	Mean (M)	0.040	0.070	0.175	0.340	0.508	0.757	0.9927
	RSD (%)	2.0	5.5	2.3	3.1	1.2	3.6	
	RE (%)	3.0	-10.3	9.4	9.7	-2.4	-1.2	
3	Mean (M)	0.036	0.090	0.167	0.297	0.499	0.783	0.9982
	RSD (%)	5.0	6.4	2.1	3.0	0.7	2.3	
	RE (%)	-8.5	9.0	7.8	-4.2	-4.3	2.2	
4	Mean (M)	0.044	0.089	0.167	0.281	0.498	0.790	0.9971
	RSD (%)	5.5	0.9	4.7	4.2	2.9	3.1	
	RE(%)	12.9	9.0	7.7	-9.4	-4.4	3.1	

a. Italic points were not included in the quantitative linear calibration.
b. Calculated mean from linear equation vs. authentic values from sample preparations.

the slurry samples into the FIA solvent would be more complete. As shown in Table 4.3, the incorporation of a post-injection slurry mixer with one and two tees into the slurry FIA/APCI-MS system did extend the upper limit of linear calibration to 21.2 and 30% (w/w) with the correlation coefficient determined to be 0.9965 and 0.9927, respectively. The RSDs of three replicates analysis also moderately decreased. This quantitative linear calibration up to 30% (w/w) concentration for the MSM slurry samples remained when three or four tees were incorporated into the post-injection slurry mixer with comparable RSDs. In order to better understand the effect of the post-injection slurry mixer, the change of peak profiles was examined as an increasing number of tees were incorporated into the post-injection slurry mixer. It appeared that as the number of tees increased, more and more Gaussian-like peak profiles were observed for the MSM slurry samples. For the 21.2% (w/w) MSM slurry sample, the asymmetry factor[48] of its peaks decreased from 11.8, 5.6, 4.2 and 2.1 to 1.9 as the number of tees increased from none, 1, 2 and 3, to 4, respectively. For optimum performance in quantitative real-time monitoring of the model batch slurry reaction, a post-injection slurry mixer with three tees was chosen to be incorporated into the slurry FIA/APCI-MS system for further tests.

4.3.2 Quantitative Calibration

In order to quantitatively monitor the model batch slurry reaction in real time, matrix effects on the mass spectrometric response need to be considered. For these experiments, this was realized by simulating the reaction progress using standard mixtures containing one reactant and the product, i.e. AMMT and MSM. The simulation

omitted the other reactant, MIB, due to its high reactivity and moisture sensitivity. Because the model slurry reaction is usually performed in commercial manufacturing at 30% (w/w) upon completion of the reaction, the simulation was carried on at the equivalent 0.77M MSM level and at 100% conversion. As shown in Table 4.3, simulated reaction mixtures containing AMMT and MSM in xylenes were prepared to represent the progress of the model slurry reaction at 0, 10, 20, 40, 60, 80, and 100%. Each simulated reaction mixture was then analyzed with five replicates by the slurry FIA/APCI-MS under optimum conditions.

Figure 4.5 shows mass spectra of the slurry samples in xylenes representing 10%, 40% and 80% completion of the reaction. As the reaction progress advanced, the signal from the $[M+H]^+$ ion of the product, MSM, at *m/z* 382 increased, while the signal from the $[M+H]^+$ of the reactant, AMMT, at *m/z* 141 decreased. Since the mass spectrometric parameters were optimized to detect MSM, the response from MSM was higher than that from AMMT even at 10% reaction progress. Quantitative calibration of MSM showed acceptable linearity and reproducibility with a correlation coefficient of 0.999 and RSDs of 2.9-6.2%. Quantitative calibration of AMMT was unsuccessful, most likely due to its adsorption onto the inner surface of the slurry FIA/APCI-MS system caused by its amine groups[8]. It should be noted that the sampling interval to use the slurry FIA/APCI-MS system in process control of the model batch slurry reaction is close to 5 min because the peak profile of *m/z* 382 extracted ion became wider and wider as the

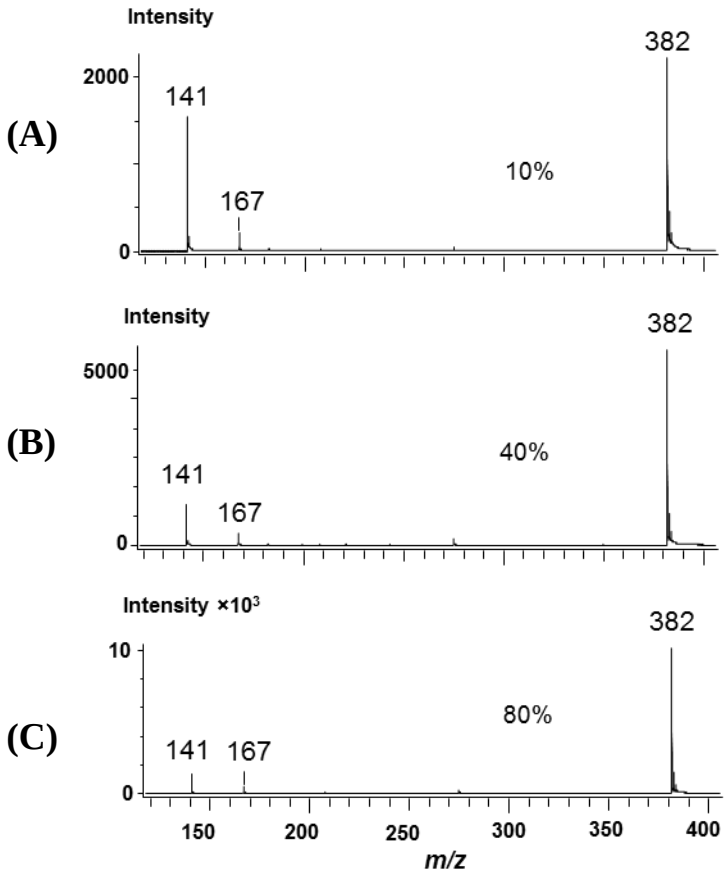

Figure 4.5 Mass spectra of simulated slurry samples representing the progress of the model batch slurry reaction at 30% (w/w) level upon completion: (A) 10%, (B) 40%; (C) 80% reaction completion.

Table 4.4 Matrix effects of AMMT on the quantitation of MSM.

Reaction progress	Simulated samples		MSM only		Deviation of PA
	PA[a] ($x10^6$)	RSD %	PA ($x10^6$)	RSD%	
10%	0.45	7.0	0.51	4.2	-12.4%
20%	0.82	6.4	0.85	2.6	-3.89%
40%	1.45	5.2	1.46	6.5	1.35%
60%	2.02	6.7	2.16	6.9	-6.08%
80%	2.56	4.8	2.66	4.4	-3.86%

a. Peak area

concentration of MSM increased, 1.7 versus 5 min for reaction completion levels of 10 versus 100%.

The matrix effect of AMMT on the quantitation of MSM was further investigated. Standard samples containing only MSM and simulated reaction mixtures containing AMMT and MSM were prepared to represent the progress of the model reaction at 10, 20, 40, 60 and 80% of a 30% (w/w) level slurry reaction upon completion. At each concentration, the simulated reaction mixtures were analyzed next to the standard MSM samples for side-by-side comparison. As summarized in Table 4.4, the matrix effect originated from the presence of AMMT lead to suppressed peak areas of *m/z* 382 extracted ion profiles and increased RSDs for simulated samples. The deviations of peak areas of *m/z* 382 between the simulated reaction mixtures and the MSM samples, however, were comparable to the RSDs of the quantitative calibration as seen for the samples where reactants were present. An exception to this was the higher deviation observed when simulating 10% competition of the reaction, where the *m/z* 382 signal were moderately suppressed by the massive AMMT present in the simulated sample. The increased RSDs might be also caused by the increased complexity in sample mixing/diffusion when two materials were present in the slurry. Nevertheless, the matrix effect of quantitative real-time reaction monitoring of the model reaction was insignificant in most case, and the calibration curve can be obtained by analyzing standard MSM samples.

4.4 Conclusion

An innovative slurry FIA/APCI-MS system for quantitative real-time monitoring of a model process-scale batch slurry reaction has been developed by modifying our previously reported auto-sampling FIA/APCI-MS system for quantitative real-time monitoring of process-scale homogeneous reactions. This slurry FIA/APCI-MS system introduced an APCI probe for slurries, a 10 μL auto-sampling valve and an aspirator to replace the commercial APCI probe, the 1 μL automatic internal sample injector and a syringe pump in the auto-sampling FIA/APCI-MS system, respectively. As a result, both sample overloading and system clogging which have been encountered in quantitative real-time monitoring of process-scale batch slurry reactions have been solved. With the further incorporation of a post-injection slurry mixer, quantitative calibration has been achieved at 30% (w/w) slurry concentration as is needed to apply this system to commercial scale monitoring of a model batch slurry reaction.

It is noted that the slurry FIA/APCI-MS system used a FIA solvent, acetonitrile, with good dissolution ability towards the solid components of the model batch slurry reaction. Under optimum operational conditions, although no evidence indicated total dissolution of AMMT and MSM before APCI nebulization, no immediate solid deposit was observed in the heated APCI chamber after APCI nebulization. The slurry FIA/APCI-MS system is applicable in quantitative real-time monitoring of process-scale heterogeneous reactions with dispersion of solid materials. It is also able to quantitatively monitor process-scale homogenous reactions in real time.

Reference

(1) Workman, J.; Lavine, B.; Chrisman, R.; Koch, M. *Anal. Chem.* **2011**, *83*. 4557-4578.

(2) U.S. Food and Drug Administration. Guidance for Industry PAT — A Framework for Innovative Pharmaceutical Development, Manufacturing, and Quality Assurance. http://www.fda.gov (accessed Feb. 20, 2013).

(3) U.S. Food and Drug Administration. Pharmaceutical cGMPs for the 21st Century - A Risk-Based Approach. http://www.fda.gov (accessed Feb. 20, 2013).

(4) ICH Expert Working Group. ICH HARMONISED TRIPARTITE GUIDELINE PHARMACEUTICAL DEVELOPMENT Q8(R2). http://www.ich.org (accessed Feb. 20, 2013).

(5) European Medicines Agency Inspections. Reflection Paper: Chemical, pharmaceutical and biological information to be included in dossiers when Process Analytical Technology (PAT) is employed. http://www.gmp-compliance.org (accessed Feb. 20, 2013).

(6) Chen, Z. P.; Lovett, D.; Morris, J. *J. Process. Contr.* **2011**, *21*. 1467-1482.

(7) Dalitz, F.; Cudaj, M.; Maiwald, M.; Guthausen, G. *Prog. Nucl. Magn. Reson. Spectrosc.* **2012**, *60*. 52-70.

(8) Zhu, Z. Q.; Bartmess, J. E.; McNally, M. E.; Hoffman, R. M.; Cook, K. D.; Song, L. G. *Anal. Chem.* **2012**, *84*. 7547-7554.

(9) Maiwald, M.; Fischer, H. H.; Kim, Y. K.; Albert, K.; Hasse, H. *J. Magn. Reson.* **2004**, *166*. 135-146.

(10) Maiwald, M.; Grutzner, T.; Strofer, E.; Hasse, H. *Anal. Bioanal. Chem.* **2006**, *385*. 910-917.

(11) Bernstein, M. A.; Stefinovic, M.; Sleigh, C. J. *Magn. Reson. Chem.* **2007**, *45*. 564-571.

(12) Khajeh, M.; Bernstein, M. A.; Morris, G. A. *Magn. Reson. Chem.* **2010**, *48*. 516-522.

(13) Skloss, T. W.; Kim, A. J.; Haw, J. F. *Anal. Chem.* **1994**, *66*. 536-542.

(14) Guthausen, G.; von Garnier, A.; Reimert, R. *Appl. Spectrosc.* **2009**, *63*. 1121-1127.

(15) Nordon, A.; Diez-Lazaro, A.; Wong, C. W. L.; McGill, C. A.; Littlejohn, D.; Weerasinghe, M.; Mamman, D. A.; Hitchman, M. L.; Wilkie, J. *Analyst* **2008**, *133*. 339-347.

(16) Vargas, M. A.; Cudaj, M.; Hailu, K.; Sachsenheimer, K.; Guthausen, G. *Macromolecules* **2010**, *43*. 5561-5568.

(17) Kuster, S. K.; Danieli, E.; Blumich, B.; Casanova, F. *Phys. Chem. Chem. Phys.* **2011**, *13*. 13172-13176.

(18) Lee, E. D.; Mueck, W.; Henion, J. D.; Covey, T. R. *J. Am. Chem. Soc.* **1989**, *111*. 4600-4604.

(19) Fabris, D. *Mass. Spectrom. Rev.* **2005**, *24*. 30-54.

(20) Colgan, S. T.; Sharp, T. R.; Hammen, P. D.; Reed, R. H.; Horna, G. J.; Gwiazda, P. W. *Talanta* **1996**, *43*. 851-857.

(21) Hathout, Y.; Fabris, D.; Han, M. S.; Sowder, R. C., 2nd; Henderson, L. E.; Fenselau, C. *Drug Metab. Dispos.* **1996**, *24*. 1395-400.

(22) Arakawa, R.; Lu, J.; Mizuno, K.; Inoue, H.; Doe, H.; Matsuo, T. *Int. J. Mass Spectrom. Ion Processes.* **1997**, *160*. 371-376.

(23) Zaia, J.; Fabris, D.; Wei, D.; Karpel, R. L.; Fenselau, C. *Protein Sci.* **1998**, *7*. 2398-404.

(24) Brum, J.; Dell'Orco, P. *Rapid Comm. Mass Spectrom.* **1998**, *12*. 741-745.

(25) Fligge, T.; Kast, J.; Bruns, K.; Przybylski, M. *J. Am. Soc. Mass Spectrom.* **1999**, *10*. 112-118.

(26) Kobayashi, N.; Fujimori, I.; Watanabe, M.; Ikeda, T. *Anal. Biochem.* **2000**, *287*. 272-278.

(27) Hogenboom, A. C.; de Boer, A. R.; Derks, R. J. E.; Irth, H. *Anal. Chem.* **2001**, *73*. 3816-3823.

(28) Dennhart, N.; Weigang, L. M. M.; Fujiwara, M.; Fukamizo, T.; Skriver, K.; Letzel, T. *J Biotechnol* **2009**, *143*. 274-283.

(29) Dell‘Orco, P.; Brum, J.; Matsuoka, R.; Badlani, M.; Muske, K. *Anal. Chem.* **1999**, *71*. 5165-5170.

(30) Brum, J.; Dell'Orco, P.; Lapka, S.; Muske, K.; Sisko, J. *Rapid Commun. Mass Spectrom.* **2001**, *15*. 1548-1553.

(31) Clinton, R.; Creaser, C. S.; Bryant, D. *Anal. Chim. Acta* **2005**, *539*. 133-140.

(32) Ma, X.; Zhang, S.; Lin, Z.; Liu, Y.; Xing, Z.; Yang, C.; Zhang, X. *Analyst* **2009**, *134*. 1863-7.

(33) Zhu, L.; Gamez, G.; Chen, H. W.; Huang, H. X.; Chingin, K.; Zenobi, R. *Rapid Commun. Mass Spectrom.* **2008**, *22*. 2993-2998.

(34) McCullough, B. J.; Bristow, T.; O'Connor, G.; Hopley, C. *Rapid Commun. Mass Spectrom.* **2011**, *25*. 1445-1451.

(35) Cho, D. S.; Gibson, S. C.; Bhandari, D.; McNally, M. E.; Hoffman, R. M.; Cook, K. D.; Song, L. G. *Rapid Commun. Mass Spectrom.* **2011**, *25*. 3575-3580.

(36) Petucci, C.; Diffendal, J.; Kaufman, D.; Mekonnen, B.; Terefenko, G.; Musselman, B. *Anal. Chem.* **2007**, *79*. 5064-5070.

(37) Ma, X. X.; Zhang, S. C.; Zhang, X. R. *Trac-trend. Anal. Chem* **2012**, *35*. 50-66.

(38) Geladi, P.; Macdougall, D.; Martens, H. *Appl. Spectrosc.* **1985**, *39*. 491-500.

(39) Barnes, R. J.; Dhanoa, M. S.; Lister, S. J. *Appl. Spectrosc.* **1989**, *43*. 772-777.

(40) Helland, I. S.; Naes, T.; Isaksson, T. *Chemometr. Intell. Lab.* **1995**, *29*. 233-241.

(41) Pedersen, D. K.; Martens, H.; Nielsen, J. P.; Engelsen, S. B. *Appl. Spectrosc.* **2002**, *56*. 1206-1214.

(42) Martens, H.; Nielsen, J. P.; Engelsen, S. B. *Anal. Chem.* **2003**, *75*. 394-404.

(43) Thennadil, S. N.; Martens, H.; Kohler, A. *Appl. Spectrosc.* **2006**, *60*. 315-321.

(44) Steponavicius, R.; Thennadil, S. N. *Anal. Chem.* **2009**, *81*. 7713-7723.

(45) Steponavicius, R.; Thennadil, S. N. *Anal. Chem.* **2011**, *83*. 1931-1937.

(46) Chen, Z. P.; Morris, J.; Martin, E. *Anal. Chem.* **2006**, *78*. 7674-7681.

(47) Jin, J. W.; Chen, Z. P.; Li, L. M.; Steponavicius, R.; Thennadil, S. N.; Yang, J.; Yu, R. Q. *Anal. Chem.* **2012**, *84*. 320-326.

(48) Foley, J. P.; Dorsey, J. G. *Anal. Chem.* **1983**, *55*. 730-737.

Chapter 5. Slurry Flow Injection Analysis coupled with APCI Mass Spectrometry for Quantitative Real-Time Monitoring of Batch Slurry Reactions: An Alternative Setup

Abstract

This study aimed to optimize the method of slurry flow injection analysis atmospheric pressure chemical ionization mass spectrometry (slurry FIA/APCI-MS), which was recently introduced and validated by us using a JEOL AccuTOF time-of-flight mass spectrometer, to be used in quantitative real-time monitoring of a model batch slurry reaction at DuPont Crop Protection where a Waters LCZ single quadrupole mass spectrometer was to be used. Both of the slurry FIA/APCI-MS setups consisted of a slurry FIA and a detached APCI-MS setup, but the new slurry FIA setup had to be incorporated with a thermostatted column compartment and a post-injection splitter because the new detached APCI-MS setup was totally different and its heater, which was adapted from a Waters Quattro II triple quadrupole mass spectrometer, lacked heating capacity. After construction, modification and optimization, the new slurry FIA/APCI-MS setup demonstrated a dynamic range of quantitation of over two orders of magnitude and a limit of detection (LOD) of 0.016% (w/w) concentration in the analysis of metsulfuron methyl (MSM) slurry samples in xylenes. It was further tested with simulated slurry mixture samples of the model batch slurry reaction at 30% (w/w) slurry concentration upon completion. A linear quantitative calibration has been achieved for the product, i.e. MSM, with a 0.9946 R^2 and 3.7-12.2% relative standard deviation (RSD) for five replicates.

5.1 Introduction

Mass spectrometry is one of the most widely used analytical tools because of its high selectivity, high sensitivity and its ability to couple separation techniques. Today, there are many types of mass analyzers such as magnetic sector, quadrupole mass filter, ion trap, time-of-flight (TOF), Fourier transform ion cyclotron resonance (FTICR) and orbitrap. They are commercialized as either standalone mass spectrometers or hybrid tandem ones after being combined with each other. Mass analyzers can be categorized into low-resolution and high-resolution. Low-resolution mass analyzers include quadrupole mass filter and ion trap[1-4], which have been coupled to either gas or liquid chromatography and are powerful tools in quantitative analysis. Traditional high-resolution mass analyzers are double-focusing magnetic sectors, which were established in the 1960s and usually coupled to gas chromatography for the analysis of volatile compounds. Other high-resolution mass analyzers include TOF, FTICR and orbitrap[5-6]. They have become very popular in recently years, often coupled to liquid chromatography and widely used in "omics" research[5-6], clinical and forensic toxicology [7], doping control[7], drug metabolism studies[8], food analysis[9] and environmental sciences[10].

Although mass spectrometers have now become quite affordable, they are still high-end instruments which are usually located in central analytical laboratories for off-site analysis. For on-site control of an industrial manufacture process, high-resolution mass spectrometers have the disadvantage of high cost and the spatial and/or environmental needs to maintain high resolving power. In contrast, low-resolution mass

spectrometers are low cost, robust, better in quantitative analysis and offer sufficient resolving power in characterization of reaction mixture samples. In addition, there has been a significant effort in making low-resolution mass spectrometers portable for on-site analysis[11-14], though the current motivation focuses in areas such as national security, emergency response, law enforcement, health care, pollution control and illicit drug detection.

Sampling and ionization are crucial to successfully applying mass spectrometry in qualitative and quantitative analysis. Because of high concentration and heterogeneity, samples from industrial batch slurry reactions pose an extreme challenge. Although atmospheric pressure ionization (API) techniques[15-28], e.g. electrospray ionization (ESI) and atmospheric pressure chemical ionization (APCI), have been used in real-time reaction monitoring, direct introduction of samples from industrial batch slurry reactions into either ESI or APCI sources will definitely result in overloading and clogging[29-30]. Many ambient ionization techniques have also been used in real-time reaction monitoring [31-43] and three of them, i.e. low temperature plasma (LTP)[32], extracted electrospray ionization (EESI)[33-34] and direct analysis in real-time (DART)[35-36], have been demonstrated to be able to analyze homogenous and/or heterogeneous reaction mixtures at molar concentrations. However, quantitative data have not been demonstrated.

To our knowledge, slurry flow injection analysis atmospheric pressure chemical ionization mass spectrometry (slurry FIA/APCI-MS)[30] is currently the only available analytical method for quantitative real-time monitoring of industrial heterogeneous

reactions. This method was recently introduced (Figure 4.1) and validated by us using a JEOL AccuTOF time-of-flight mass spectrometer because its APCI source could be easily adapted for the sampling and ionization of heterogeneous samples at up to molar concentration. In this study, an alternative slurry FIA/APCI-MS setup was developed using a Waters Quattro II triple quadrupole mass spectrometer in our lab. It aimed to develop the slurry FIA/APCI-MS method to be used at DuPont Crop Protection where a Waters LCZ single quadrupole mass spectrometer, which was retired from its central analytical laboratory and used an identical APCI source as the Waters Quattro II triple quadrupole mass spectrometer, was identified to be used in quantitative real-time monitoring of a model batch slurry reaction.

5.2 Experimental

5.2.1 Reagent

2-Amino-4-methoxy-6-methyl-1,3,5-triazine (AMMT) and metsulfuron methyl (MSM) were industrial grade and provided by DuPont Crop Protection (Newark, Delaware). Certified A.C.S. grade xylenes, generally a mixture of the *ortho*-, *meta*- and *para*-isomers and perhaps containing some ethylbenzene, was purchase from Fisher Scientific (Pittsburgh, PA). It was used as the liquid component of simulated slurry samples because the corresponding industrial grade reagent is currently used in industrial manufacturing of MSM by DuPont Crop Protection. AMMT and MSM have very limited solubility in xylenes, approximately 1.73 mM (0.245 mg/mL) and 2.76 mM (1.05

mg/mL), respectively, by experiments in our lab after sufficient time of ultrasonication. HPLC grade acetonitrile was also purchased from Fisher Scientific (Pittsburgh, PA). It was used as FIA solvent. The solubility of AMMT and MSM in acetonitrile was approximately 10.0 mM (1.40 mg/mL) and 65.6 mM (21.2 mg/mL), respectively, by experiments in our lab, again after sufficient time of ultrasonication.

5.2.2 Model batch slurry reaction

The same model batch slurry reaction was studied as in our previous study[30]. As shown in Scheme 5.1, MSM, a sulfonylurea herbicide for broadleaf weeds and some annual grasses, is synthesized by a coupling reaction between AMMT and methyl 2-(isocyanatosulfonyl) benzoate (MIB) in xylenes. This is a typical batch slurry reaction due to the extremely low solubility of AMMT and MSM in xylenes. Of the three compounds involved in this reaction, MIB has much higher solubility in xylenes than AMMT and MSM and can remain dissolved up to 1 M. However, MIB is moisture sensitive and can be easily hydrolyzed in air. In industrial manufacture, this slurry reaction is usually performed at 30.0% (w/w) upon completion of the reaction; and an average particle size of less than 10 μm has been determined for MSM.

5.2.3 Instrumentation

The slurry FIA/APCI-MS method was recently introduced and validated using a JEOL AccuTOF time-of-flight mass spectrometer (Peabody, MA). In this study, an alternative slurry FIA/APCI-MS setup was constructed using a Waters Quattro II triple

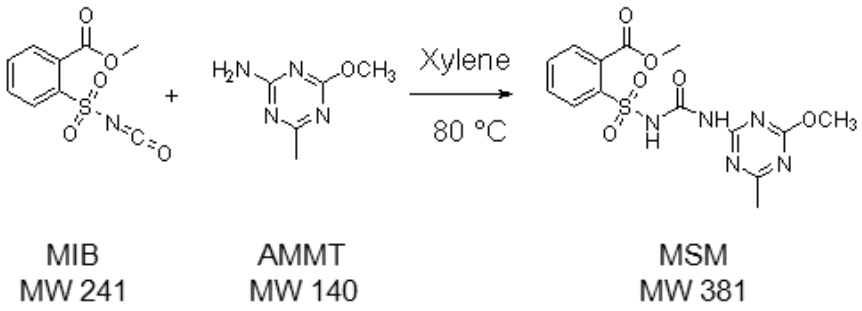

Scheme 5.1 The model batch slurry reaction: coupling reaction of AMMT and MIB for the production of MSM.

quadrupole mass spectrometer (Milford, MA). However, both of the setups consisted of a slurry FIA setup and a detached APCI-MS setup (Figure 5.1).

Detached APCI-MS setup. Because the configuration of the commercial APCI sources between the JEOL AccuTOF time-of-flight mass spectrometer and the Waters Quattro II triple quadrupole mass spectrometer were totally different, the construction of the two detached APCI-MS setups differed significantly. Figure 5.2 shows the difference between the commercial APCI-MS setup (Figure 5.2A) and the detached APCI-MS setup (Figure 5.2B) for the Waters Quattro II triple quadrupole mass spectrometer. The commercial APCI source featured an outward-to-inward orientation relative to the mass spectrometer, whereas the detached APCI source chose a top-to-bottom orientation to minimize contamination by high concentration heterogeneous samples.

Figure 5.3A shows a detailed schematic diagram of the detached APCI-MS setup, which from left to right consisted of a Vapur interface adapter (Ionsense, Saugus, MA), an ion-transport capillary and a detached APCI source. It is noted that the commercial Vapur interface adapter was designed for other models of mass spectrometers from Waters and therefore could only fit onto the sample cone nozzle after careful machining the side next to the mass spectrometer to be much thinner and smoother. The ion-transport capillary was a 6.0 inch long, 1.47 mm outer diameter (O.D.) and 1.07 mm inner diameter (I.D.) stainless steel tubing (Hamilton, Reno, Nevada), which was 1.5 inch longer than previously used with the JEOL AccuTOF time-of-flight mass spectrometer [30] due to spatial limitation (Figure 5.2B). A VacTorr 20 vacuum pump (Gca/Precision

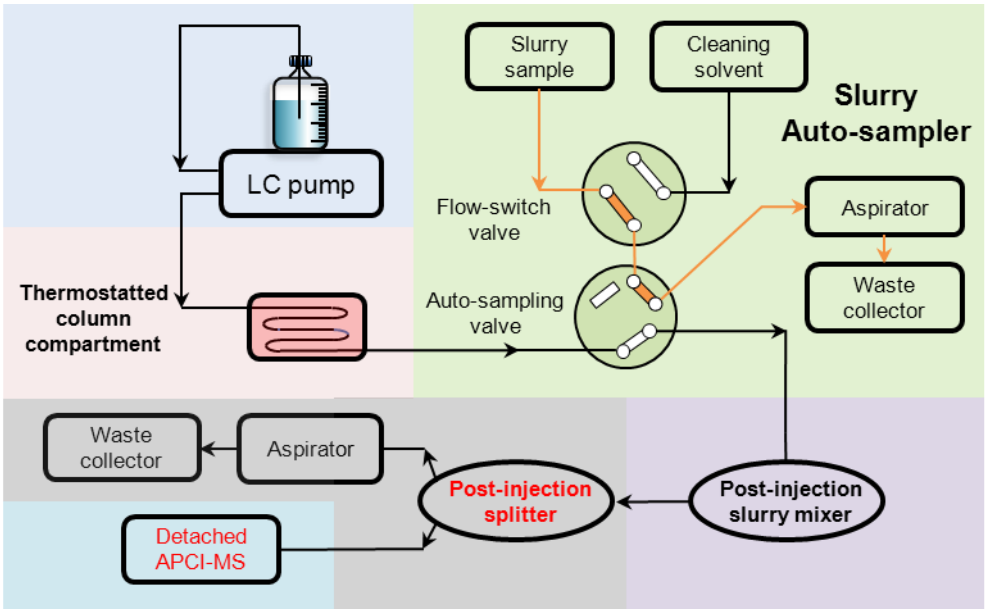

Figure 5.1 Schematic diagram of the new slurry FIA/APCI-MS setup.

(A)

(B)

Figure 5.2 Waters Quattro II triple quadrupole mass spectrometer with A) the commercial APCI-MS source, and B) the detached APCI-MS source.

Figure 5.3 Detailed schematic diagrams of: A) the detached APCI-MS setup, B) the base of the detached APCI source and C) the commercial APCI probe (left) and the slurry APCI probe (right).

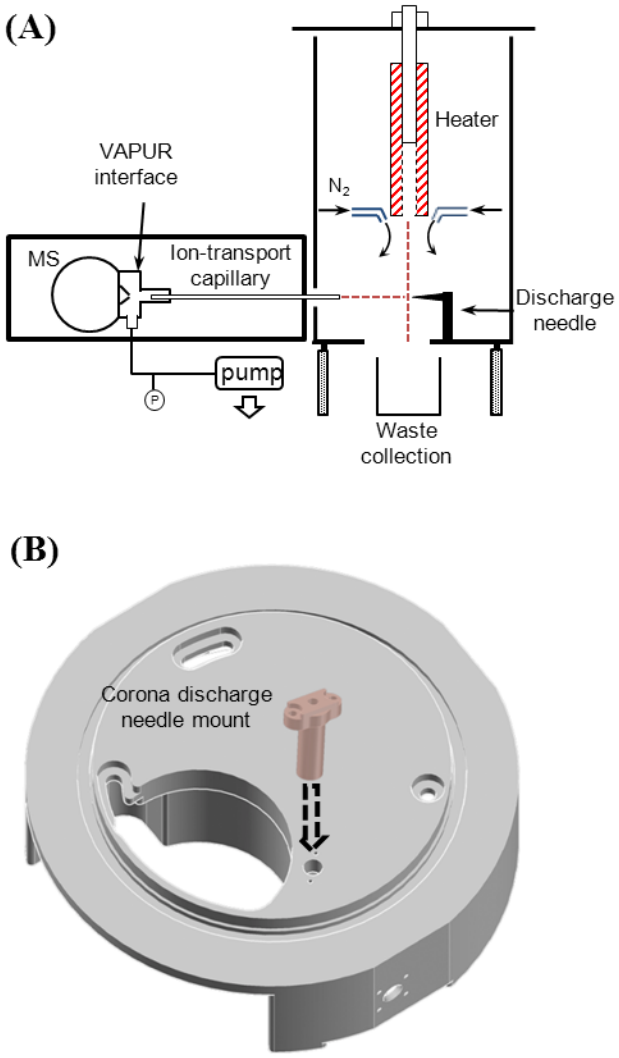

Figure 5.3 Continued.

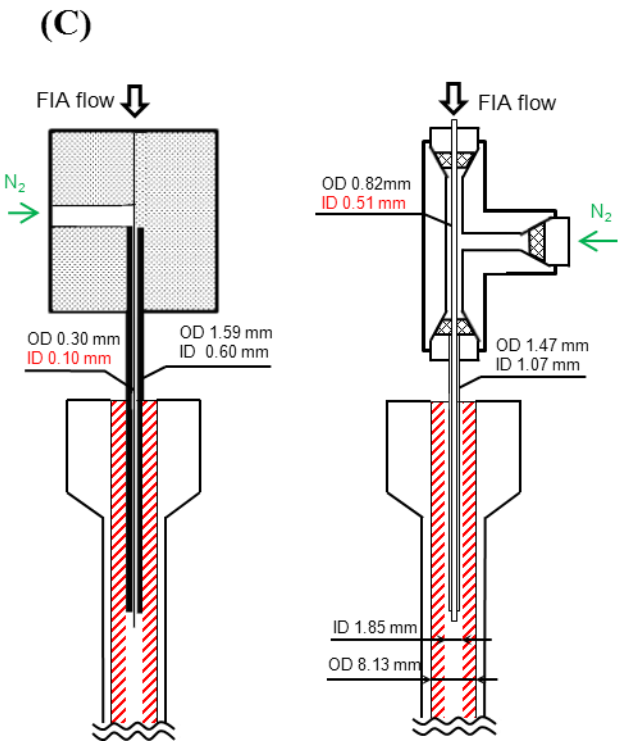

Figure 5.3 Continued.

Scientific, Chicago, IL) was used with the Vapur interface adapter to create pressure differential along the ion-transport capillary. The pressure in the intermediate region at the exit of the ion-transport capillary was measured to be approximately 526 Torr.

From bottom to top, the detached APCI source consisted of a source base, a cylindrical glass to create a source chamber, a probe base and a slurry APCI probe. The source base is home-made and illustrated in Figure 5.3B. On the top of the source base, three metal poles would be installed so that the cylindrical glass would be fitted outside and the probe base could rest on top. A corona discharge needle mount would also be installed on the top of the source base for corona discharge. The big opening on the source base was designed to exhaust waste and to reduce deposition of solid particles of heterogeneous samples inside the source chamber. On the bottom of the source base, three supporting metal legs could be installed to allow bigger waste collectors (Figure 5.2B). The cylindrical glass was home-cut to length and a glass tube was horizontally attached to it off axis so that the ion-transport capillary could be inserted inside the APCI source chamber and underneath the slurry APCI probe (Figure 5.2B). The commercial probe base was used in the detached APCI source without any modification (Figure 5.2B).

It was necessary to preplace the original APCI probe with a slurry APCI probe so that clogging would not occur due to the introduction of high concentration heterogeneous samples [30]. As shown in Figure 5.3C, both the commercial and slurry APCI probe used the same cylindrical heater assembly with 8.13 mm O.D. and 1.85 mm

I.D. In the original APCI probe (Figure 5.3C left), desolvation/nebulizing gas flowed through a stainless steel tube with 1.59 mm O.D. and 0.60 mm I.D, inside which there was a fused silica capillary with 0.30 mm O.D. and 0.10 mm I.D to accommodate a liquid flow. The slurry APCI probe (Figure 5.3C right) was assembled by using a stainless steel tube (Hamilton, Reno, Nevada) with 1.47 mm O.D., 1.07 mm I.D. and 3 inch length, inside which was centered another stainless steel tube (Hamilton, Reno, Nevada) with 0.82 mm O.D., 0.51 mm I.D. and 4.5 inch length. These two stainless steel tubes were connected together through an appropriate tee (Upchurch Scientific, Oak Harbor, WA), where heterogeneous samples could flow through the inner tubing and the desolvation/nebulizing gas flowed in between the tubing.

For optimum performance, it was found that the ends of the ion-transport capillary, the corona discharge needle and the slurry APCI probe should be aligned as shown in Figure 5.3A. The distance between the ends of the ion-transport capillary and the corona discharge needle was approximately 1.2 inch, whereas the distance between the ends of the corona discharge needle and the slurry APCI probe was approximately 1.6 inch.

Slurry FIA setup. As illustrated in Figure 5.1, the slurry FIA system consisted of an Agilent 1100 Series HPLC pump (Santa Clara, CA), an Agilent 1100 Series thermostatted column compartment (Santa Clara, CA), a slurry auto-sampler, a post-injection slurry mixer and a post-injection splitter. These components were connected together with 1/8 inch O.D. and 0.06 inch I.D. PEEK tubing (Upchurch Scientific, Oak

Harbor, WA). The slurry auto-sampler, which consisted of a flow-switch valve (Valco, Huston, TX), an auto-sampling valve (Valco, Huston, TX) and an home-made aspirator, was described in detail previously [30]. So was the post-injection slurry mixer, which was constructed by introducing three tees (Valco, Huston, TX) into the FIA flow path to force the FIA flow to make 90 degree turns.

Because the heater of the slurry APCI probe, which was adapted from the commercial APCI probe of the Waters Quattro II triple quadrupole mass spectrometer without modification, was unable to totally evaporate the FIA solvent at a flow rate of 2 mL/min, the thermostatted column compartment and the post-injection splitter was incorporated into the new slurry FIA/APCI-MS setup. The optimum temperature of the thermostatted column compartment was found to be 65 ℃ because bubbles would form in the FIA flow at higher temperature.

Following the post-injection slurry mixer, the post-injection splitter was assembled by incorporating an appropriate tee (Upchurch Scientific, Oak Harbor, WA) (Figure 5.4). To the tee, two pieces of identical PEEK tubing with 1/8 inch O.D., 0.02 inch I.D. and 18 inch length were attached, and to the two tubes the slurry APCI probe and an aspirator were connected. The aspirator was constructed similarly to the slurry APCI probe by using a stainless steel tube (Hamilton, Reno, Nevada) with 1.47 mm O.D., 1.07 mm I.D. and 4.5 inch length, inside which centered another stainless steel tube (Hamilton, Reno, Nevada) with 0.57 mm O.D., 0.31 mm I.D. and 2.5 inch length. These two stainless steel tubes were connected together through an appropriate tee

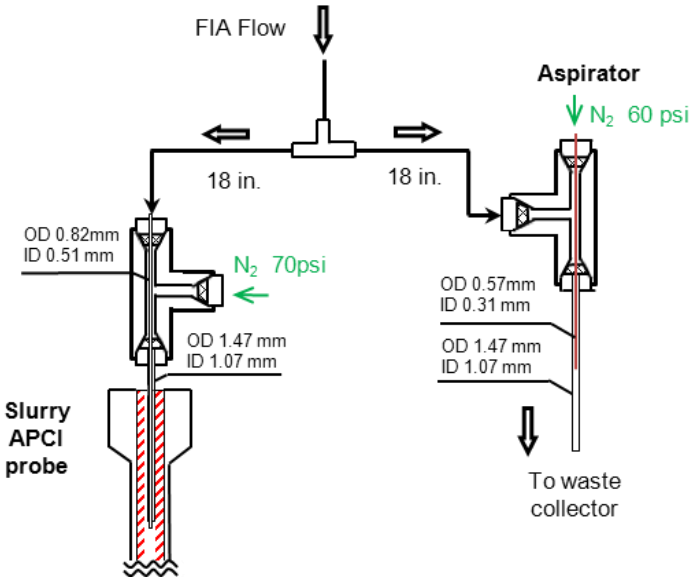

Figure 5.4 Detailed schematic diagram of the post-injection splitter using an aspirator.

(Upchurch Scientific, Oak Harbor, WA), where nitrogen gas flowed through the inner tubing and heterogeneous samples could flow in between the tubing. Alternatively, the aspirator could be replaced by a withdrawing syringe pump (Harvard Apparatus, Holliston, MA).

5.2.4 Instrumental conditions

The FIA flow rate delivered by the HPLC pump was 2 mL/min. The parameters of the detached APCI source were set as follows: capillary voltage, 4500 V; desolvation temperature, 500 ℃; desolvation gas flow, 4 L/min. Nitrogen was used as desolvation gas at a pressure of 70 psi. The parameters of the mass spectrometer were set as follows: cone voltage, 20 V; source block temperature, 120 ℃; LM Res, 14.0; HM Res, 14.0; multiplier 1, 650 V; multiplier 2, 650 V. Single ion recording (SIR: mass, *m/z* 382; dwell, 0.5 s; inter-channel delay, 0.03 s; repeat, 1; span, 1) mode was used to monitor the $[MSM + H]^+$ ion for the analysis of standard MSM slurry samples. Identical SIR followed by MS1 scan (mass, *m/z* 100-400; scan time, 2 s; inter-channel delay, 0.5 s; repeat, 1) was used for the analysis of simulated batch slurry reaction mixture samples. Integration of peaks from SIR chromatogram was performed with MassLynx 4.0 software (Waters, Milford, MA). In order to minimize exposure to vapors, the detached APCI source was put inside a home-made thick cardboard box which was connected to the lab exhaust pipe with good ventilation.

5.2.5 Quantitative calibration

Because the slurry auto-sampler was designed to load a slurry sample with a constant volume, the quantitative calibration for the analysis of slurry samples by the slurry FIA/APCI-MS should be still a linear relationship between the peak areas and the equivalent molar concentration of the slurry samples (which was calculated assuming that they were prepared as homogeneous samples). Therefore, the weight/weight concentration, which is generally used for slurry samples in industrial manufacture, e.g. a 30.0% (w/w) MSM slurry sample in xylenes, had to be converted into equivalent molar concentration before a linear regression of the quantitative calibration was performed. Standard MSM slurry samples in xylenes were prepared at 1.71, 3.41, 6.70, 13.1, 21.2, 30.0% (w/w) concentration and their equivalent molar concentration is shown in Table B1. These samples were used to investigate the upper limit of quantitative calibration during the development of the slurry FIA/APCI-MS setup. When the MSM concentration in xylenes was lower than 0.55% (w/w), MSM was totally dissolved. Three MSM solution samples in xylenes were prepared at 0.026, 0.21 and 0.43% (w/w) concentration and their equivalent molar concentration is also shown in Table B1. These samples were used together with the slurry samples to investigate the limit of detection (LOD) and the dynamic range of the quantitative calibration of the slurry FIA/APCI-MS setup.

In order to create a calibration curve for quantitative real-time monitoring of the model batch slurry reaction, simulated batch slurry reaction mixture samples containing AMMT, MSM and xylenes were further prepared to represent 0%, 1%, 5%, 10%, 20%,

40%, 60%, 80% and 100% reaction progress. Table B2 shows the required AMMT amount, MSM amount and xylenes volume when they were mixed into 25 mL volumetric flasks. This preparation omitted MIB because it is soluble in xylenes, but moisture sensitive and not expected to be hydrolyzed before the slurry samples are exposed to air in the APCI chamber. To further assess the existence of AMMT on the calibration, corresponding slurry samples containing only the MSM and xylenes were also prepared to represent 1%, 5%, 10%, 20%, 40%, 60% and 80% reaction progress. Table B2 also shows the required MSM amount and xylenes volume when they were mixed into 25 mL volumetric flasks.

All slurry samples were sonicated for 20 min and thoroughly stirred before being sampled by the slurry auto-sampler.

5.3 Results and Discussions

5.3.1 Evaluation of the detached APCI-MS setup

An FIA/APCI-MS setup consisted of a slurry FIA setup and a detached APCI-MS setup. Therefore, in principle the new FIA/APCI-MS setup using a Waters Quattro II triple quadrupole mass spectrometer could inherit the identical slurry FIA setup previously used by the FIA/APCI-MS setup using a JEOL AccuTOF time-of-flight mass spectrometer. However, the two detached APCI-MS setups differed significantly because the configuration of the commercial APCI sources for the two mass spectrometers was totally different.

The new slurry APCI probe was first tested off-line to assess its tolerance to slurry samples. Sampling was accomplished by using a short piece of 0.06 inch I.D. PEEK tubing with one end being connected to the slurry APCI probe and the other end being immersed in MSM slurry samples. Once the desolvation/nebulizing gas was turned on, MSM slurry samples were aspirated into the slurry APCI probe and then sprayed out of it. When the desolvation/nebulizing gas pressure was higher than 100 psi, a 30% (w/w) MSM slurry sample in xylenes was successfully sprayed without clogging.

The new detached APCI-MS setup was then evaluated for the analysis of MSM slurry samples with an identical slurry FIA setup as previously reported, i.e. without incorporation of the thermostatted column compartment and the post-injection splitter as shown in Figure 5.1. MSM slurry samples with 1.71, 3.41, 6.70, 13.1, 21.2 and 30.0% (w/w) concentration were sampled and analyzed in three replicates. Potential clogging by undissolved particles was not observed for any of the slurry samples. Repetitive chromatographic peaks of the $[MSM + H]^+$ ion at *m/z* 382 were recorded in SIR mode. Peak areas were integrated and plotted against the equivalent molar concentrations of the MSM slurry samples. However, the obtained upper-limit of linearity was only at 6.7% (w/w) concentration. When lower FIA flow rates, e.g. 1.5 mL/min and 1.0 mL/min, were used, the linear calibrations were improved and the upper-limit was at 21.2 % (w/w) concentration at 1.0 mL/min FIA flow rate, which probably indicated insufficient heating by the slurry APCI probe. Although lower FIA flow rate could alleviate the insufficient heating issue, longer delay time and considerably larger peak widths were inevitable, e.g.

120 s delay and 10 min peak width at 1 mL/min vs 63 s delay and 5 min peak width at 2 mL/min when analyzing 30.0% (w/w) MSM slurry sample, which was not preferred for real-time reaction monitoring. Because the slurry APCI probe adapted the same cylindrical heater assembly from the commercial APCI probe, there was not an easy solution to improve its heating capability.

5.3.2 Evaluation of the slurry FIA setup

In order to address the insufficient heating issue, a thermostatted column compartment and a post-injection splitter were incorporated into the new slurry FIA setup. The effects of FIA solvent preheating and post-injection splitting of the FIA flow were evaluated by analyzing MSM slurry samples with 1.71, 3.41, 6.70, 13.1, 21.2 and 30.0% (w/w) concentration in three replicates at 2 mL/min FIA flow rate.

As demonstrated in Figure 5.5A and 5.5B, smoother chromatographic peaks of *m/z* 382 were observed with less scattered noise at the top when the thermostatted column compartment was set at 65 ℃. In addition, signal-to-noise ratio (S/N) increased about 2.7 times for all the samples, i.e. averagely 176 vs. 66, while relative standard deviations (RSDs) slightly decreased, i.e. 0.6-5.8% vs. 2.2-9.0%. However, a "valley" in each chromatographic peak of the 13.1, 21.5 and 30.0% (w/w) MSM slurry samples was observed, which did not occur for 1.71, 3.41 and 6.70% (w/w) MSM slurry samples (Figure 5.5B). It appeared that the higher the concentration the more obvious was the "valley". When the FIA solvent was not preheated, possible "valleys" in the corresponding chromatographic peaks might be concealed by the higher scattered noise

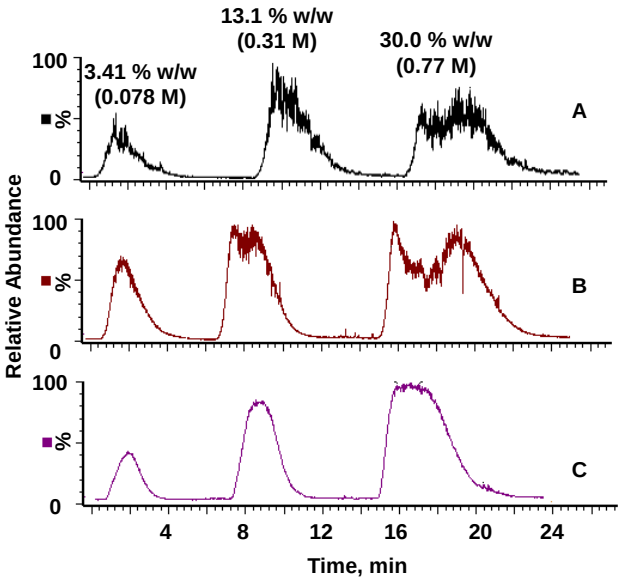

Figure 5.5 Effect of solvent preheating and post-injection splitting on the chromatographic peaks of the $[MSM + H]^+$ ion at *m/z* 382: A) without solvent preheating and post-injection splitting, B) with solvent preheating only, and C) with both solvent preheating and post-injection splitting.

(Figure 5.5A). Nevertheless, only minor improvement was achieved in establishing linear calibration and the upper-limit of linearity remained at 6.7% (w/w) concentration

Post-injection splitting would decrease the flow input to the slurry APCI probe and put less demand on the heating capacity of its heater. However, steady control of a desired split ratio was required for quantitation, which was challenging because 0.02 inch I.D. tubing had to be used for the two outlets of the post-injecting splitter to avoid clogging by slurry samples (Figure 5.4). In order to simplify the construction of the splitter, two pieces of 0.02 inch I.D. tubing with identical length, i.e. 18 inch, were used for the two outlets. Because one outlet of the splitter was connected to the slurry APCI probe where the desolvation/nebulizing gas (usually at 70 psi for optimum performance) was applied and subsequently a negative pressure was generated, flow splitting could not be achieved when the other outlet was left open. Instead, gas bubbles were observed in the FIA flow. Therefore, the construction of the splitter was focused on connecting a device to the other outlet of the splitter so that the negative pressure generated by the operation of the slurry APCI probe could be balanced. An aspirator, which was assembled similarly to the slurry APCI probe, was therefore used (Figure 5.4).

The aspirator-driven splitter was evaluated in the analysis of MSM slurry sample at 21.5% (w/w) concentration in three replicates, and the results are shown in Table 5.1. At an aspirator gas pressure of 40, 50, 55, 60 and 65 psi, chromagraphic peak areas of the $[MSM + H]^+$ ion at *m/z* 382 were compared to those without splitting, i.e. the aspirator was disconnected and the corresponding outlet was plugged. As the aspirator gas pressure

Table 5.1 Evaluation of the post-injection splitting using an aspirator.

Pressure (psi)	Plg[a]	40	50	55	60	65
RPA[b]	1.00	0.86	0.66	0.43	0.35	NA
RSD (%)	3.85	2.13	2.46	4.44	5.54	--

a. The aspirator was disconnected and the corresponding outlet of the tee was plugged.
b. Relative peak area.

increased, the peak area decreased and finally no peak was observed at 65 psi, possibly indicating a sample-to-waste splitting ratio of 0:1 due to excessive negative pressure generated by the aspirator. No significant differences in the RSDs were found with different aspirator gas pressure, which indicated a stable control of the splitting. However, it is noted that when the I.D. of the PEEK tubing in the two outlets of the splitter increased from 0.02 to 0.06 inch, the splitting became extremely difficult to control.

Alternatively, a withdrawing syringe pump was used to replace the aspirator in the splitter, which was also evaluated in the analysis of MSM slurry sample at 21.5% (w/w) concentration in three replicates and the results are shown in Table 5.2. One advantage in using a withdrawing syringe pump in the splitter was that the split flow rates were easily controlled at 0.50, 1.00, 1.25, 1.50, and 1.75 mL/min, resulting in a sample-to-waste splitting ratio of 3:1, 1:1, 5:3, 1:3 and 1:7, respectively. As shown in Table 5.2, the chromatographic peak area of the $[MSM + H]^+$ ion at *m/z* 382 slightly increased when the splitting flow started at 0.50 mL/min and the corresponding input flow to the APCI probe became 1.50 mL/min, which probably suggested that the heating of the slurry APCI probe was insufficient without splitting. As the splitting flow further increased, the peak area steadily decreased, but no significant differences in the RSDs were observed.

Another advantage in using a withdrawing syringe pump in the splitter was that 0.06 I.D. PEEK tubing could also be used with the splitter, though RSDs were slightly larger than the use of 0.02 I.D. PEEK tubing as shown in Table 5.2, which was possibly

Table 5.2 Evaluation of the post-injection splitting using a withdrawing syringe pump.

Split flow (mL/min)			0.00	0.50	1.00	1.25	1.50	1.75
Split ratio			1:0	3:1	1:1	3:5	1:3	1:7
Tubing I.D. (Inch)	0.02	RPA[a]	1.00	*1.04*	0.63	0.48	0.36	0.18
		RSD (%)	3.85	2.49	3.53	2.80	2.90	5.32
	0.06	RPA	1.00	*1.14*	0.87	0.52	0.31	0.15
		RSD (%)	2.82	8.03	3.42	9.02	6.73	8.84

a. Relative peak area.

due to less stable control of the splitting. It is noted that the peak area of the $[MSM + H]^+$ ion at *m/z* 382 slightly increased again when the splitting flow started at 0.50 mL/min, probably indicating that the heating of the slurry APCI probe was insufficient without splitting.

By comparing the data between Table 5.1 and 5.2, the sample-to-waste splitting ratio of the aspirator-driven splitter could be estimated at different aspirator gas pressure. For example, it was approximately 1:1 and 1:3, respectively, at 50 and 60 psi gas pressure.

Although the splitter using a withdrawing syringe pump provided better control of the splitting, the length of the experiments were limited by the syringe size and splitting flow rate. On the other hand, the aspirator-driven splitter did not have this limitation. Eventually in our experiments, the aspirator-driven splitter using 18 inch long and 0.02 inch I.D. PEEK tubing at 60 psi with an estimated sample-to-waste splitting ratio of 1:3 was chosen for the new slurry FIA setup. Under optimal parameter settings, MSM slurry samples at 1.71, 3.41, 6.70, 13.1, 21.2 and 30.0% (w/w) concentration were analyzed in three replicates. Gaussian-like peaks were observed without any "valley" (Figure 5.5C), and the upper-limit of quantitative linear calibration reached 30.0% w/w concentration.

5.3.3 Dynamic range of quantitation and LOD

When the MSM concentration in xylenes was lower than 0.55% (w/w), MSM was totally dissolved. Because the slurry auto-sampler was designed to load a sample with a constant volume, the slurry FIA/APCI-MS method was able to simultaneously quantify

MSM solution and slurry samples. MSM samples in xylenes at 0.026, 0.21, 0.43, 1.71, 3.41, 6.70, 13.1, 21.2 and 30.0% (w/w) concentration were analyzed in five replicates with the new slurry FIA/APCI-MS setup. The calibration was found to be linear from 0.21 to 30.0% (w/w) concentration with 0.9988 R^2 and 0.5-6.5% RSDs. Therefore, the dynamic range of quantitation by the new slurry FIA/APCI-MS setup was over two orders of magnitude, which should be enough for quantitative real-time monitoring of any batch slurry reactions. Although the MSM solution sample at 0.026% (w/w) concentration deviated from linear calibration, a LOD was subsequently calculated to be 0.016% (w/w) concentration using one-tail T test with 99% confidence.

5.3.4 Quantitative calibration

In order to quantitatively monitor the model batch slurry reaction in real time, matrix effects on the mass spectrometric response of the component(s) to be quantitated should be considered. This was realized by simulating the reaction progress using standard mixtures containing one reactant, the product and the solvent, i.e. AMMT, MSM and xylenes. The simulation omitted the other reactive reactant, i.e., MIB, due to its high reactivity and moisture sensitivity. Because the model batch slurry reaction is usually performed in industrial manufacture at 30% (w/w) concentration upon completion of the reaction, the simulation was performed at the equivalent 0.77 M MSM level. As shown in Table B2, simulated slurry reaction mixtures containing AMMT and MSM in xylenes were prepared to represent the progress of the model slurry reaction at 0, 1, 5, 10, 20, 40,

60, 80 and 100%. Each simulated reaction mixture was then analyzed in five replicates using the new slurry FIA/APCI-MS setup with SIR mode followed by MS1 scan mode.

Figure 5.6 shows mass spectra of the simulated slurry reaction mixtures in xylenes representing 5%, 20% and 100% completion of the reaction. $[MSM + H]^+$ at *m/z* 382, [AMMT + Acetonitrile + H]$^+$ at *m/z* 182 and $[AMMT + H]^+$ at *m/z* 141 were observed. As the reaction progressed, the $[MSM + H]^+$ ion signal increased as expected. However, $[AMMT+H]^+$ ion signal increased from 5% to 20 % reaction progress, then decreased and did not totally disappear at 100% reaction progress, which could be ascribed to the fragmentation of $[MSM + H]^+$ and/or the adsorption of AMMT onto the inner surface of the slurry FIA/APCI-MS system due to its amine groups [29-30]. Consequently, quantitative calibration of AMMT was unsuccessful, whereas quantitative calibration of MSM showed good linearity and reproducibility with a 0.9946 R^2 and 3.7-12.2% RSDs. It is believed that quantitative calibration of MIB should be similar to MSM once the new slurry FIA/APCI-MS system is used in process control of the model batch slurry reaction. The sampling interval to use the new slurry FIA/APCI-MS system in process control of the model batch slurry reaction should be maintained at 5 min because the chromatographic peak of *m/z* 382 became wider and wider as the concentration of MSM increased, i.e. 1.5 vs. 4.7 min for reaction completion at 1 vs. 100%.

The matrix effects of AMMT on the quantitation of MSM were further

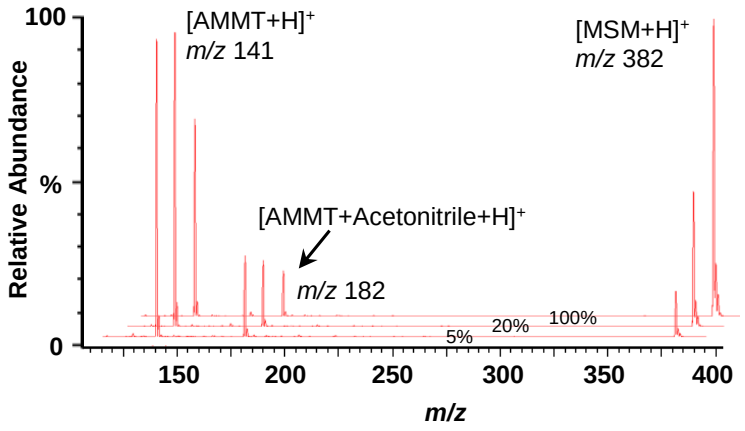

Figure 5.6 Mass spectrum acquired by MS1 scan for simulated slurry mixture samples with reaction progress at 5%, 20% and 100% completion.

investigated. Slurry samples containing only MSM and simulated slurry reaction mixtures containing AMMT and MSM were prepared to represent the progress of the model reaction at 1, 5, 10, 20, 40, 60 and 80% of a 30.0% (w/w) level slurry reaction upon completion. Then, each simulated slurry reaction mixtures were analyzed next to the corresponding standard MSM slurry samples for side-by-side comparison in five replicates. As shown in Table 5.3, when the progress of the model batch slurry reaction was at 1%, the matrix effect originated from the presence of AMMT led to an obvious suppressed peak area of *m/z* 382. However, as the reaction progressed, the deviations between the simulated slurry reaction mixtures and the standard MSM slurry samples became so close that they were comparable to the RSDs of the quantitative calibration as described above. This leaded to a conclusion that the matrix effects of quantitative real-time reaction monitoring of the model batch slurry reaction were insignificant within an order of magnitude below the upper limit of calibration. Consequently, a linear calibration curve could be simply obtained by analyzing standard MSM slurry samples. The insignificant matrix effects of AMMT on the mass spectrometric response of the MSM were possibly because APCI was not severely subject to ion suppression and/or the MSM had a stronger proton affinity (PA) than AMMT.

5.4 Conclusions

An alternative slurry FIA/APCI-MS setup for quantitative real-time monitoring of process-scale batch slurry reactions has been developed using a Waters Quattro II triple quadruple mass spectrometer. Similar to the previously introduced slurry FIA/APCI-MS

Table 5.3 Matrix effects of AMMT on the quantitation of MSM.

Simulated progress	Standards containing only MSM			Simulated sample containing AMMT & MSM				Deviation of averaged MSM PA
	Molar Conc. of MSM	PA[a]	RSD	Molar Conc. of MSM	Molar Conc. of AMMT	PA	RSD	
1%	0.0077	13592	3.2%	0.0077	0.76	10417	12.3%	-23.4%
5%	0.038	43677	3.6%	0.038	0.73	39456	5.7%	-9.7%
10%	0.077	72245	8.0%	0.077	0.69	67934	8.1%	-6.0%
20%	0.15	140743	3.4%	0.15	0.61	137512	6.4%	-2.3%
40%	0.31	251516	3.5%	0.31	0.46	259513	3.7%	3.2%
60%	0.46	343587	6.6%	0.46	0.31	355522	7.7%	3.5%
80%	0.61	468326	2.8%	0.61	0.15	458603	3.9%	-2.1%

a. Peak area.

setup using a JEOL AccuTOF time-of-flight mass spectrometer, the new setup also consisted of a slurry FIA and a detached APCI-MS setup. However, a thermostatted column compartment and a post-injection splitter were incorporated into the new slurry FIA setup because the new detached APCI-MS setup was totally different from the previous one with its lack of heating capacity. The new slurry FIA/APCI-MS setup has been demonstrated to be feasible for quantitative real-time monitoring of a model batch slurry reaction at 30% (w/w) slurry concentration upon completion at DuPont Crop Protection where a Waters LCZ single quadrupole mass spectrometer, which used an identical APCI source as the Waters Quattro II triple quadrupole mass spectrometer, was identified to be used.

With the development of two slurry FIA/APCI-MS setups using two totally different mass spectrometers, the slurry FIA/APCI-MS method has been demonstrated to have good flexibility for quantitative real-time monitoring of batch slurry reactions. It is believed that the method is applicable to most commercial mass spectrometers, but low-resolution mass spectrometers, which may be retired from central analytical laboratories, are definitely more attractive due to their low cost, good sensitivity and sufficient resolving power. We hope that the method will also provide the mass spectrometric manufacturers with a motivation to develop portable low-resolution mass spectrometers for on-site industrial analysis.

References

(1) March, R. E. *Mass Spectrom. Rev.* **2009**, *28*. 961-989.

(2) Douglas, D. J. *Mass Spectrom. Rev.* **2009**, *28*. 937-960.

(3) March, R. E.; Todd, J. F. J. *Quatrupole Ion Trap Mass Spectrometry.* 2nd Ed. John Wiley & Sons, Ltd. 2005.

(4) Douglas, D. J.; Frank, A. J.; Mao, D. M. *Mass Spectrom. Rev.* **2005**, *24*. 1-29.

(5) Xian, F.; Hendrickson, C. L.; Marshall, A. G. *Anal. Chem.* **2012**, *84*. 708-719.

(6) Marshall, A. G.; Hendrickson, C. L. *Annual. Rev. Anal. Chem.* **2008**, *1*. 579-599.

(7) Ojanpera, I.; Kolmonen, M.; Pelander, A. *Anal. Bioanal. Chem.* **2012**, *403*. 1203-1220.

(8) Meyer, M. R.; Maurer, H. H. *Anal. Bioanal. Chem.* **2012**, *403*. 1221-1231.

(9) Kaufmann, A. *Anal. Bioanal. Chem.* **2012**, *403*. 1233-1249.

(10) Hernandez, F.; Sancho, J. V.; Ibanez, M.; Abad, E.; Portoles, T.; Mattioli, L. *Anal. Bioanal. Chem.* **2012**, *403*. 1251-1264.

(11) Peng, Y.; Austin, D. E. *Anal. Chem.* **2011**, *30*. 1560-1567.

(12) Xu, W.; Manicke, N. E.; Cooks, G. R.; Ouyang, Z. *Jala* **2010**, *15*. 433-439.

(13) Ouyang, Z.; Noll, R. J.; Cooks, R. G. *Anal. Chem.* **2009**, *81*. 2421-2425.

(14) Ouyang, Z.; Cooks, R. G. *Annu. Rev. Anal. Chem.* **2009**, *2*. 187-214.

(15) Lee, E. D.; Mueck, W.; Henion, J. D.; Covey, T. R. *J. Am. Chem. Soc.* **1989**, *111*. 4600-4604.

(16) Fabris, D. *Mass Spectrom. Rev.* **2005**, *24*. 30-54.

17. Colgan, S. T.; Sharp, T. R.; Hammen, P. D.; Reed, R. H.; Horna, G. J.; Gwiazda, P. W. *Talanta* **1996**, *43*. 851-857.

(18) Hathout, Y.; Fabris, D.; Han, M. S.; Sowder, R. C., 2nd; Henderson, L. E.; Fenselau, C. *Drug Metab. Dispos.* **1996**, *24*. 1395-1400.

(19) Arakawa, R.; Lu, J.; Mizuno, K.; Inoue, H.; Doe, H.; Matsuo, T. *Int. J. Mass Spectrom. Ion Processes* **1997**, *160*. 371-376.

(20) Zaia, J.; Fabris, D.; Wei, D.; Karpel, R. L.; Fenselau, C. *Protein Sci.* **1998**, *7*. 2398-2404.

(21) Brum, J.; Dell'Orco, P. *Rapid Commun. Mass Spectrom.* **1998**, *12*. 741-745.

(22) Fligge, T.; Kast, J.; Bruns, K.; Przybylski, M. *J. Am. Soc. Mass Spectrom.* **1999**, *10*. 112-118.

(23) Kobayashi, N.; Fujimori, I.; Watanabe, M.; Ikeda, T. *Anal. Biochem.* **2000**, *287*. 272-278.

(24) Hogenboom, A. C.; de Boer, A. R.; Derks, R. J. E.; Irth, H. *Anal. Chem.* **2001**, *73*. 3816-3823.

(25) Dennhart, N.; Weigang, L. M. M.; Fujiwara, M.; Fukamizo, T.; Skriver, K.; Letzel, T. *J. Biotechnol.* **2009**, *143*. 274-283.

(26) Dell‘Orco, P.; Brum, J.; Matsuoka, R.; Badlani, M.; Muske, K. *Anal. Chem.* **1999**, *71*. 5165-5170.

(27) Brum, J.; Dell'Orco, P.; Lapka, S.; Muske, K.; Sisko, J. *Rapid Commun. Mass Spectrom.* **2001**, *15*. 1548-1553.

(28) Clinton, R.; Creaser, C. S.; Bryant, D. *Anal. Chim. Acta* **2005**, *539*. 133-140.

(29) Zhu, Z. Q.; Bartmess, J. E.; McNally, M. E.; Hoffman, R. M.; Cook, K. D.; Song, L. G. *Anal. Chem.* **2012**, *84*. 7547-7554.

(30) Zhu, Z. Q.; Bartmess, J. E.; McNally, M. E.; Hoffman, R. M.; Cook, K. D.; Song, L. G. *Anal. Chem.* **2014**, *To be submitted*.

(31) Li, J.; Dewald, H. D.; Chen, H. *Anal. Chem.* **2009**, *81*. 9716-9722.

(32) Ma, X.; Zhang, S.; Lin, Z.; Liu, Y.; Xing, Z.; Yang, C.; Zhang, X. *Analyst* **2009**, *134*. 1863-1867.

(33) Zhu, L.; Gamez, G.; Chen, H. W.; Huang, H. X.; Chingin, K.; Zenobi, R. *Rapid Commun. Mass Spectrom.* **2008**, *22*. 2993-2998.

(34) McCullough, B. J.; Bristow, T.; O'Connor, G.; Hopley, C. *Rapid Commun. Mass Spectrom.* **2011**, *25*. 1445-1451.

(35) Cho, D. S.; Gibson, S. C.; Bhandari, D.; McNally, M. E.; Hoffman, R. M.; Cook, K. D.; Song, L. *Rapid Commun. Mass Spectrom.* **2011**, *25*. 3575-3580.

(36) Petucci, C.; Diffendal, J.; Kaufman, D.; Mekonnen, B.; Terefenko, G.; Musselman, B. *Anal. Chem.* **2007**, *79*. 5064-5070.

(37) Yu, Z.; Chen, L. C.; Erra-Balsells, R.; Nonami, H.; Hiraoka, K. *Rapid Commun. Mass Spectrom.* **2010**, *24*. 1507-1513.

(38) Cheng, C.-Y.; Yuan, C.-H.; Cheng, S.-C.; Huang, M.-Z.; Chang, H.-C.; Cheng, T.-L.; Yeh, C.-S.; Shiea, J. *Anal. Chem.* **2008**, *80*. 7699-7705.

(39) Santos, V. G.; Regiani, T. s.; Dias, F. F. G.; Romão, W.; Jara, J. L. P.; Klitzke, C. c. F.; Coelho, F.; Eberlin, M. N. *Anal. Chem.* **2011**, *83*. 1375-1380.

(40) Nørgaard, A. W.; Vaz, B. G.; Lauritsen, F. R.; Eberlin, M. N. *Rapid Commun.Mass Spectrom.* **2010**, *24*. 3441-3446.

(41) Chen, T.-Y.; Chao, C.-S.; Mong, K.-K. T.; Chen, Y.-C. *Chem. Commun.* **2010**, *46*. 8347-8349.

(42) Hsieh, C. H.; Chao, C. S.; Mong, K. K. T.; Chen, Y. C. *J. Mass Spectrom.* **2012**, *47*. 586-590.

(43) Ma, X. X.; Zhang, S. C.; Zhang, X. R. *Trac-Trends Anal. Chem.* **2012**, *35*. 50-66.

Appendix B

for

Chapter 5. Slurry Flow Injection Slurry Flow Injection Analysis coupled with APCI Mass Spectrometry for Quantitative Real-Time Monitoring of Batch Slurry Reactions: An Alternative Setup

Table B1 Preparation of MSM solution and slurry samples in xylenes with 25 mL volumetric flasks.

Entry	W_{MSM}(g)	V_{xylene}(mL)	Concentration	
			% (w/w)	M
1	5.7×10^{-3}	24.97	0.026	6.0×10^{-4}
2	0.046	24.93	0.21	4.8×10^{-3}
3	0.092	24.85	0.43	9.7×10^{-3}
4	0.369	24.52	1.71	0.039
5	0.741	24.29	3.41	0.078
6	1.48	23.82	6.70	0.16
7	2.95	22.62	13.1	0.31
8	4.96	21.40	21.2	0.52
9	7.30	19.70	30.0	0.77

Table B2 Preparation of simulated slurry samples to represent the progress of the model batch slurry reaction at 30% (w/w) level upon completing using 25 mL volumetric flasks.

Reaction progress	Simulated samples			Product only	
	W_{AMMT} (g)	W_{MSM} (g)	V_{xylene} (mL)	W_{MSM} (g)	V_{xylene} (mL)
0%	2.68	0	23.20	--	--
1%	2.66	0.073	22.85	0.073	24.90
5%	2.55	0.365	22.79	0.365	24.62
10%	2.41	0.730	22.65	0.730	24.30
20%	2.15	1.46	22.38	1.46	23.78
40%	1.61	2.92	21.66	2.92	22.75
60%	1.07	4.38	21.23	4.38	21.83
80%	0.537	5.84	20.56	5.84	20.82
100%	0	7.30	19.70	--	--

Chapter 6. Quantitative Real-time Monitoring of Heterogeneous-Catalyzed Reactions by Slurry FIA/APCI-MS

Abstract

For the first time, a heterogeneous-catalyzed Pechmann reaction at molar concentration level was monitored quantitatively in real time. A slurry flow injection analysis coupled to atmospheric pressure ionization mass spectrometry (FIA/APCI-MS) setup was introduced to circumvent sample overloading caused by analytes in molar concentrations, as well as instrumental contamination and/or clogging by solid particles. The synthesis of hymecromone catalyzed by 50 g/L silica supported perchloric acid ($HClO_4/SiO_2$, extent of loading: 0.35 mmol/g) via Pechmann condensation was quantitatively monitored in real time with a sampling rate of every 5 minutes for 2 hours, and a conversion ratio of 22% was obtained for hymecromone.

6.1 Introduction

Coumarin and its derivatives have an important place in the realm of synthetic organic and medicinal chemistry.[1] Suitably substituted coumarins have various applications in food additives, pharmaceutical, perfume, and cosmetic industries.[1,2] Hymecromone, 7-hydroxy-4-methylcoumarin, is used commercially as a biliary antispasmodic, and it is also the substrate material for the production of several insecticides. Pechmann condensation is a well-established route to synthesize coumarins from activated phenols and ethyl acetoacetate in acidic media, with the by-products ethanol and water produced.[3] Despite its homogeneity, this reaction usually involves the use of non-reusable acids[4-7] in an excess amount, resulting in environmental pollution.

For eco-friendly reasons, some solid-supported catalysts such as silica supported zinc chloride ($ZnCl_2/SiO_2$)[8], silica supported perchloric acid ($HClO_4/SiO_2$)[9], polystyrene-supported $GaCl_3$[10], Polyvinylpolypyrrolidone-bound BF_3[11], ion-exchange resins[12], etc. as alternatives to acids have been employed.

Real-time monitoring during coumarins synthesis via homogenous Pechmann condensation was recently reported using Raman spectroscopy when an acid catalyst was used.[13] However, there has not been a technique applied for the real-time monitoring of heterogeneous-catalyzed Pechmann condensation reactions. In Chapter 4 and 5, slurry flow injection analysis coupled with atmospheric pressure chemical ionization mass spectrometry (slurry FIA/APCI-MS) was introduced for quantitative real-time monitoring of a batch slurry reaction, where sample overloading and sample clogging were avoided, and slurry samples up to 30%(w/w) were quantified. Here the slurry FIA/APCI-MS was further utilized for quantitative real-time monitoring of a model Pechmann condensation reaction.

6.2 Experimental

6.2.1 Reagent

Acetonitrile (HPLC grade) was purchased from Fisher Scientific (Suwanee, GA). Resorcinol (ACS grade, ≥99%), ethyl acetoacetate (EAA, ≥99%), 7-hydroxy-4-methylcoumarin (hymecromone, ≥98%), and silica supported perchloric acid ($HClO_4/SiO_2$, extent of loading: 0.35 mmol/g) were purchased from Sigma-Aldrich (St.

Louis, MO). Silica gel (SiO_2, 60Å) was purchased from Sorbent technology (Norcross, GA).

6.2.2 Model reaction

A Pechmann condensation reaction of resorcinol and EAA using $HClO_4/SiO_2$ as the catalyst to produce hymecromone, ethanol and water, was used as the model reaction (Scheme 6.1). 8.25 g resorcinol (75 mmol) and 15 mL EAA (115 mmol) along with 2.5g $HClO_4/SiO_2$ were mixed in acetonitrile to give a total 50 mL mixture, which was refluxed at 110 ℃ for 2h. The catalyst $HClO_4/SiO_2$ was the only undissolved particles throughout the reaction.

6.2.3 Instrumentation

The slurry FIA/APCI-MS setup used in this study consists of an HPLC pump, a slurry auto-sampler and a detached APCI-MS setup (Figure 6.1). The slurry auto-sampler included a gas-flow valve, an aspirator and a 1 μL auto-sampling valve in order to interface with the reactor and achieve auto-sampling of the heterogeneous reaction mixture. The movement of gas-flow valve and the auto-sampling valve were synchronized. When the auto-sampling valve was at the “loading” position, the gas-flow valve was “on” to introduce N_2 at 80 psi to the aspirator and create the sample flow at approximately 1.5 mL/second, which resulted in a slot of the auto-sampling valve filled with reaction mixture. After 1 second, the auto-sampling valve moved to the “injection” position and the gas-flow valve was “off” to stop the sample flow, when the mixture trapped in the slot was injected into the FIA flow for APCI-MS analysis.

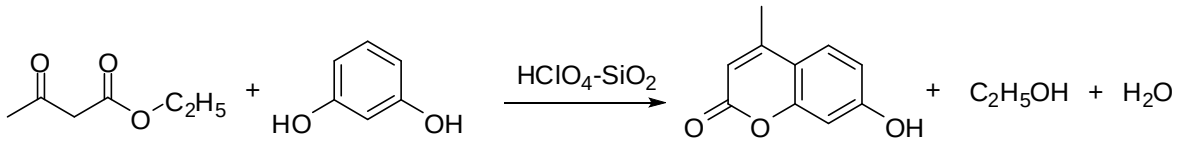

Ethyl acetoacetate (EAA) | Resorcinol | 7-hydroxy-4-methylcoumarin (Hymecromone)

Scheme 6.1 The model reaction to synthesis hymecromone via Pechmann condensation

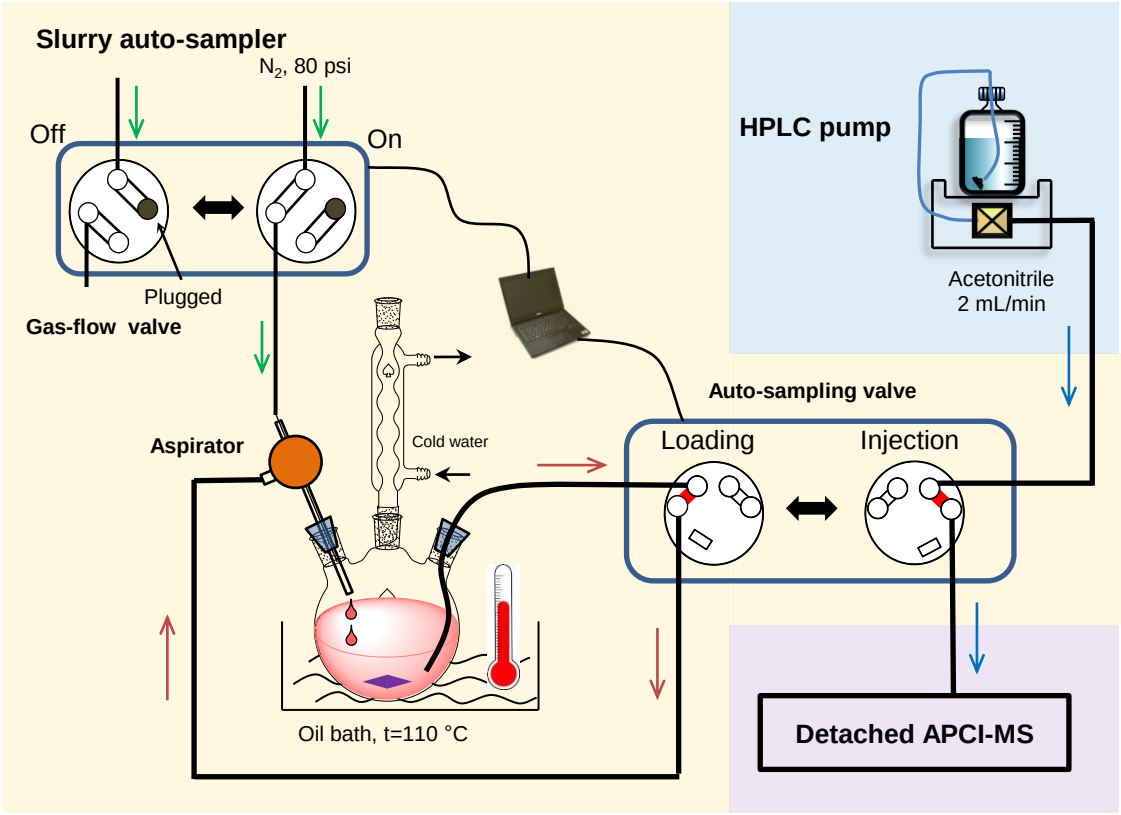

Figure 6.1 The slurry FIA/APCI-MS setup used for quantitative real-time monitoring of the model reaction.

The detached APCI-MS for an AccuTOF JMS-100LC time-of-flight (TOF) mass spectrometer (JEOL, Peabody, MA) was introduced in Chapter 2, where the potential sample overloading was avoided with the help of a 4.5 inch long stainless-steel ion-transport capillary and a low-capacity pump. The use of a detached APCI-MS would also prevent mass spectrometric contamination by the solid particles. In addition, the commercial APCI probe was replaced with a slurry APCI probe, introduced in Chapter 4, to avoid instrumental clogging. The parameters of the APCI source were briefly optimized for 2 mL/min FIA flow rate with acetonitrile as solvent and set as follows: needle voltage, -4500 V; desolvation chamber temperature, 500 ℃; desolvation gas flow, 4 L/min; nebulizing gas pressure, 80 psi. Nitrogen was used for both desolvation gas and nebulizing gas. The parameters of TOF mass spectrometer were briefly optimized for the detection of MSM and set as follows: orifice 1 voltage, -20 V; orifice 2 voltage, -10 V; ring voltage, -15 V; peak voltage, 600 V. Chromatogram-like ion intensity profiles were recorded with a mass range of *m/z* 100 to 500 and scan interval of 1.0 s. Integration of peaks from the extracted ion profiles (XIPs) were performed with TSSPRO 3.0 software (JEOL, Peabody, MA). In order to minimize exposure to vapors, the APCI ion source was put inside a wooden box which was connected to the well ventilated lab exhaust pipe.

6.2.4 Quantitative calibration

In order to create a calibration curve for quantitative real-time monitoring of the model reaction using the slurry FIA/APCI-MS setup, standard mixtures were prepared to

simulated the progress at 0, 1, 5, 10, 20 and 50% completion of the model reaction (Table 6.1). For each standard mixture, 0.5 g SiO_2 (60Å) was added to simulate the $HClO_4/SiO_2$ added in the reaction, and total volume was 10 mL. All the standard mixtures were heated at 65 ℃ analyzed in three replicates for quantitative calibration.

6.2.5 Quantitative real-time monitoring of the model reaction

Quantitative real-time monitoring of the model reaction was performed using the slurry FIA/APCI-MS at the sampling rate 5 min/injection for 2h. As a result, total 24 injections were completed.

6.3 Results and Discussions

To evaluate the tolerance of the slurry FIA/APCI-MS setup to the undissolved catalyst, 48 mL acetonitrile and 2.5g silica gel (60Å) were stirred in the reactor at 110 ℃ to simulate the real reaction mixture, and the aspirator was initiated for 1s every 5 min. Due to the wide passage of the slurry flow tube, i.e. 0.03 inch, and its high flow rate, i.e. approximately 0.5 mL/second, clogging was not observed for 24 injections, which was long enough for the model reaction to complete. However, the solvent vapor was carried out each time when the aspirator was on, and the reduction of acetonitrile was observed at approximately 3.5 mL after the 2-hour reaction, averaging 0.15 mL/aspiration.

Quantitative calibration was established by analyzing the simulated standard mixtures using the slurry FIA/APCI-MS. Linear calibration was obtained between the molar concentration of hymercomone and the corresponding peak areas of its XIPs at

Table 6.1 Preparation of standard mixtures simulating the progress of the model reaction.

Compound	Amount of each compound[a]					
	Simulated reaction progress					
	0	**1%**	**5%**	**10%**	**20%**	**50%**
Resorcinol (g)	1.65	1.63	1.57	1.49	1.32	0.83
EAA (mL)	3.00	2.98	2.90	2.80	2.61	2.02
Hymecromone (g)	0	0.026	0.132	0.264	0.528	1.32
Aectonitrile (mL)	5.40	5.40	5.50	5.60	5.50	5.80
SiO_2 (60Å) (g)	0.500	0.500	0.500	0.500	0.500	0.500

a. Total volume is 10 mL for each standard mixture.

m/z 175 for the $[Hymecromone-H]^-$ ion with correlation coefficient R^2=0.9986 and relative standard deviations (RSDs) 6.7-11.3% in three replicates. However, simultaneous quantification of resorcinol and EAA were not achieved due to the weak responses of their respective ions, i.e. ($[M-H]^-$ ion at *m/z* 109 and 129. This was not a surprise because our experiment had showed that in (-)-APCI-MS, the sensitivity of hymecromone was approximately 2.5 orders of magnitude higher than that of EAA and 1.5 order of magnitude higher than that of resorcinol; and the dynamic range of the mass spectrometer used in this study was approximately two orders of magnitude.

Real-time monitoring of the model reaction was performed and no clogging was observed. Mass spectra of *m/z* 100-200 at 5, 25 and 45 min of reaction time were presented in Figure 6.2, where the peak observed at *m/z* 175 ($[Hymecromone-H]^-$) was abundant and its intensity kept increasing as the reaction proceeded. The peak intensity of the $[Resorcinol-H]^-$ ion at *m/z* 109 was low in the beginning and became lower as resorcinol was consumed, while the $[EAA-H]^-$ ion at *m/z* 129 was not observed. After the correction of volume changes, i.e. 0.15 mL/injection, the production of hymecromone was calculated based on the quantitative calibration curve and demonstrated in Figure 6.3. The reaction proceeded quickly in the first 10 min and reached its equilibrium at around 50 min, with a conversion ratio of 22% for hymecromone obtained. In a previous study using 18g/L $ZnCl_2/SiO_2$ as the catalyst and acetonitrile as the solvent, low conversion ratio of hymecromone, i.e. 10%, was also reported.[8] Although solvent-free

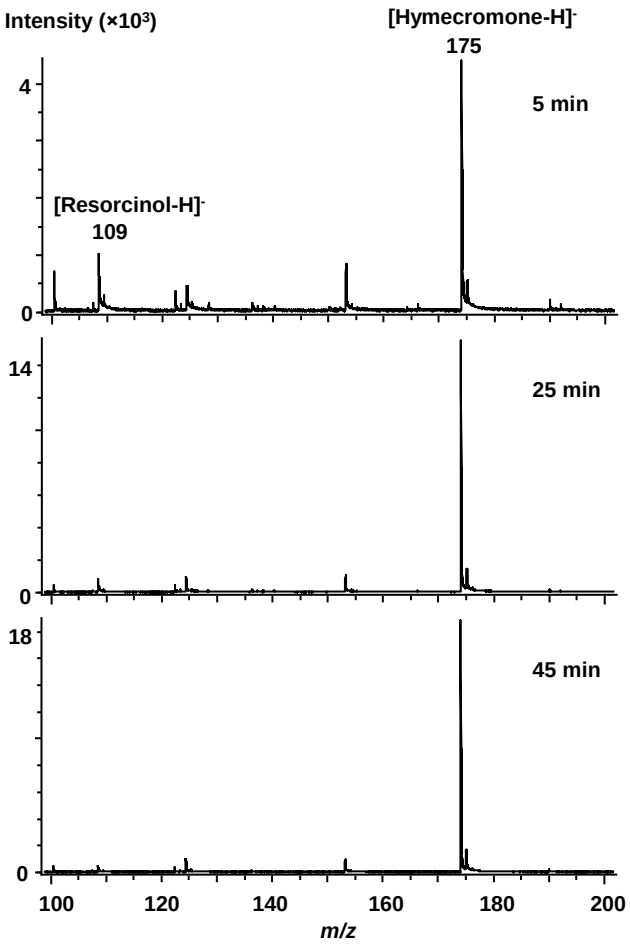

Figure 6.2 Mass spectra of reaction mixtures at 5, 25 and 45 min of reaction time.

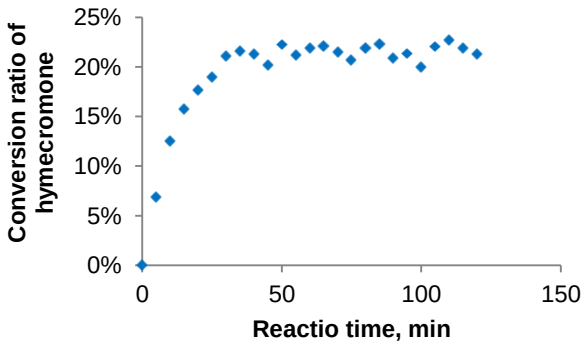

Figure 6.3 Yield-time profile of hymecromone obtained by quantitative real-time reaction monitoring using slurry FIA/APCI-MS.

condition could offer high conversion ratio, i.e. 95%[8], the use of *ca.* 200 g/L $ZnCl_2/SiO_2$ catalyst would require a wider slurry flow path of the slurry FIA/APCI-MS setup, e.g. 0.06 inch, to avoid clogging.

6.4 Conclusion

In summary, slurry FIA/APCI-MS has been proven to be feasible in quantitative real-time monitoring of heterogeneous-catalyzed reactions. Sample overloading caused by analytes in molar concentrations, and instrumental contamination and/or clogging by 50 g/L catalyst were avoided. Higher concentration of heterogeneous catalyst may not pose additional problem if an auto-sampling valve with a wider flow path is incorporated. Although the use of an aspirator to generate a recycling slurry flow caused loss of solvent, it was convenient and economy in lab testing. In addition, a variable speed pump is usually used in industry to create recirculation of the reaction mixture and loss of solvent will not be a problem.

Reference

(1) O'Kennedy, R.; Thornes, R. D. *Coumarins: Biology, Applications and Mode of Action*; Wiley, 1997.

(2) Harborne, J. B. *Plant Cell Environ.* **1982**, 5, 435-436.

(3) Srinivasan, P.; Rao, V. J.; Chandrasekaran, S.; Rampally, C.; Google Patents, 2004.

(4) Sethna, S. M.; Shah, N. M. *Chem. Rev.* **1945**, 36, 1-62.

(5) Shirini, F.; Marjani, K.; Nahzomi, H. T.; Zolfigol, M. A. *Chin. Chem. Lett.* **2007**, 18, 909-911.

(6) Bose, D. S.; Rudradas, A. P.; Babu, M. H. *Tetrahedron Lett.* **2002**, 43, 9195-9197.

(7) De, S. K.; Gibbs, R. A. *Synthesis-Stuttgart* **2005**, 1231-1233.

(8) Datta, B.; Pasha, M. A. *ISRN Org. Chem.* **2013**, 2013, 5.

(9) Maheswara, M.; Siddaiah, V.; Damu, G. L. V.; Rao, Y. K.; Rao, C. V. *J. Mol. Catal. A: Chem.* **2006**, 255, 49-52.

(10) Rahmatpour, A.; Mohammadian, S. *C. R. Chimie* **2013**, 16, 271-278.

(11) Mokhtary, M.; Najafizadeh, F. *C. R. Chimie* **2012**, 15, 530-532.

(12) Sabou, R.; Hoelderich, W. F.; Ramprasad, D.; Weinand, R. *J. Catal.* **2005**, 232, 34-37.

(13) Calvino-Casilda, V.; Banares, M. A.; LozanoDiz, E. *Catal. Today* **2010**, 155, 279-281.

Chapter 7. Differentiation of Underivatized Monosaccharides by Atmospheric Pressure Chemical Ionization Quadrupole Time-of-Flight Mass Spectrometry

A version of this chapter was originally published by Zhu, Z., Song, L.and Bartmess, J. E.:

Zhu, Z.; Song, L.; Bartmess, J. E. *Rapid Comm. Mass Spectrom.* **2012**, *26*, 1320-1328.

Abstract

In order to distinguish underivatized monosaccharides from their stereoisomers, a convenient approach has been developed using atmospheric pressure chemical ionization quadrupole time-of-flight mass spectrometry (APCI/QTOF-MS). Glucose was distinguished from mannose and galactose due to the different MS^2 spectra of their $[M + NH_4]^+$ ions, while mannose was further distinguished from galactose due to the different MS^2 spectra of their $[M - H]^-$ ions. The MS^2 spectra of $[M + NH_4]^+$ ions were also used to distinguish methyl *α*-D-glucose and methyl *β*-D-glucose, while the *pseudo*-MS^3 spectra of $[M + H]^+$ ions were utilized to differentiate the three hexosamine and *N*-acetylhexosamine stereoisomers. Unique $[M + O_2]^-$ ions were observed and their distinctive fragmentation patterns were also utilized to differentiate the three hexosamine stereoisomers. Furthermore, the identity of the ionization products of the underivatized monosacharides and their corresponding fragment ions were assigned after accurate mass measurement by QTOF-MS. Consequently, the identity of the adduct ions of hexoses generated by APCI/MS using H_2O and D_2O as solvents were proven to be $[M + NH_4]^+$ and $[M_{d5} + ND_4]^+$, respectively, rather than $[M + H_2O]^{+\cdot}$ and $[M_{d5} + D_2O + D]^+$ as previously reported.

7.1 Introduction

Extensive studies have shown that oligosaccharides are closely involved in many life process by modulating proteins or mediating a variety of interactions among cells and molecules.[1, 2] An understanding of these biological processes is closely associated to the knowledge of their structures. The structure elucidation of oligosaccharides usually includes the differentiation of the monosaccharide stereoisomers, the determination of the oligosaccharide sequence, and the identification of the linkage location and branching sites.[3]

Mass spectrometry has been widely used in structure elucidation of oligosaccharides due to its high accuracy, analytical versatility and high sensitivity.[4] In earlier studies, fast atom bombardment mass spectrometry (FAB/MS) was utilized to determine the sequence and linkage position[5, 6] of both derivatized and underivatized oligosaccharides[6]. Later on, electrospray ionization mass spectrometry (ESI/MS) gained predominant popularity in the analysis of oligosaccharides.[7-20] Particularly, the differentiation of underivatized monosaccharides including hexoses[13-20], hexosamines[10, 12, 20], *N*-acetylhexsamines[12, 20] and methyl D-glucopyranosides[16, 20] was achieved by investigating the fragmentation behavior of their protonated/deprotonated ions and/or their metal[11-16], ammonium[18, 20] and $NH_2NH_2H^+$ adducts[19]. The tandem mass spectra were usually acquired using ion trap[11, 12, 14, 15, 19, 20], triple-quadrupole[13, 16, 18] or quadrupole time-of-flight (QTOF)[17] mass spectrometers.

Although atmospheric pressure chemical ionization mass spectrometry (APCI/MS) has not been widely used in the analysis of monosacharides so far, both Liang *et al*[21] and Ullah *et al*[22] showed that APCI/MS was advantageous over ESI/MS in quantification due to less matrix effects. Recently, Choi and Kim[23] reported the differentiation of glucosamine, mannosamine and galactosamine by APCI/MS using the fragmentation patterns of either their $[M + H]^+$ or $[M_{d6} + D]^+$ ions when H_2O and D_2O were respectively used as the solvent. Shortly after, they also reported the differentiation of galactose from glucose and mannose by APCI/MS using the fragmentation patterns of their $[M + H_2O]^{+\cdot}$ ion, and the differentiation of glucose from galactose and mannose by APCI/MS using the fragmentation behavior of their $[M_{d5} + D_2O + D]^+$ ions.[24] Apparently, according to Choi and Kim[23, 24], the difference between H_2O and D_2O resulted in different types of ionization products from hexoses, but not from hexosamines. This contradiction could be caused by the incorrect assignment of the ionization products from hexoses, i.e. $[M + H_2O]^{+\cdot}$ and $[M_{d5} + D_2O + D]^+$. In consideration that ubiquitous trace amount of ammonia is present in the atmosphere[25] and ammonia can interact with hexoses through hydrogen bond[26], the identity of the ionization products from hexoses could be $[M + NH_4]^+$ and $[M_{d5} + ND_4]^+$. A possible incorrect assignment could be a result of inaccurate mass measurement by the single quadrupole mass spectrometer used in the study because the nominal *m/z* of the $[M + NH_4]^+$ and $[M + H_2O]^{+\cdot}$, and the $[M_{d5} + ND_4]^+$ and $[M_{d5} + D_2O + D]^+$ ions were identical.

In this report, APCI/MS has been explored in the analysis of total eleven underivatized monosaccharides (Figure C1). A quadrupole time-of-flight (QTOF) mass spectrometer was specially selected due to its accurate mass measurement ability. The identity of the ionization products of the underivatized monosacharides and their corresponding fragment ions were assigned after accurate mass measurement. Differentiation of underivatized monosacharides by APCI/QTOF-MS has been achieved for three hexoses, two methyl D-glucopyranosides, three hexosamines and three *N*-acetylhexosamines.

7.2 Experimental

7.2.1 Chemicals

Water (H_2O) and methanol were HPLC grade and purchased from Fisher Scientific (Suwanee, GA, USA). Deuterium oxide (D_2O) and ammonium acetate (NH_4Ac) were purchased from Sigma-Aldrich (St. Louis, MO, USA). D-(+)-Glucose (Glc), D-(+)-Mannose (Man), D-Glucosamine hydrochloride (GlcN·HCl), D-Mannosamine hydrochloride (ManN·HCl), *N*-Acetyl-D-mannosamine (ManNAc), *N*-Acetyl-D-galactosamine (GalNAc) and Methyl α-D-glucopyranoside (MeαGlc) were also purchased from Sigma-Aldrich (St. Louis, MO, USA). D-Galactosamine hydrochloride (GalN·HCl) and Methyl β-D-glucopyranoside hemihydride (MeβGlc·1/2H_2O) were purchased from Tokyo Chemical Industry Co. (Tokyo, Japan). D-(+)-Galactose (Gal) was purchased from Thermo Fisher Scientific Inc. (Pittsburgh, PA, USA). *N*-Acetyl-D-

glucosamine (GlcNAc) was purchased from Ferro Pfanstiehl Laboratories Inc. (Waukegan, IL, USA). Individual monosaccharides were dissolved either in H_2O, D_2O, methanol, or methanol containing 10 mM NH_4Ac. The concentration of the monosaccharide was either 0.1 mM for positive-ion or 0.5 mM for negative-ion mass spectrometric experiments.

7.2.2 Mass spectrometry

Mass spectrometric analysis was performed using a QSTAR Elite quadrupole time-of-flight (QTOF) mass spectrometer equipped with an APCI heated nebulizer ion source and an integrated syringe pump (AB Sciex, Forster City, CA, USA). Nitrogen (Airgas, Bowling Green, KY, USA) was used as nebulizer, auxiliary, curtain and collision gas. The mass spectrometric parameters in the instrumental control panel were briefly optimized to minimize in-source fragmentation. In positive-ion MS mode, they were: nebulizer current, 1.0 μA; heater temperature, 250 ℃; auxiliary gas, 40; nebulizer gas, 40; curtain gas, 40; collision gas: 3; declustering potential, 30 V; focusing potential, 100 V; declustering potential 2: 10 V. In positive-ion MS^2 mode, all the mass spectrometric parameters remained the same except that collision gas was adjusted to 4. Collision energy was varied over an appropriate range and is described in detail in the RESULTS AND DISCUSSION section. In negative-ion MS and MS^2 mode, the absolute values of the spectrometric parameters remained the same as in positive-ion mode, but the voltages were inverted. The accumulation time of each mass spectrometric scan was 1 second. Data acquisition was performed in multiple channel averaging (MCA) mode and

all mass spectra obtained were an accumulation of 10 scans. The monosaccharide solutions were infused into the mass spectrometric system using a Hamilton (Reno, NV, USA) gastight syringe. The infusion flow rate was either 30 μL min^{-1} in positive-ion mode or 50 μL min^{-1} in negative-ion mode. Each monosaccharide solution was analyzed in five replicates.

7.3 Results and Discussion

7.3.1 Ionization products of hexoses by positive-ion APCI

Figure 7.1 shows an APCI/QTOF mass spectrum of 1.0 mM Glc in H_2O. Besides a adduct ion at nominal *m/z* 198, other ions at nominal *m/z* 180, 163, 145 and 127 were also observed due to inevitable in-source fragmentation by APCI[27]. A similar mass spectrum with ions at the same nominal *m/z* values was reported by Choi and Kim[24] using APCI single quadrupole mass spectrometry, though the adduct ion at nominal *m/z* 198 was observed to be the base peak, which might be a result of different ambient environment and/or instrumental conditions. A MS^2 mass spectrum of a nominal *m/z* 198 precursor ion, similar to the APCI/QTOF mass spectrum in Figure 7.1, was also reported by Zhu and Sato[20] using ESI ion trap mass spectrometry. Among the three studies, there is an obvious disagreement in the identities of the ions at nominal *m/z* 198 and 180, i.e. $[M + H_2O]^{+\cdot}$ and $M^{+\cdot}$ by Choi and Kim *vs.* $[M + NH_4]^+$ and $[M + NH_4 - H_2O]^+$ by us in this study, and Zhu and Sato[20]. However, there is an agreement in the elemental

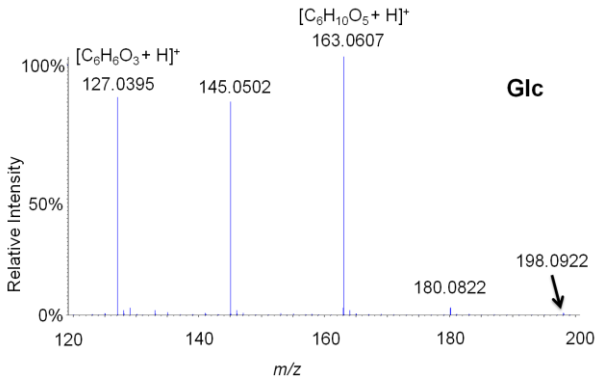

Figure 7.1 Positive-ion APCI/QTOF mass spectrum of 1.0 mM Glc in H_2O. The mass spectrum was calibrated using the peaks representing ions of $[C_6H_{10}O_5 + H]^+$ and $[C_6H_6O_3 + H]^+$ with theoretical *m/z* values of 163.0607 and 127.0395, respectively. The *m/z* values of other peaks measured by APCI/QTOFMS are indicated in the figure.

composition of the fragment ions at *m/z* 163, 145 and 127 being $[C_6H_{10}O_5 + H]^+$, $[C_6H_8O_4 + H]^+$ and $[C_6H_6O_3 + H]^+$ (accurate *m/z* values: 163.0607, 145.0501 and 127.0395, respectively). As a result of this agreement, the mass spectrum shown in Figure 7.1 was able to be calibrated using the peaks representing ions of $[C_6H_{10}O_5 + H]^+$ and $[C_6H_6O_3 + H]^+$. The mass measurement accuracy by APCI/QTOF-MS was then verified by the experimental and accurate *m/z* value of the peak representing ion $[C_6H_8O_4 + H]^+$, i.e. 145.0502 *vs.* 145.0501. Because the experimental *m/z* value of the adduct ion was 198.0922, its identity was obviously more reasonable to be assigned as $[M + NH_4]^+$ with an accurate *m/z* value of 198.0978, rather than $[M + H_2O]^{+\cdot}$ with an accurate *m/z* value of 198.0740. With regard to the ion with an experimental *m/z* value of 180.0822, its identity was obviously more reasonable to be assigned as $[M + NH_4 - H_2O]^+$ with an accurate *m/z* value of 180.0872, rather than $M^{+\cdot}$ with an accurate *m/z* value of 180.0634. The mass accuracies were 5.6 and 5.0 mamu for the $[M + NH_4]^+$ and $[M + NH_4 - H_2O]^+$ ions, respectively. They were slightly larger than that for the $[C_6H_8O_4 + H]^+$ ion, i.e. 0.1 mamu. This was because the *m/z* values of the $[M + NH_4]^+$ and $[M + NH_4 - H_2O]^+$ ions were beyond the calibration range, i.e. *m/z* 163.0607 to 127.0395. Because the adduct ion was confirmed to be $[M + NH_4]^+$, the identities of the fragment ions at *m/z* 163.0607, 145.0502 and 127.0395 were $[M + NH_4 - H_2O - NH_3]^+$, $[M + NH_4 - 2H_2O - NH_3]^+$ and $[M + NH_4 - 3H_2O - NH_3]^+$, respectively.

APCI/QTOF mass spectra of 1.0 mM Man and Gal in H_2O were also acquired and calibrated similarly. Their adduct ions were also verified to be $[M + NH_4]^+$. APCI/QTOF

mass spectra of 1.0 mM Glc, Man and Gal in D_2O were further acquired and calibrated as described. Their adduct ions were confirmed to be $[M + ND_4]^+$. In order to enhance the relative abundance of $[M + NH_4]^+$ ion to other in-source fragmentation ions, 0.1 mM Glc, Man and Gal were prepared in methanol containing 1, 10 and 100 mM NH_4Ac. The best result was obtained with methanol containing 10 mM NH_4Ac.

7.3.2 Differentiation of Glc, Man and Gal

Positive-ion APCI/QTOF mass spectra of Glc, Man and Gal did not show significant differences. Therefore, their $[M + NH_4]^+$ ions were selected as parent ions for further MS^2 experiments. Figure 7.2A shows positive-ion APCI/QTOF-MS^2 spectra of the $[M + NH_4]^+$ precursor ions at *m/z* 198.098 generated from 0.1 mM Glc, Man and Gal in methanol containing 10 mM NH_4Ac. Accurate mass measurement determined that the identities of product ions at nominal *m/z* 181, 180, 163 and 145 were $[M + NH_4 - NH_3]^+$, $[M + NH_4 - H_2O]^+$, $[M + NH_4 - H_2O - NH_3]^+$ and $[M + NH_4 - 2H_2O - NH_3]^+$, respectively. Glc can be differentiated from Man and Gal due to obviously larger relative intensity of peaks at *m/z* 180 to 163. Figure 7.2B shows the relative intensity of peaks at *m/z* 180 to 163 of Glc, Man and Gal under different collision energy from 7 to 14 V. As the collision energy increased from 7 to 14 V, the relative intensity of peaks at *m/z* 180 to *m/z*163 from Glc decreased from 1.7 to 0.2, while they were below 0.3 and almost identical for both Man and Gal. Thus, Glc can be better differentiated from Gal and Man under lower collision energy, e.g. 8 V in Figure 7.2A.

(A)

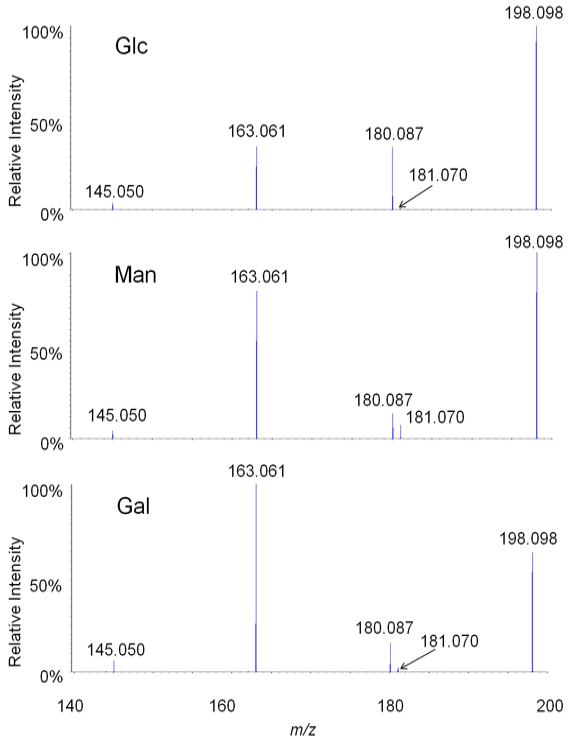

(B)

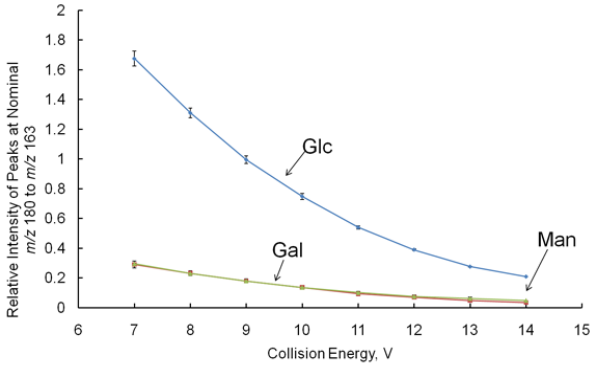

Figure 7.2 (A) Positive-ion APCI/QTOF-MS^2 spectra of the $[M + NH_4]^+$ precursor ions at *m/z* 198.098 generated from 0.1 mM Glc, Man, and Gal in methanol containing 10 mM NH_4Ac. Collision energy was 9 V. Product ions are identified to be $[M + NH_4 - NH_3]^+$(*m/z* 181), $[M + NH_4 - H_2O]^+$ (*m/z* 180), $[M + NH_4 - H_2O - NH_3]^+$ (*m/z* 163) and $[M + NH_4 - 2H_2O - NH_3]^+$ (*m/z* 145). (B) Relative intensities of peaks at nominal *m/z* 180 to 163 in the APCI/QTOF-MS^2 spectra under different collision energy for Glc, Man and Gal.

In order to further differentiate Man from Gal, negative-ion APCI/QTOF mass spectra of 0.5 mM Man and Gal in methanol were further acquired. The ionization products of hexoses by negative-ion APCI were $[M + O_2]^-$ ions (data not shown) due to the generation of $O_2^{-\cdot}$ during the APCI process and its hydrogen-bond interaction with the hexoses.[28] Abundant deprotonated molecular ions, i.e. $[M - H]^-$, and other in-source fragment ions, e.g. $[M - H - H_2O]^-$, were also detected at *m/z* 179.056 and 161.044, respectively. The $O_2^{-\cdot}$ has $\Delta_{acid}G$ of 1450.5 kJ/mol[29], while the hexoses have free energies of acidity for the hexopyranose forms in the 1407-1419 kJ/mol range[30]. Therefore, dissociation of $[M + O_2]^-$ ions may be largely responsible for the observation of abundant deprotonated molecular ions of hexoses.[31] The deprotonation process induced by $O_2^{-\cdot}$ is expected to occur at the most acidic site of hexoses, presumably the anomeric -OH on C_1 for Glc and the -OH groups on C_4 for Gal, while the acidities of -OH groups on C_1, C_2 and C_4 are close for Man.[30-32] The gas-phase acidities of hexoses could also be affected due to possible ring-opening process of their anions.[33] Nevertheless, negative-ion APCI/QTOF-MS spectra of Man and Gal did not show significant differences.

$[M - H]^-$ ions from Man and Gal were selected as precursor ions for further MS^2 experiments. Figure 7.3A shows negative-ion APCI/QTOF-MS^2 spectra of the $[M - H]^-$ precursor ions at *m/z* 179.056 generated from 0.5 mM Man and Gal in methanol. Accurate mass measurement determined that the identities of product ions at nominal *m/z* 161, 119 and 89 were $[M - H_2O - H]^-$, $[M - C_2H_4O_2 - H]^-$ and $[M - C_3H_6O_3 - H]^-$,

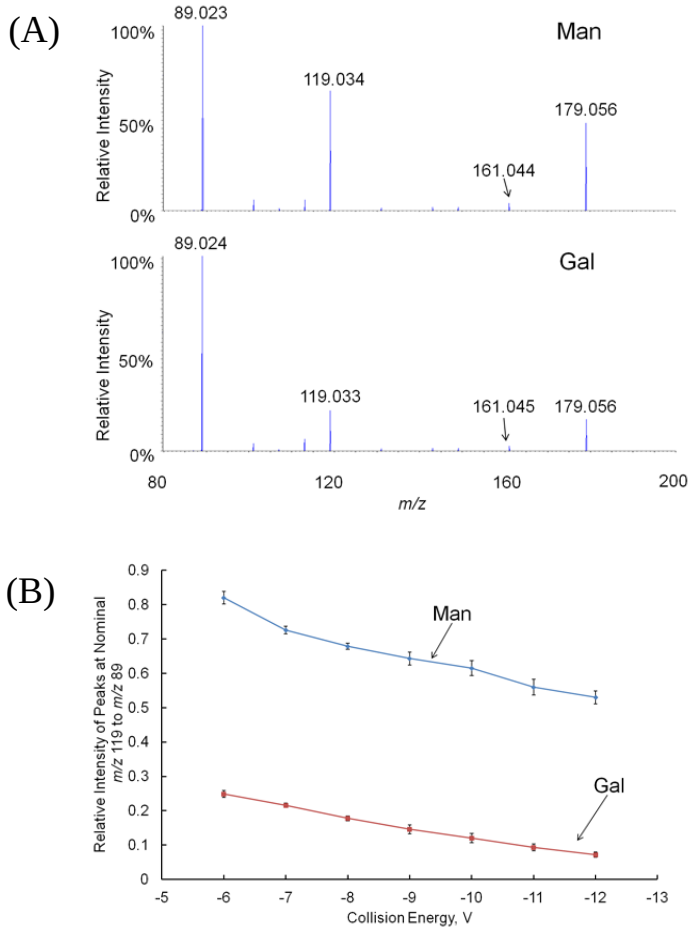

Figure 7.3 (A) Negative- ion APCI/QTOF-MS^2 spectra of the $[M - H]^-$ ions at *m/z* 179.056 generated from 0.5 mM Man and Gal in methanol. Collision energy was at -10 V. Product ions are identified to be $[M - H_2O - H]^-$ (*m/z* 161), $[M - C_2H_4O_2 - H]^-$ (*m/z* 119) and $[M - C_3H_6O_3 - H]^-$ (*m/z* 89). (B) Relative intensities of peaks at nominal *m/z* 119 to 89 in the APCI/QTOF-MS^2 spectra under different collision energy for Man and Gal.

respectively. Man can be differentiated from Gal due to obviously larger relative intensity of peaks at *m/z* 119 to 89. Figure 7.3B shows the relative intensity of peaks at *m/z* 119 to 89 of Man and Gal under different collision energy from -6 to -12 V. The relative intensities of peaks at *m/z* 119 to *m/z* 89 were above 0.5 from Man and below 0.25 from Gal. Thus, Man can be differentiated from Gal.

7.3.3 Differentiation between Me*α*Glc and Me*β*Glc

In order to study the fragmentation behavior of monosaccharides influenced by different anomeric configurations, anomers of methyl D-glucopyranoside, i.e. Me*α*Glc and Me*β*Glc, were selected. Me*α*Glc and Me*β*Glc differ from Glc by replacing the anomeric hydroxyl group with a methoxy group. Consequently, they are able to maintain their own configuration in solvent due to the substantially increased energy barrier for mutarotation process.

Positive-ion APCI/QTOF mass spectra of Me*α*Glc and Me*β*Glc were acquired (data not shown). A relative larger intensity of the peaks representing $[M + NH_4]^+$ ions at *m/z* 212.113 were observed from Me*α*Glc than from Me*β*Glc under the same mass spectrometric conditions. It is possible that the anomeric oxygen in axial position is a more favorable configuration than that in equatorial position when hydrogen bonds are formed between methyl D-glucopyranosides and NH_4^+. Such difference was not observed among Glc, Man and Gal as the result of the fast mutarotation at room temperature in their solutions[1].

However, the difference observed between the mass spectra of Me*α*Glc and Me*β*Glc was not sufficient to distinguish them. Therefore, their $[M + NH_4]^+$ ions were selected as precursor ions for further MS^2 experiments. Figure 7.4A shows positive-ion APCI/QTOF-MS^2 spectra of the $[M + NH_4]^+$ precursor ions at *m/z* 212.113 generated from 0.1 mM Me*α*Glc and Me*β*Glc in methanol containing 10 mM NH_4Ac. Accurate mass measurement determined that the identities of the peaks at *m/z* 212, 195, 180, 163 and 145 were $[M + NH_4]^+$, $[M + NH_4 - NH_3]^+$, $[M + NH_4 – CH_4O]^+$, $[M + NH_4 - CH_4O - NH_3]^+$ and $[M– CH_6O_2 + H]^+$, respectively. The observation of $[M + NH_4 - CH_4O]^+$ rather than $[M + NH_4 - H_2O]^+$ supports a previous deduction that the anomeric center is the most active site of monosaccharides.[18] Me*α*Glc could be differentiated from Me*β*Glc due to the larger abundance of $[M + NH_4 - CH_4O]^+$ ions than $[M+NH_4-NH_3]^+$ ions. Figure 7.4B shows the relative intensity of peaks at *m/z* 180 to 195 of Me*α*Glc and Me*β*Glc under different collision energy from 8 to 14 V. As the collision energy increased from 8 to 14 V, the relative intensity of peaks at *m/z* 195 to *m/z* 180 from Me*α*Glc increased from 1.7 to 4.9, while they were below 0.4 for Me*β*Glc. Therefore, Me*α*Glc can be better differentiated from Me*β*Glc under higher collision energy, e.g. 14 V in Figure 7.4B.

In the negative-ion APCI/QTOF mass spectra of 0.5 mM Me*α*Glc and Me*β*Glc in methanol (data not shown), abundant peaks were observed for both $[M + O_2]^-$ ions at *m/z* 226.0646 and $[M - H]^-$ ions at *m/z* 193.0732. As described in the last section, this is quite different from the negative-ion APCI/QTOF mass spectra of hexoses, where the

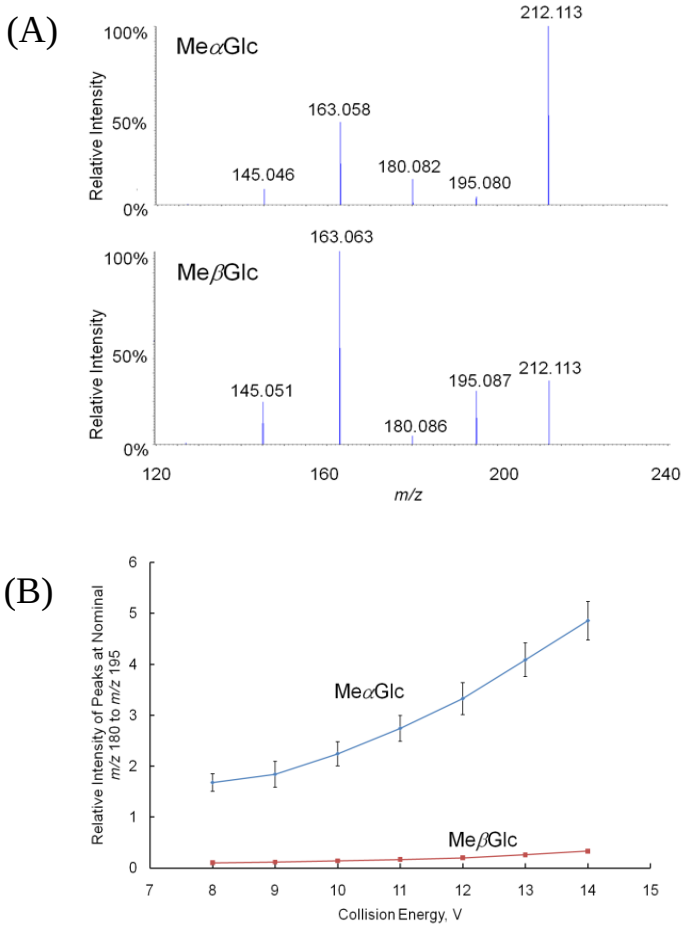

Figure 7.4 (A) Positive-ion APCI/QTOF-MS^2 spectra of the $[M + NH_4]^+$ precursor ions at *m/z* 212.113 generated from 0.1 mM Me*α*Glc and Me*β*Glc in methanol containing 10 mM NH_4Ac. Collision energy was 11 V. Product ions are identified to be $[M - 2H_2O + H]^+$ (*m/z* 144), $[M - 3H_2O + H]^+$ (*m/z* 126), $[M - CH_8O_4 + H]^+$ (*m/z* 96), $[M - C_2H_8O_4 + H]^+$ (*m/z* 84) and $[M - C_3H_8O_4 + H]^+$ (*m/z* 72). (B) Relative intensities of peaks at nominal *m/z* 180 to 195 in the APCI/QTOF-MS^2 spectra under different collision energy for Me*α*Glc and Me*β*Glc.

dissociation of $[M + O_2]^-$ ions was considered favorable to form much more abundant $[M - H]^-$ ions. This is probably because the most acidic hydrogen[30-32] on the anomeric oxygen in D-glucose has been replaced by a methyl group in methyl D-glucopyranosides. A higher energy barrier is therefore created in the dissociation process of the $[M + O_2]^-$ ions of methyl D-glucopyranosides to $[M - H]^-$ ions. Consequently, much more abundant $[M + O_2]^-$ ions were observed in the negative-ion APCI/QTOF mass spectra of Me*α*Glc and Me*β*Glc.

APCI/QTOF-MS^2 spectra of the $[M + O_2]^-$ and $[M - H]^-$ precursor ions generated from 0.5 mM Me*α*Glc and Me*β*Glc in methanol were further acquired. No significant differences were observed.

7.3.4 Differentiation of GlcN, ManN, and GalN

Positive-ion APCI/QTOF-MS spectra of 0.1 mM GlcN HCl, ManN HCl and GalN HCl in methanol containing 10 mM NH_4Ac showed abundant $[M + H]^+$ ions at *m/z* 180 (data not shown). However, unlike the corresponding hexoses, peaks representing $[M + NH_4]^+$ ions were not detected. This is because the proton affinity (PA) value of NH_3, i.e. 853.6 kJ/mol[34], is much weaker than that of GlcN, ManN or GalN, i.e. 937.7, 942.0, and 940.8 kJ/mol[11], respectively. Therefore, $[M + H]^+$ ions of GlcN, ManN and GalN could be formed by abstracting protons from NH_4^+. Even if the $[M + NH_4]^+$ ions were temporarily formed by collision, they could be ready to undergo dissociation process to form $[M + H]^+$ and NH_3, a favorable process when an analyte molecule has a much stronger PA value than that of NH_3.[26] Other in-source fragment ions were also observed

in positive-ion APCI/QTOF mass spectra of 0.1 mM GlcN·HCl, ManN·HCl and GalN·HCl in methanol containing 10 mM NH_4Ac. Accurate mass measurement determined that the major fragment ions were $[M - H_2O + H]^+$, $[M - 2H_2O + H]^+$ and $[M - 3H_2O + H]^+$ with theoretical *m/z* values of 162.076, 144.066 and 126.055.

Neither positive-ion APCI/QTOF mass spectra of GlcN, ManN and GalN nor the MS^2 spectra of their $[M + H]^+$ precursor ions (data not shown) showed any significant differences. Conventional MS^3 spectra, commonly acquired by using ion-trap mass spectrometers[12, 15, 20, 35], could not be acquired by using QTOF mass spectrometers. However, *pseudo*-MS^3 experiment could be performed by utilizing the in-source fragment ions as the precursor ions according to previous studies[36, 37]. In our case, the *pseudo*-MS^3 spectra of their $[M + H]^+$ ions could be acquired when the abundant in-source fragment ions, i.e. $[M - H_2O + H]^+$ ions at *m/z* 162.076, were utilized as the precursor ions. Figure 7.5A shows positive-ion APCI/QTOF-MS^2 spectra of the $[M - H_2O + H]^+$ precursor ions at *m/z* 162.076 generated from 0.1 mM GlcN, ManN and GalN in methanol containing 10 mM NH_4Ac. Accurate mass measurement determined that the identities of product ions at nominal *m/z* 144, 126, 96, 84 and 72 were $[M - 2H_2O + H]^+$, $[M - 3H_2O + H]^+$, $[M - CH_8O_4 + H]^+$, $[M - C_2H_8O_4 + H]^+$ and $[M - C_3H_8O_4 + H]^+$, respectively. Abundant $[M - CH_8O_4 + H]^+$ ions at *m/z* 96 were only detected for GalN, while peaks representing $[M - C_2H_8O_4 + H]^+$ ions at *m/z* 84 were observed with large relative intensity for GlcN and ManN, but not for GalN. In addition, peaks representing $[M - C_3H_8O_4 + H]^+$ ions at *m/z* 72 were the most abundant for both GlcN and GalN, but

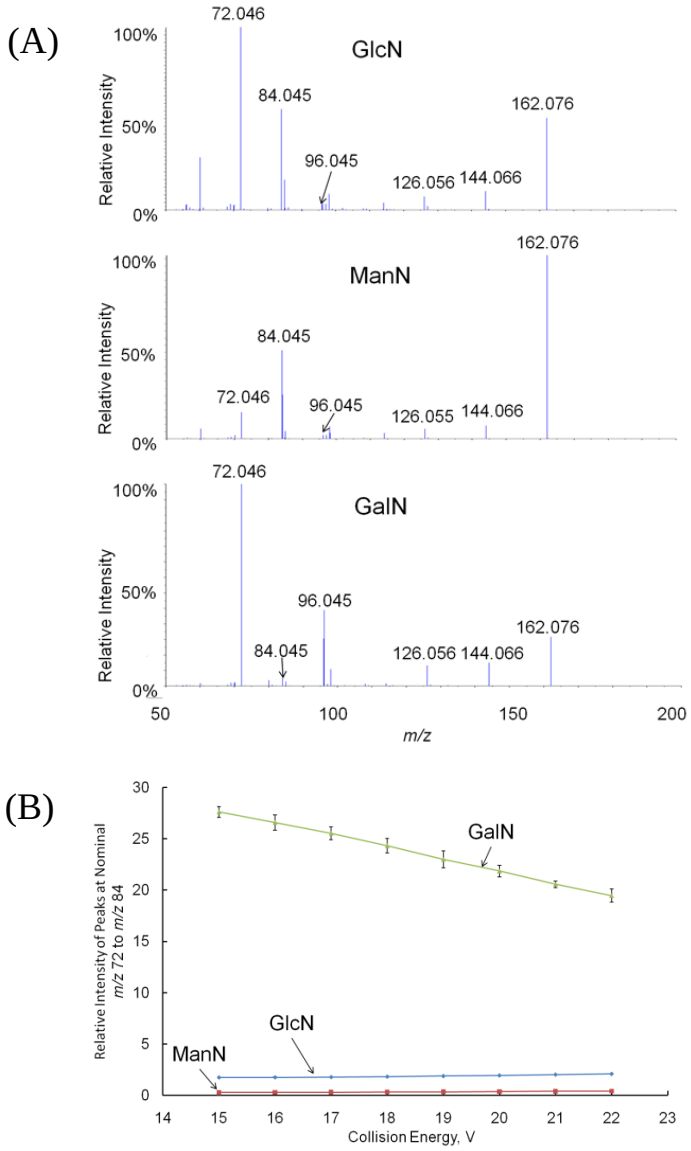

Figure 7.5 (A) Positive-ion APCI/QTOF-MS^2 spectra of the $[M - H_2O + H]^+$ precursor ions at *m/z* 162.076 generated from 0.1 mM GlcN, ManN and GalN in methanol containing 10 mM NH_4Ac. Collision energy was 18 V. Product ions are identified to be $[M - 2H_2O + H]^+$ (*m/z* 186) and $[M - C_2H_8O_4 + H]^+$ (*m/z* 126). (B) Relative intensities of peaks at nominal *m/z* 72 to 84 in the APCI/QTOF-MS^2 spectra under different collision energy for GlcN, ManN and GalN.

not for ManN. Figure 7.5B shows the relative intensity of peaks at *m/z* 72 to 84 of GlcN, ManN and GalN under different collision energy from 15 to 22 V. As the collision energy increased from 15 to 22 V, the relative intensity of peaks at *m/z* 72 to 84 from GalN decreased from 27 to 19, while they were between 1.5 and 2.5 for GlcN and below 0.5 for ManN. Therefore, GlcN, ManN and GalN were clearly distinguished.

Negative-ion APCI/QTOF mass spectra of 0.5 mM GlcN·HCl, ManN·HCl and GalN·HCl in methanol showed chloride adducts, i.e. $[M + {}^{35}Cl]^-$ ions at *m/z* 214.056 and $[M + {}^{37}Cl]^-$ at *m/z* 216.051, with the characteristic 3 to 1 isotopic ratio (data not shown). $[M + O_2]^-$ ions of GlcN, ManN and GalN at *m/z* 211.072 were also observed with a much lower abundance. This could be because $O_2^{-\cdot}$ formed less stable hydrogen bonds with hexosamines than Cl^- , which was also reflected in the negative-ion APCI/QTOF-MS^2 spectra of $[M + O_2]^-$ and $[M + {}^{35}Cl]^-$ ions where no fragment ions were observed beyond *m/z* 100 for the $[M + {}^{35}Cl]^-$ ions.

Figure 7.6A shows negative-ion APCI/QTOF-MS^2 spectra of the $[M + O_2]^-$ precursor ions at *m/z* 211.070 generated from 0.5 mM GlcN·HCl, ManN·HCl and GalN·HCl in methanol. Accurate mass measurement determined that the identities of product ions at nominal *m/z* 178, 177, and 160 were $[M - H]^-$, $[M - 2H]^-$ and $[M - H - H_2O]^-$, respectively. The $[M - 2H]^-$ ions can best be rationalized as loss of hydrogen peroxide from the $[M + O_2]^-$ ions. The relative intensity of the peaks representing $[M - 2H]^-$ ions at *m/z* 177 were larger than that of $[M - H]^-$ ions at *m/z* 178 for GalN, while the opposite was observed for ManN and GlcN. Meanwhile, ManN showed smaller relative

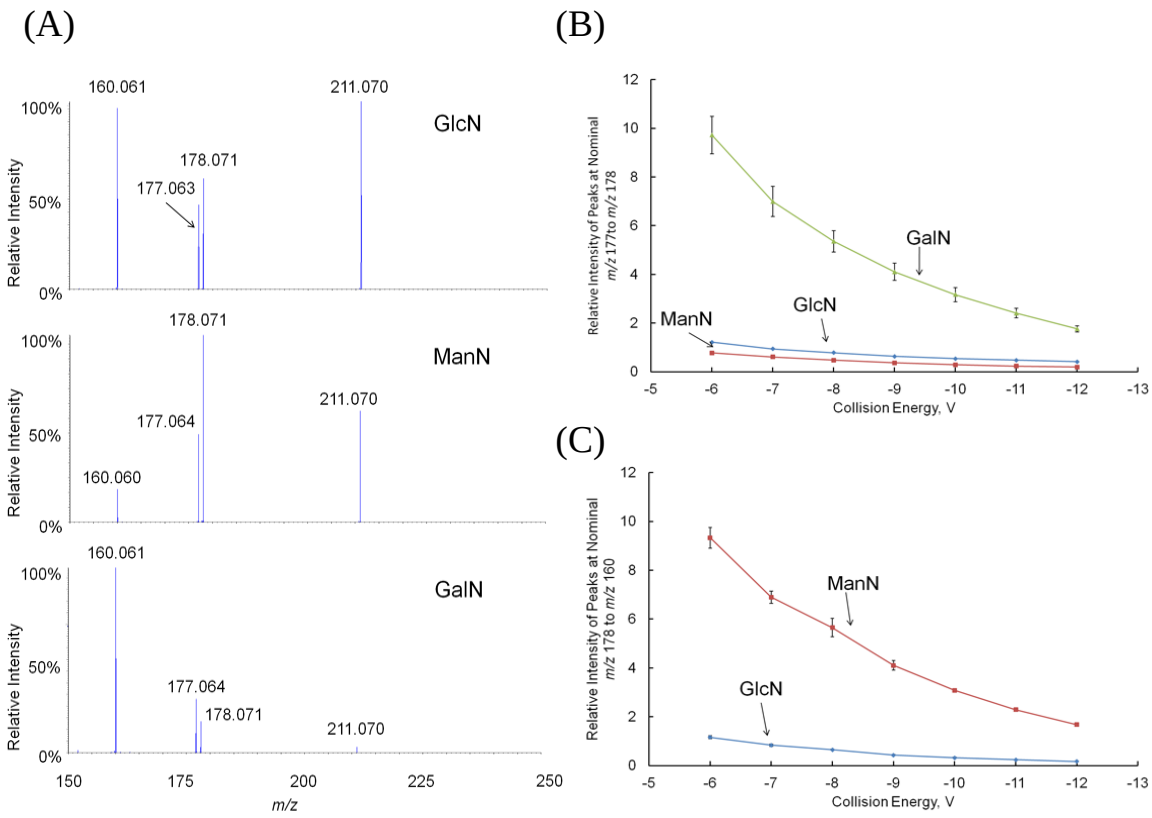

Figure 7.6 (A) Negative-ion APCI/QTOF-MS^2 spectra of the $[M + O_2]^-$ ions at *m/z* 211.070 generated from 0.5 mM GlcN, ManN and GalN. Collision energy was -8 V. Product ions are identified to be $[M - H]^-$ (*m/z* 178), $[M - 2H]^-$ (*m/z* 177), and $[M - H - H_2O]^-$ (*m/z* 160). (B) Relative intensities of peaks at nominal *m/z* 177 to 178 in the APCI/QTOF-MS^2 spectra under different collision energy for GlcN, ManN and GalN. (C) Relative intensities of peaks at nominal *m/z* 178 to 160 in the same spectra under same collision energies as in (B).

intensity of peaks representing $[M - H - H_2O]^-$ ions at *m/z* 160, different from GlcN and GalN. Figure 7.6B shows the relative intensity of peaks at *m/z* 177 to 178 of GlcN, ManN and GalN under different collision energy from 6 to 12 V. As the collision energy increased from 6 to 12 V, the relative intensity of peaks at *m/z* 177 to 178 from GalN decreased from 10 to 1.6, while they were below 1.2 for both GlcN and ManN. Figure 7.6C shows the relative intensity of peaks at *m/z* 178 to 160 of GlcN, and ManN under different collision energy from 6 to 12 V. As the collision energy increased from 6 to 12 V, the relative intensity of peaks at *m/z* 178 to 160 were between 1.5 to 9.5 for ManN and less than 1 for GlcN. Therefore, differentiation of three hexosamine isomers was also successful using negative-ion APCI/QTOF-MS.

7.3.5 Differentiation of GlcNAc, ManNAc, and GalNAc

Positive-ion APCI/QTOF mass spectra of 0.1 mM GlcNAc, ManNAc and GalNAc in methanol containing 10 mM NH_4Ac were obtained (data not shown). Similar to hexosamines, abundant $[M + H]^+$ ions at *m/z* 222.096 were observed, but $[M + NH_4]^+$ ions were absent (The PA values of GlcNAc, ManNAc and GalNAc are 925.7, 926.1 and 927.8 kJ/mol, respectively[38], which are also much stronger that the PA value of NH_3, i.e. 853.6 kJ/mol.) Other in-source fragment ions were also observed. Accurate measurement determined the major fragment ions were $[M - H_2O + H]^+$, $[M - 2H_2O + H]^+$ and $[M - 3H_2O + H]^+$ with theoretical *m/z* values of 204.087, 186.076, and 168.066.

Neither positive-ion APCI/QTOF mass spectra of GlcN, ManN and GalN nor the MS^2 spectra of their $[M + H]^+$ precursor ions (data not shown) showed any significant

differences. Figure 7.7A shows positive-ion APCI/QTOF-MS^2 spectra of the $[M - H_2O + H]^+$ precursor ions at *m/z* 204.087 generated from 0.1 mM GlcNAc, ManNAc and GalNAc in methanol containing 10 mM NH_4Ac. Accurate mass measurement determined that the identities of the product ions at nominal *m/z* 186 and 126 were $[M - 2H_2O + H]^+$ and $[M - C_2H_8O_4 + H]^+$, respectively. Figure 7.7B shows the relative intensity of peaks at *m/z* 186 to 126 of GlcN, ManN and GalN under different collision energy from 9 to 15 V. As the collision energy increased from 9 to 15 V, the relative intensity of peaks at *m/z* 186 to 126 from GlcNAc decreased from 3 to 0.3, while they decreased from 1.3 to 0.1 for both ManNAc and GalNAc. Thus, GlcNAc can be differentiated from ManNAc and GalNAc under lower collision energy, e.g. 9 V in Figure 7.7B. To further distinguish ManNAc and GalNAc, positive-ion APCI/QTOF-MS^2 spectra of the $[M + H - 3H_2O]^+$ precursor ions at *m/z* 168.066 were studied and shown in Figure 7.8A. Accurate mass measurement determined that the identities of the product ions at nominal *m/z* 138 and 126 were $[M - CH_8O_4 + H]^+$ and $[M - C_2H_8O_4 + H]^+$, respectively. Figure 7.8B shows the relative intensity of peaks at *m/z* 138 to 126 of ManNAc and GalNAc under different collision energy from 7 to 13 V. As the collision energy increased from 7 to 13 V, the relative intensity of peaks at *m/z* 138 to 126 from GalNAc increased from 1 to 2.9, while they were below 0.5 from ManNAc. As a result, GlcNAc, ManNAc and GalNAc could be successfully distinguished by positive-ion APCI/QTOF-MS.

Negative-ion APCI/QTOF-MS spectra of 0.5 mM GlcNAc, ManNAc and GalNAc in methanol were also obtained, but no significant differences were observed.

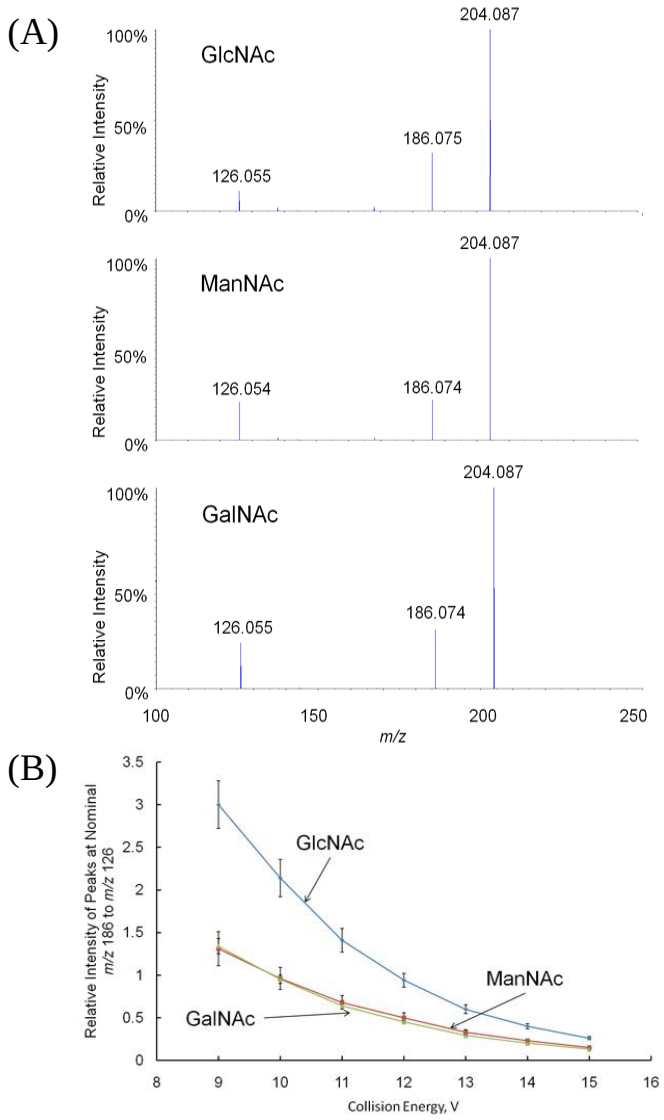

Figure 7.7 (A) Positive-ion APCI/QTOF-MS^2 spectra of the $[M - H_2O + H]^+$ precursor ions at *m/z* 204.087 generated from 0.1 mM GlcNAc, ManNAc and GalNAc in methanol containing 10 mM NH_4Ac. Collision energy was 9 V. Product ions are identified to be $[M - 2H_2O + H]^+$ (*m/z* 186) and $[M - C_2H_8O_4 + H]^+$ (*m/z* 126). (B) Relative intensities of peaks at nominal *m/z* 186 to 126 in the APCI/QTOF-MS^2 spectra under different collision energy for GlcNAc, ManNAc and GalNAc.

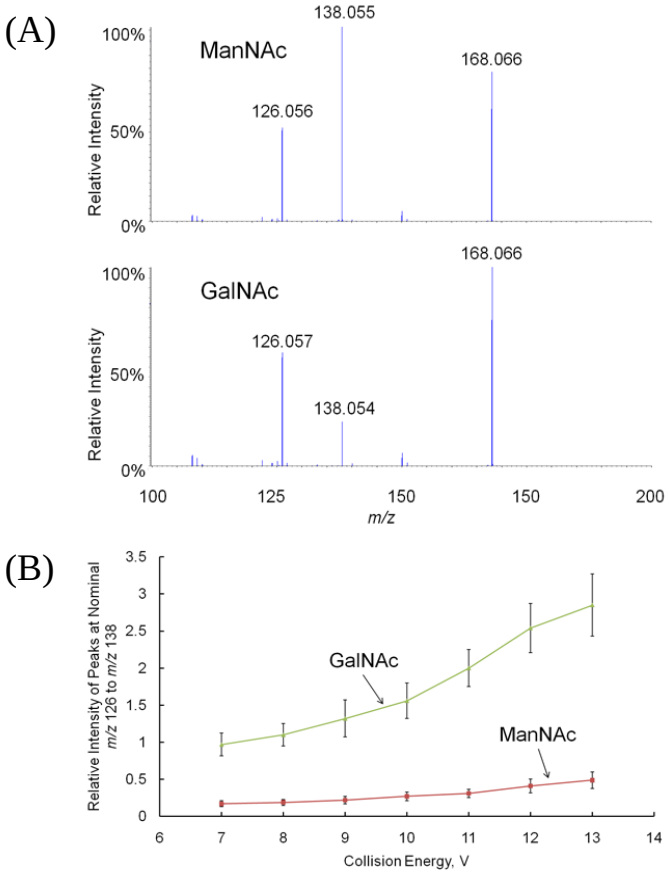

Figure 7.8 (A) Positive-ion APCI/QTOF-MS^2 spectra of the $[M - 3H_2O + H]^+$ precursor ions at *m/z* 168.066 generated from 0.1 mM GlcNAc, ManNAc and GalNAc in methanol containing 10 mM NH_4Ac. Collision energy was 9 V. Product ions are identified to be $[M - 2H_2O + H]^+$ (*m/z* 186) and $[M - C_2H_8O_4 + H]^+$ (*m/z* 126). (B) Relative intensities of peaks at nominal *m/z* 126 to 138 in APCI/QTOF-MS^2 spectra under different collision energy for GlcNAc, ManNAc and GalNAc.

Abundant $[M-H]^-$ ions at *m/z* 220.083 and trace amount of $[M + O_2]^-$ ions at nominal *m/z* 253 were obtained. Further MS^2 spectra of the parent $[M + O_2]^-$, $[M - H]^-$ and other in-source fragment ions were also acquired, but the differentiation of GlcNAc, ManNAc and GalNAc was not achieved after carefully inspection of the fragmentation patterns.

7.4 Conclusion

In this report, APCI/QTOF has been proven to be a convenient and efficient technique for differentiation of underivatized monosaccharides. For hexoses, Glc was differentiated from Man and Gal through the different MS^2 spectra of their $[M + NH_4]^+$ ions; Man was further differentiated from Gal through the different MS^2 spectra of their $[M - H]^-$ ions. For methyl D-glucopyranosides, Me*α*Glc was differentiated from Me*β*Glc through the different MS^2 spectra of their $[M + NH_4]^+$ ions. For hexosamines, GlcN, ManN and GalN were differentiated by either the different *pseudo*-MS^3 spectra of their $[M + H]^+ \rightarrow [M + H - H_2O]^+$ ions or the different MS^2 spectra of their $[M + O_2]^-$ ions. For N-acetylhexosamines, GlcNAc, ManNAc and GalNAc were differentiated by the different *pseudo*-MS^3 spectra of their $[M + H]^+ \rightarrow [M + H - H_2O]^+$ ions.

Although ESI has been widely utilized in the differentiation of monosaccharides, this report demonstrated that APCI had its own ability to achieve the same goal. With ESI, $[M + NH_4]^+$, $[M + H]^+$, metal adduct, $[M + Cl]^-$ ions of monosaccharides were usually produced. In comparison with ESI, APCI is unable to produce metal adduct ions, but it could generated more abundant $[M - H]^-$ and unique $[M + O_2]^-$ ions due to the generation of $O_2^{-\cdot}$ in the APCI process and its strong basicity. Both $[M - H]^-$ and [M +

$O_2]^-$ ions were proven to be useful in the differentiation of certain underivatized monosaccharides.

Although single or triple quadrupole and ion trap mass spectrometry have been predominantly used in the analysis of (oligo- and mono-)saccharides, this report demonstrated that QTOF-MS could be advantageous due to its accurate mass measurement ability. While QTOF mass spectrometers are unable to perform MS^n analysis, it appeared to us that their *psduo*-MS^3 capability could also meet the requirements as $MS^{n(>3)}$ analyses have been rarely used in the analysis of (oligo- and mono-)saccharides.

Reference

(1) A. Varki. *Essentials of glycobiology*, 2nd ed., Cold Spring Harbor Laboratory Press, Cold Spring Harbor, N.Y., **2009**.

(2) A. Varki. *Glycobiology* **1993**, *3*, 97.

(3) M. F. Chaplin, J. F. Kennedy, *Carbohydrate analysis : a practical approach*, 2nd ed., ILR Press, Oxford ; New York, **1994**.

(4) J. Zaia. *Mass Spectrom. Rev.* **2004**, *23*, 161.

(5) D. Garozzo, M. Giuffrida, G. Impallomeni, A. Ballistreri, G. Montaudo. *Anal. Chem.* **1990**, *62*, 279.

(6) H. Egge, J. Peter-Katalinić. *Mass Spectrom. Rev.* **1987**, *6*, 331.

(7) S. Gaucher, J. Leary. *J. Am. Soc. Mass Spectrom.* **1999**, *10*, 269.

(8) K. L. Duffin, J. K. Welply, E. Huang, J. D. Henion. *Anal. Chem.* **1992**, *64*, 1440.

(9) D. M. Sheeley, V. N. Reinhold. *Anal. Chem.* **1998**, *70*, 3053.

(10) V. Nagaveni, S. Prabhakar, M. Vairamani. *Anal. Chem.* **2004**, *76*, 3505.

(11) H. Desaire, J. A. Leary. *Anal. Chem.* **1999**, *71*, 4142.

(12) H. Desaire, J. A. Leary. *Anal. Chem.* **1999**, *71*, 1997.

(13) J. Y. Salpin, J. Tortajada. *J. Mass Spectrom.* **2002**, *37*, 379.

(14) V. Carlesso, C. Afonso, F. Fournier, J. C. Tabet. *Int. J. Mass spectrom.* **2002**, *219*, 559.

(15) S. P. Gaucher, J. A. Leary. *Anal. Chem.* **1998**, *70*, 3009.

(16) K. P. Madhusudanan, S. Kanojiya, B. Kumar. *J. Mass Spectrom.* **2005**, *40*, 1044.

(17) R. E. March, C. J. Stadey. *Rapid Commun. Mass Spectrom.* **2005**, *19*, 805.

(18) K. P. Madhusudanan. *J. Mass Spectrom.* **2006**, *41*, 1096.

(19) G. Giorgi, M. Speranza. *Int. J. Mass spectrom.* **2006**, *249*, 112.

(20) X. Zhu, T. Sato. *Rapid Commun. Mass Spectrom.* **2007**, *21*, 191.

(21) H. R. Liang, T. Takagaki, R. L. Foltz, P. Bennett. *Rapid Commun. Mass Spectrom.* **2005**, *19*, 2284.

(22) S. Ullah, J. Wahren, O. Beck. *Scand. J. Clin. Lab. Invest.* **2009**, *69*, 837.

(23) S. S. Choi, J. C. Kim. *Rapid Commun. Mass Spectrom.* **2009**, *23*, 3969.

(24) S. S. Choi, J. C. Kim. *Carbohydr. Res.* **2010**, *345*, 408.

(25) M. A. Sutton, J. W. Erisman, F. Dentener, D. Moller. *Environ. Pollut.* **2008**, *156*, 583.

(26) H. Nakata, H. Konishi, N. Takeda, A. Tatematsu, M. Suzuki. *J. Mass Spectrom. Soc. Jpn.* **1983**, *31*, 275.

(27) L. Song, D. S. Cho, D. Bhandari, S. C. Gibson, M. A. McNally, R. Hoffman, K. D. Cook, "Ionization mechanisms related to atmospheric pressure chemical ionizatoin (APCI) and direct analysis in real time (DART)", (2011). Conference Presentation, Published. Bibliography: The PITTCON Conference & Expo 2011, Atlanta, GA, USA

(28) D. F. Hunt, C. N. McEwen, T. M. Harvey. *Anal. Chem.* **1975**, *47*, 1730.

(29) J. E. Bartmess. "Negative Ion Energetics Data" in **NIST Chemistry WebBook, NIST Standard Reference Database Number 69**, Eds. P.J. Linstrom and W.G.

Mallard, National Institute of Standards and Technology, Gaithersburg MD, 20899, http://webbook.nist.gov, (retrieved May 1, 2011)

(30) Based on G3(MP2)B3 calculations, J. E. Bartmess,

(31) Y. Cai, R. B. Cole. *Anal. Chem.* **2002**, *74*, 985.

(32) J. Y. Salpin, J. Tortajada. **2004**, *39*, 930.

(33) D. J. Brown, S. E. Stefan, G. Berden, J. D. Steill, J. Oomens, J. R. Eyler, B. Bendiak. *Carbohydr. Res.* **2011**, *346*, 2469.

(34) E. P. Hunter, S. G. Lias. "Pronton Affinity Evaluation" in **NIST Chemistry WebBook, NIST Standard Reference Database Number 69**, Eds. P. J. Linstrom and W. G. Mallard, National Institute of Standards and Technology, Gaithersburg MD, 20899, http://webbook.nist.gov, (retrieved May 1, 2011)

(35) H. Desaire, J. A. Leary. *J. Am. Soc. Mass Spectrom.* **2000**, *11*, 1086.

(36) H. P. Chen, K. Tabei, M. M. Siegel. *J. Am. Soc. Mass Spectrom.* **2001**, *12*, 846.

(37) J. J. Li, Z. Wang, E. Altman. *Rapid Commun. Mass Spectrom.* **2005**, *19*, 1305.

(38) N. Voleti, M. Vairamani. *Rapid Commun. Mass Spectrom.* **2003**, *17*, 1089.

Appendix C

for

Chapter 7. Differentiation of Underivatized Monosaccharides by Atmospheric Pressure Chemical Ionization Quadrupole Time-of-Flight Mass Spectrometry

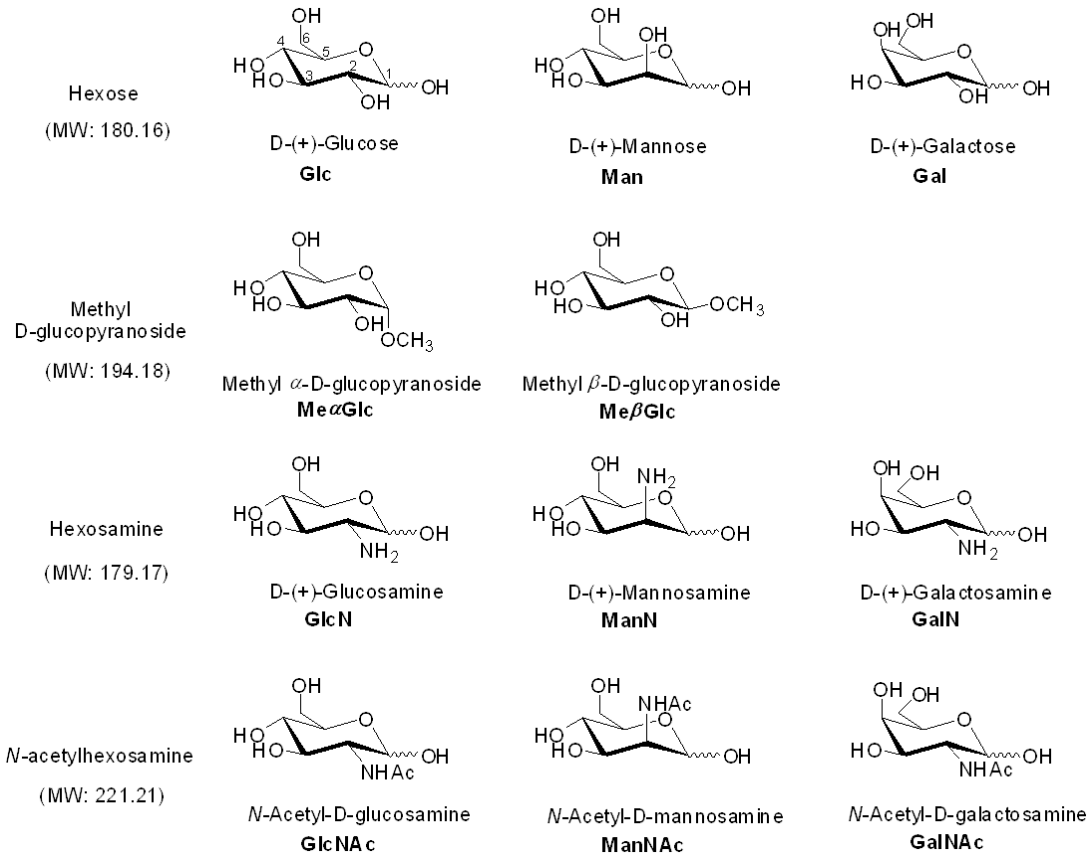

Figure C1 Structures of monosaccharides studied in this chapter.

Chapter 8. Conclusion

APCI-MS based systems have been successfully developed for quantitative real-time monitoring of molar-level chemical reactions from homogenous liquid (Chapter 2) to heterogeneous liquid-liquid (Chapter 3) and further to heterogeneous solid-liquid systems (Chapter 4-6).

In Chapter 2, the potential sample overloading in quantitative real-time monitoring of process-scale reactions was avoided using a novel auto-sampling FIA/APCI-MS system. The system incorporated a 1 μL automatic internal sample injector, a post-injection splitter with 1:10 splitting ratio, and a detached APCI source, to extend the upper-limit of quantitative calibration by approximately 10^3 times. In addition, the performance of the injector, the splitter and the ion-transport capillary were compound-independent, which allows the auto-sampling FIA/APCI-MS to be widely employed for quantitative real-time reaction monitoring. The ability of the auto-sampling FIA/APCI-MS to monitor more complex reactions quantitatively in real time was further explored in Chapter 3, where the transesterfication of a triglyceride to produce biodiesel through three reversible reactions were investigated. Chapter 3 also presents the efforts in compensating the matrix effects observed in FIA/APCI-MS. Quantitative results of reactant, product and intermediates were obtained and in a great agreement with quantitative data obtained off-line using HPLC/APCI-MS where matrix effects were considered minimum.

The slurry FIA/APCI-MS introduced in Chapter 4 and 5 allowed routine quantitative analysis of not only liquid samples but also solid-liquid mixtures, where sample pretreatment, e.g. filtration, was otherwise inevitable. Both sample overloading and

instrumental clogging in quantitative real-time monitoring of process-scale batch slurry reactions have been solved. Quantitative calibration has been achieved at 30% (w/w) slurry concentration as is needed to apply this system to monitor a model batch slurry reaction in industry. Components of the slurry FIA/APCI-MS, including a HPLC pump, a column thermostatted compartment, a slurry auto-sampler, a post-injection slurry mixer, a post-injection splitter, a slurry APCI probe and a detached APCI-MS setup, guaranteed its flexibility to be adapted to diverse chemical processes and different mass spectrometers. In Chapter 6, the slurry FIA/APCI-MS was adapted for the quantitative real-time monitoring of a heterogeneous-catalyzed Pechmann condensation reaction, where sample overloading caused by analytes in molar concentrations, and instrumental contamination and/or clogging by 50 g/L catalyst were successfully avoided.

The next level of the research is the evaluation of the slurry FIA/APCI-MS on the quantitative real-time monitoring of industrial reactions performed in the pilot plants. The slurry FIA/APCI-MS can be conveniently interfaced with the recirculation loop, which is commonly used in industrial reactors, so that the slurry auto-sampler can be easily loaded with slurry samples. Meanwhile, an integrated slurry FIA and detached APCI setup, with independent power supply and software control, can be developed to be a portable device. Such a device is expected to universally bridge diverse chemical reactors and mass spectrometers for quantitative real-time reaction monitoring of industrial reactions.

Chapter 7 presents the characteristic mass spectra and fragmentation patterns of underivertized monosaccharides by APCI-MS and APCI-MS/MS. APCI has been found

as an alternative ionization method to ESI to distinguish stereoisomers of underivertized monosaccharides.

Vita

Zhenqian Zhu was born in a beautiful town in Nantong, China. He attended East China University of Science and Technology from 2005 to 2009, where he received his B.S. in Pharmaceutics in Shanghai, China. After graduation, he enrolled as a graduate student in Department of Chemistry at the University of Tennessee-Knoxville and joined Professor John E. Bartmess' group in October, 2010. His PhD work mainly focused on developing mass spectrometry based systems for quantitative real-time reaction monitoring at high concentration levels. Zhenqian Zhu received a Doctor of Philosophy Degree in Analytical Chemistry from the University of Tennessee in May, 2014.